INVESTIGATION OF EFFECTS OF BIRD STRIKE ON A ROTARY-WING AIRCRAFT

DÖNER KANATLI BİR HAVA ARACINA KUŞ ÇARPMASININ ETKİLERİNİN İNCELENMESİ

MURAT FEHMİ BÜLENT ALTINDAĞ

PROF. DR. BORA YILDIRIM
Supervisor

Submitted to
Graduate School of Science and Engineering of Hacettepe University
as a Partial Fulfillment to the Requirements
for the Award of the Degree of Master of Science
in Mechanical Engineering

2021

ABSTRACT

INVESTIGATION OF EFFECTS OF
BIRD STRIKE ON
A ROTARY-WING AIRCRAFT

Murat Fehmi Bülent ALTINDAĞ

Master of Science, Department of Mechanical Engineering
Supervisor: Prof. Dr. Bora YILDIRIM
June 2021, 87 pages

Bird strike incidents have been important issue since begining of aviation, and importance of bird strikes increase day by day. Number of bird strike incident are going to continue increasing because of developing aviation industry and increasing air traffic. Airspeed of rotary wing aircraft changes with pitch angle. Therefore, effect of bird strikes at different airspeeds changes with not only airspeed but also impact angle. Within the scope of this study, effect of bird strike on a rotary wing aircraft was investigated and it is aimed to bring an example study to the literature of our country. After history of bird strike was mentioned chronologically, information was given about effects of bird strike incident to general aviation and helicopters which are rotary wing aircraft. Also, one helicopter crash occured because of bird strike was mentioned. After giving information about applying forces on flying helicopter and explaining how helicopters fly, impact scenarios were determined for anayses. Finite element methods were explained and compared with each other for bird strike analysis. After defining a geometry, dimensions and density of bird, analyses were done using each bird geometry using Lagrangian, SPH and ALE methods according to speed and mass given in literature. Results were evaluated and the optimal finite element method–bird shape combination was determined.

Strike analyses were done using determined finite element method – bird shape combination in accordance with data of previous experimental bird strike study before analysis setup was verified. After defining impact surface, impact speed and strike angle, final analyses were done at 80, 85, 102, 110 ve 120 knots impact speeds with excluding effect of strike angle and including effect of stike anglei respectively. Finaly, effects of bird strike on a rotary-wing aircraft were investigated.

Keywords: Bird, Strike, Bird Strike, Helicopter, Rotary-Wing, Lagrange, ALE, SPH

ÖZET

DÖNER KANATLI BİR HAVA ARACINA KUŞ ÇARPMASININ ETKİLERİNİN İNCELENMESİ

Murat Fehmi Bülent ALTINDAĞ

Yüksek Lisans, Makina Mühendisliği Bölümü
Tez Danışmanı: Prof. Dr. Bora YILDIRIM
Haziran 2021, 87 sayfa

Kuş çarpması olayları havacılık tarihinin ilk zamanlarından itibaren var olan ve havacılık sektörü için önemi her geçen gün artan önemli bir olaydır. Gelişen havacılık sektörü ve artan hava aracı trafiği sonucunda kuş çarpması olayları artmaya devam edecektir. Döner kanatlı hava aracının hava sürati yunuslama açısı ile değişmektedir. Bu sebeple farklı hızlarda meydana gelen kuş çarpması olaylarında, çarpmanın etkisi yalnızca hız ile değil aynı zamanda çarpma açısı ile değişmektedir. Bu çalışmada döner kanatlı hava aracına kuş çarpması durumunda oluşan etkiler incelenerek, sonuçları ülkemiz literatürüne kazandırmak amaçlanmıştır. Kuş çarpması olaylarının tarihçesinden kronolojik sırayla bahsedilmesinin ardından hava aracına kuş çarpması olayının genel havacılığa ve döner kanatlı hava araçları olan helikopterlere etkileri hakkında istatistiksel veriler kullanılarak bilgi verilmiştir. Ayrıca, kuş çarpması sonucunda oluşan bir helikopter kazasından bahsedilmiştir. Helikopterlere uçuşta etki eden kuvvetler ve helikopterlerin nasıl uçtuğu hakkında bilgi verilmesinin ardından analizlerde kullanılacak farklı hızlardaki kuş çarpması senaryoları belirlenmiştir. Analizlerde kullanılması planlanan sonlu eleman yöntemleri hakkında bilgi verilip, birbirlerine göre avantajları ve dezavantajları belirtilmiştir. Kuş modellemesi için kullanılacak olan geometriler, geometrilerin ağırlığına bağlı olarak boyutlarıı ve özkütlelerinin belirtilmesinin ardından lagrange, SPH ve ALE metodları kullanılarak her bir kuş geometrisi ile litertürde yer alan hız ve ağırlıkta analizler gerçekleştirilmiş olup, çıkan

sonuçlar değerlendirilerek tez çalışmasında kullanılacak metod ve kuş geometrisi belirlenmiştir. Belirlenen metod ve geometri kullanılarak literatürde yer alan deneysel kuş çarpması çalışmasındaki şartlarda analiz gerçekleştirilmiş olup, çıkan sonuçlar ve deneysel çalışma sonuçları karşılaştırılarak kullanılan metod ve kuş geometrisinin uygun olduğu doğrulanmıştır. Kuş çarpmasının gerçekleşeceği yüzey, çarpma hızı ve hıza bağlı olarak değişen çarpma açısıları belirlenmesinin ardından, 80, 85, 102, 110 ve 120 knots hızlarda, hıza bağlı olarak değişen çarpma açısının etkisi dahil edilmeden ve dahil edilerek analizler gerçekleştirilmiş ve döner kanatlı bir hava aracına kuş çarpmasının etkileri incelenmiştir.

Anahtar Kelimeler: Kuş, Çarpma, Kuş Çarpması, Helikopter, Döner Kanat, Lagrange, ALE, SPH

ACKNOWLEDGEMENTS

Firstly, I would like to express my deepest gratitude to my supervisor Prof. Dr. Bora YILDIRIM who made a great contribution in the creation of this thesis, supported me with his knowledge, guidance, and experience at every stage of my study. I would also thank to my thesis committee members for their valuable feedbacks and suggestions.

I would like to express my thankfulness to all my family, my lovely wife Doğa TEZAL ALTINDAĞ, my brother Ömer Utku ALTINDAĞ, and my parents Sevgi ALTINDAĞ and Murat ALTINDAĞ who have always supported me with their love and devotion. I am very grateful for their love and endless support.

Murat Fehmi Bülent ALTINDAĞ

June 2021, Ankara

TABLE OF CONTENTS

LIST OF FIGURES

LIST OF TABLES

LIST OF SYMBOLS AND ABBREVIATIONS

Symbols

$\vec{F}_R$,	Resultant Aerodynamic Force
$\vec{F}_P$	Pressure Force
$\vec{F}_\tau$	Shear Force
$\vec{F}_D$	Drag Force
$\vec{F}_L$	Lift Force
$\vec{n}$	Unit Vector Normal to Surface
$\vec{k}$	Unit Vector Parallel to Surface
$\vec{V}_\infty$	Free Stream Velocity/Relative Velocity
A	Cross Section Area
C	Coefficient
C_D	Drag Coefficient
c_0	Speed of Sound
D_{bird}	Bird Model Diameter
dS	Segment of Surface
E_i	Internal Energy
K	Bulk Modulus
k	Experimental Constant of EOS
L_{bird}	Bird Model Length
m_{bird}	Bird Model Mass
P	Pressure
$P_{stagnation}$	Stagnation Pressure
p	Local Pressure

q_∞	Dynamic Pressure
V_{bird}	Bird Model Volume
V_H	Maximum Speed in Level Flight with Maximum Continuous Power
V_{impact}	Impact Velocity
V_{NE}	Velocity Never Exceed
v_s	Velocity of A Shock
v_p	Velocity of Particle
α	Angle of Attack
a_{Corr}	First Order Correction to Gruneisen Coefficient
ρ	Current Density
ρ_0	Reference Density of Medium
$\rho_{impactor}$	Density of Impactor
ρ_{air}	Air Density
ρ_{bird}	Bird Model Density
μ	Change in Density
τ	Local Shear Stress
γ_0	Gruneisen Coefficient

Abbreviations

AGL	Above Ground Level
CPU	Central Processing Unit
CST	Central Standard Time
CVR	Cockpit Voice Recorder
FDR	Flight Data Recorder
inHg	Inch of Mercury
NTSB	National Transportation Safety Board
RPM	Revolution Per Minute
STC	Supplemental Type Certificate

1 INTRODUCTION

Bird strike have been an important issue for aviation since beginning of aviation. Structural deformations which occur as a result of bird strike could cause serious accidents. Flight safety is the one of the important issues of aviation. Therefore, bird proof design of aircraft has importance for aviation. Because of the potential bird strike accidents, aircrafts should be designed and produced considering bird strike incidents [1, 2].

Physical tests are expensive, time consuming and inefficient method because it is required to setup qualified test infrastructure to use produced aircraft structure. Unsuccessful result after production and testing means changing of design or material then producing and testing of new design, respectively. As a result of developing computer processor technology, computational methods, and solvers; design and evaluation are done at the same time using FEM solvers. Use of FEM analyses instead of physical tests reduce time and cost.

In this study effects of bird strike on a rotary-wing aircraft were investigated. After creating analysis environments in LS-PrePost, then LS-DYNA was used to make impact analyses. Analyses were done for differend forward airspeeds. At the speeds of strike, the bird has soft body behavior and flows in a fluid-like manner on impact surface. High deformation of spreading material is important issue for finite element method analysis [3]. Lagrangian method, Arbitrary Lagrangian - Eulerian method and Smoothed Particle Hydrodynamics methods were used with three different bird shapes to decide appropriate method and bird shape combination for the bird strike analyses. At the end of the analyses, results were compared. Combination of Smoothed Particle Hydrodynamics method and cylindrical bird shape with hemispherical ends was chosen for final analyses.

Airspeed of rotary-wing aircraft changes with pitch angle. Beauce of the correlation between pitch angle and speed of rotary wing aircraft, bird strikes to surface with higher speeds and steeper angle while flying with higher speed. Therefore, effect of bird strike to a rotary-wing aircraft is different than the fixed-wing aircrafts. In this thesis work, effects of bird strike on a rotary-wing aircraft were investigated.

2 BIRD STRIKE INCIDENT

2.1 History

History of bird strike dates back to beginning of 20th century by the first reported bird strike incident. Just two years after first flight, Orville Wright who was the one of the Wright brothers struck a bird in Dayton/Ohio/USA in 1905. Bird strike incidents continued in the course of time. Some of the best-known accidents called Hudson River Miracle and Sikorsky S-76C happened in 2009.

The accident of Hudson River Miracle happened because of ingestion of Canada geese into both engines of Airbus 320. It resulted with engine loss and emergency forced landing of aircraft with 155 passengers and crew to the Hudson River.

The accident Sikorsky S-76C happened because of collision of red-tailed hawk and Sikorsky S-76C helicopter. It resulted loss of helicopter in 17 seconds and death of two pilots and six of seven passengers at the time of accident.

Table 1 Important Bird Strike Incidents in History [4]

Year	Place	Accident	Result
1912	Over Long Beach, CA	Calbraith Rodgers' aircraft struck a gull.	The first fatal bird strike incident. After the collision with a gull, bird jammed in aircraft control cables.
1960	Boston Logan Airport	The aircraft stroked a flock of European Starlings on take-off then crashed in the Boston harbor.	The first commercial aviation disaster involving a bird strike. As a result of accident 62 people died and 9 people injured.
1995	Elmendorf AFB	The aircraft struck Canada geese and was destroyed.	The worst recorded military disaster involving birds in the U.S. Result of accident was 24 fatalities.
2009	Hudson River	Ingestion of Canada geese in both engines of Airbus 320.	Known as Hudson Miracle. Emergency forced landing of aircraft with 155 passengers and crew.
2009	Morgan City, LA	Collision of red-tailed hawk and Sikorsky S-76C.	Loss of helicopter in 17 seconds and death of six of seven passengers at the time of accident.

2.2 Effects of Bird Strike to Aviation

The FAA started to collect bird strike data in 1965. The National Wildlife Strike Database was created by cooperation of FAA and United States Department of Agriculture, Wildlife Service (USDA/WS). Wildlife strike data, not only bird strike, was collected, analyzed, and annually drawn up in a report named Wildlife Strikes to Civil Aircraft in the United States. According to 24th issue of report, birds and other animal strikes responsible for loss of more than 263 aircrafts and 287 people from 1988 through November 2018, internationally [5].

According to reported wildlife strikes to civil aircraft in the United States 1990-2005 [6], for 16 years, it is observed that 64734 bird strike incidents were reported. 43495 bird strike reports included time of occurrence of strikes. 62,9 percent of incidents occurred in daytime of a day, 27,2 percent of incidents occurred in nighttime of a day, and 9,9 percent of incidents occurred in dawn and dusk time of a day. 53309 bird strike reports included damage information of bird strike incident. 7875 reports resulted as damaged component, and 2156 reports (27,4 percent of reported damages) resulted in substantial or higher damage. 59049 bird strike reports included information of components reported as struck. According to reported incidents, 10265 windshields were reported as struck, and 546 windshields were reported as damaged. Windshields were the most reported component as struck with 17,4 percent.

Similarly, according to reported wildlife strikes to civil aircraft in the United States 1990-2017 [5], for 28 years, It is observed that 187343 bird strike incidents were reported. 119673 bird strike reports included time of occurrence of strikes. 62,8 percent of incidents occurred in daytime of a day, 29,4 percent of incidents occurred in nighttime of a day, and 7,8 percent of incidents occurred in dawn and dusk time of a day. 133531 bird strike reports included damage information of bird strike incident. 14744 reports resulted as damaged component, and 3595 reports (24,4 percent of reported damages) resulted in substantial or higher damage. 165670 bird strike reports included information of components reported as struck. According to reported incidents, 26167 windshields were reported as struck and 1087 windshields were reported as damaged. Windshields were the most reported component as struck with 15,8 percent.

After observation and comparison of statistical data collected for 16 years and 28 years, it was seen from bird strike data that statistical distribution of strike data stayed almost constant while number of reported strike incidents increased. It was observed that windshield is going to stay as the most reported component as struck. Increase of bird population and air traffic are going to increase both number of bird strike incidents and importance of bird strike.

2.3 Helicopter Bird Strike

According to reported wildlife strikes to civil aircraft in the United States 1990-2005 [6], for 16 years, 64734 bird strike incidents were reported for civil aircrafts. 53309 reports included damage information. 7875 reports (14,8 percent of 53309 reports) resulted in damage and 2140 reports (4 percent of 53309 reports) resulted in substantial damage. However, 370 bird strike incidents (0,6 percent of 64734 bird strike incidents) were reported for rotary-wing aircrafts. 186 reports (50,3 percent of 370 reports) resulted in damage and 67 reports (18,1 percent of 370 reports) resulted in substantial damage. It is observed that for rotary-wing aircrafts, number of strikes are seen less compared to all aircraft types. However, bird strike incidents with rotary-wing aircraft resulted in higher percentage of aircraft damage.

En route phase of flight constitutes a large part of flights. In the en route flight, the average cruise altitude of fixed-wing aircrafts is higher than the average altitude of bird populations. However, at the take-off run, climb, approach and landing roll phases of flight which are closer to the ground level, aircrafts and many bird species use same airfield. Therefore, most of the bird strike incidents of fixed wing aircrafts occur at those flight phases as seen in the Table 2 which was generated using reported strikes data including flight phase and aircraft type information in USA between 1990 and 2005.

Table 2 Reported Flight Phase of Bird Strikes to Civil Aircrafts [6]

	Total Strike Reports (Known Flight Phases)	Flight Phase	Strike Report	Percentage
Civil Aircrafts (Including Civil Helicopters)	48638	Approach	18813	38,68 %
		Take-off Run	9562	19,66 %
		Climb	8978	18,46 %
		Landing Roll	7939	16,32 %
		Other	3346	6,88 %
Only Civil Helicopters	352	En route	221	62,78 %
		Climb	55	15,63 %
		Approach	44	12,50 %
		Other	32	9,09 %

On the other hand, traffic density of rotary-wing aircraft density is less than traffic density of fixed-wing aircrafts. Therefore, compared to bird strike incidents of fixed-wing aircrafts, number of bird strike incidents of rotary-wing aircrafts were less. However, probability of bird strike to rotary-wing aircraft is higher because rotary-wing aircrafts and many bird species fly at lower altitude AGL compared to fixed-wing aircrafts. Therefore, much higher strike rate for rotary-wing aircrafts was observed in en route flight as seen in Table 2.

Table 3 Reported Bird Strikes Including Flight Phase and Damage Information [6]

	Total Reported (Including Flight Phase and Damage Information)		Strikes in En Route Flight			
	Strike	Damage	Report Number		Percentage	
			Strike	Damage	Strike	Damage
Civil Fixed Wing Aircrafts	47711	6499	1051	465	2,2 %	7,2 %
Civil Helicopters	352	179	221	137	62,8 %	76,5 %

Table 3 was generated using reported strikes data which includes flight phase and damage information in USA between 1990 and 2005.

It was seen from Table 3 that, number of bird strike incidents to rotary-wing aircrafts was less than fixed-wing aircrafts in en route flight. For fixed-wing aircrafts, 2,2 percent (1051 strikes) of 47711 strikes occurred during en route flight and 7,2 percent (465 strikes) of 6499 damaging strikes occurred during en route flight. However, 62,8 percent (211 strikes) of the 352 strikes and 76,5 percent (137 strikes) of the 179 damaging strikes for rotary-wing aircraft occurred during the en route phase of flight.

Table 4 The Most Reported Component Struck by Bird [6]

	Total Reported Components		The Most Reported Component as Struck				
	Strike	Damage	Component	Number of Report		Percentage to Total	
				Strike	Damage	Strike	Damage
Civil Aircrafts	59049	9244	Windshield	10265	546	17,4 %	5,9 %
Only Civil Helicopters	442	238	Windshield	157	98	35,5 %	41,2 %

Table 4 shows number of reported components of civil aircrafts as struck and damaged because of bird strike in the United States between 1990-2005. 59049 civil aircraft components were reported as struck and 9244 civil aircraft components were reported as damaged. For only civil helicopters, 442 and 238 components were reported as struck and damaged because of bird strike, respectively. According to reports, windshield was the most reported component as struck and damaged for not only rotary-wing aircraft but also civil aircrafts. For civil aircrafts, 17,4 % of 59049 reports (10265 reports) stated windshield as struck and 5,9 % of 9244 reports (546 reports) stated that windshield was damaged after strike. For only civil helicopters, 35,5 % of 442 reports (157 reports) stated windshield as struck and 41,2 % of 238 reports (98 reports) stated that windshield was damaged after strike. Comparison of data shows that, windshields of helicopters were exposed to bird strike almost twice as often compared to windshields of other civil aircraft types. Helicopter windshields were damaged after bird strike about six times higher in percertage than windshield of all civil aircrafts. The high percentage of helicopter windshields reveals importance of bird strike incidents for helicopters. Figure 2-1 and Figure 2-2 show seriousness of bird strike incidents for rotary-wing aircraft.

Figure 2-1 Sikorsky UH-60 Helicopter after Birds Strike, Outside

Figure 2-2 Sikorsky UH-60 Helicopter after Birds Strike, Inside

2.4 Sikorsky S-76C Accident

On January 4, 2009, at 14:09 CST, the Sikorsky S-76 model helicopter departed from its home base of Lake Palourde Base Heliport (Ameliai LA). The helicopter was en route to an offshore oil platform with two pilots and seven passengers. Weather at the time of the accident was suitable for flight. Lowest cloud condition was scattered at 1500 feet AGL with ten miles visibility. Air temperature was 24°C with 19°C dew point. Wind was 6 knots from 160°. Approximately seven minutes after take-off, it crashed into marshy terrain, 12 miles southeast of takeoff location. The helicopter had CVR and FDR. According to flight data recorder, helicopter flew in level cruise flight condition at 8500 feet MSL (Mean Sea Level) and 135 knots indicated air speed. Investigation of cockpit voice recorder elicited a loud impact and rushing wind sound respectively because of a hitting average weight of approximately 2.4 pounds (~1,09 kg) red-tailed hawk. As a result of bird strike incident, helicopter lost power of both engines, and main rotor RPM in order. It was followed by loss of control and rapid descent of helicopter. The helicopter crashed into marshy terrain with 9 people in 17 seconds just after the bird strike. Two pilots and six of seven passengers died at the time of accident. One of the passengers was seriously injured. According to investigation of the NTSB, collision with red-tailed hawk was the reason of accident. After collision of red-tailed hawk, it fractured the cast acrylic windshield and went to engine power control levers (ECL). It changed engine power to idle position. The pilots were not able to recover from unplanned loss of power [7-12].

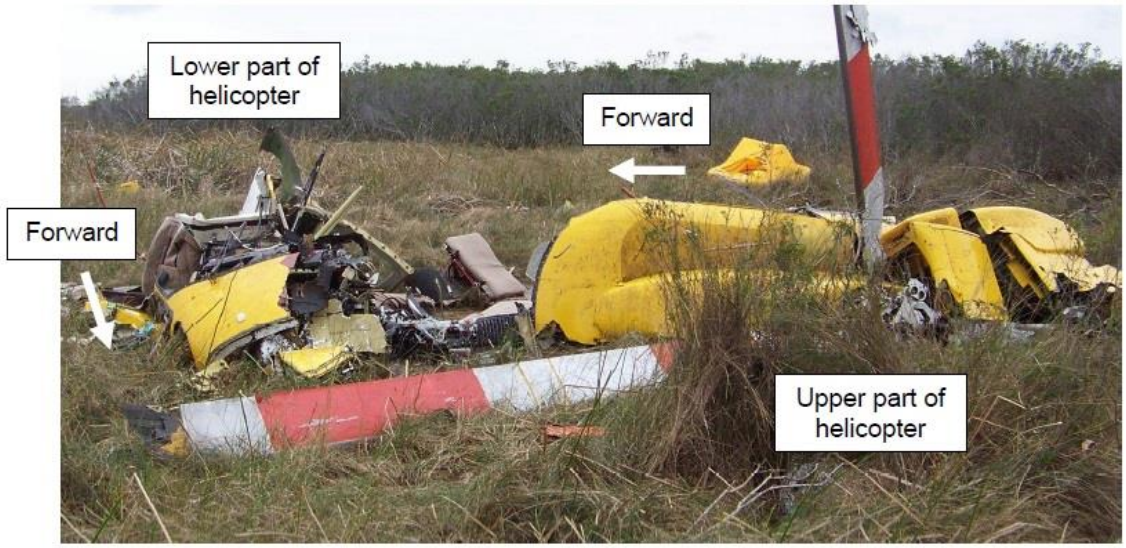

Figure 2-3 Wreckage of Sikorsky S-76A++ after Bird Strike [13]

Figure 2-4 Reconstruction of the Sikorsky S-76A++ Canopy and Windshield [13]

Figure 2-5 Bird Strike on Sikorsky S-76A++ with the STC Acrylic Windshield [13]

3 AERODYNAMIC FORCES

The surface of an object is exerted by aerodynamic forces in airflow because of pressure distribution and shear stress distribution on surface. Pressure is locally perpendicular to the surface and shear stress is locally parallel to surface. The resultant aerodynamic force applied on body is the sum of the integral of the pressure distribution over the exposed surface and the integral of the shear stress distribution over the exposed surface. In another word, the resultant aerodynamic force $\vec{F}_R$, is the sum of the pressure force $\vec{F}_P$, and the shear force $\vec{F}_\tau$, where p, τ, $\vec{n}$, $\vec{k}$, dS are local pressure, local shear stress, unit vector normal to surface, unit vector parallel to surface, and segment of surface, respectively. The specific point on body where $\vec{F}_R$ acts is called center of pressure. On center of pressure point, moment created by aerodynamic forces is equal to zero.

$$\vec{F}_P = -\iint_S p\vec{n}\, dS \tag{3.1}$$

$$\vec{F}_\tau = \iint_S \tau\vec{k}\, dS \tag{3.2}$$

$$\vec{F}_R = \vec{F}_P + \vec{F}_\tau \tag{3.3}$$

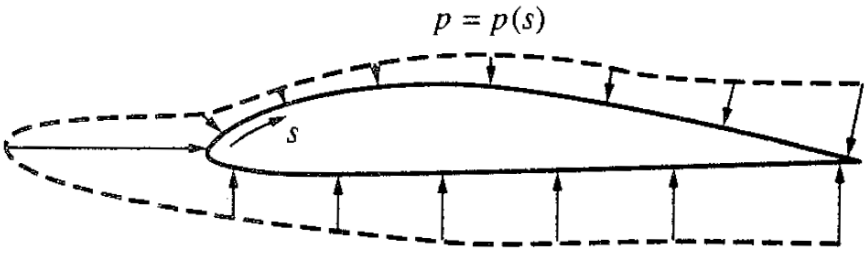

Figure 3-1 Pressure Distribution (Schematic only; distorted for clarity) [14]

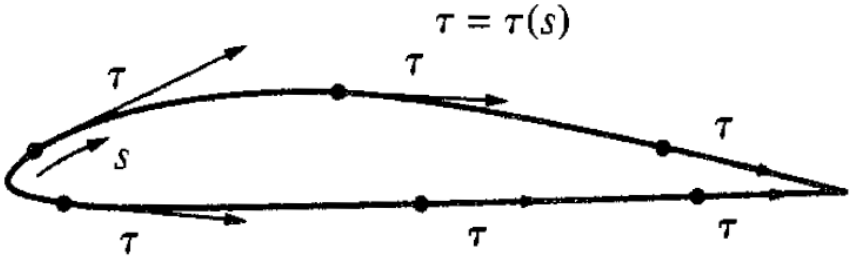

Figure 3-2 Shear Stress Distribution [14]

Free stream velocity also called relative velocity is symbolled $\vec{V}_\infty$. Component of $\vec{F}_R$ parallel to the $\vec{V}_\infty$ is called drag force, $\vec{F}_D$. Similarly, component of $\vec{F}_R$ perpendicular to the $\vec{V}_\infty$ is called lift force, $\vec{F}_L$. In another word, Direction of lift force is always perpendicular to flow direction and direction of drag force is always parallel to flow direction.

4 ROTARY-WING AIRCRAFT

Rotary wing aircrafts are heavier-than-air aircrafts. Helicopter, autogiro and gyrodyne are some of the rotary-wing aircraft types. In this study helicopter is going to be used as rotary-wing aircraft.

Four main forces which are lift, drag, thrust, and weight act on aircraft. Weight force is generated by mass and gravity. A big part of aerodynamic forces is generated by rotor system and fuselage as they move in air. Helicopters provide both lift and thrust forces from rotor system. Drag force occurs because of movement of aircraft in air. Therefore, thrust force is a necessary force against to drag force. For the level flight of helicopter, thrust force is equal to drag force, and lift force is equal to weight.

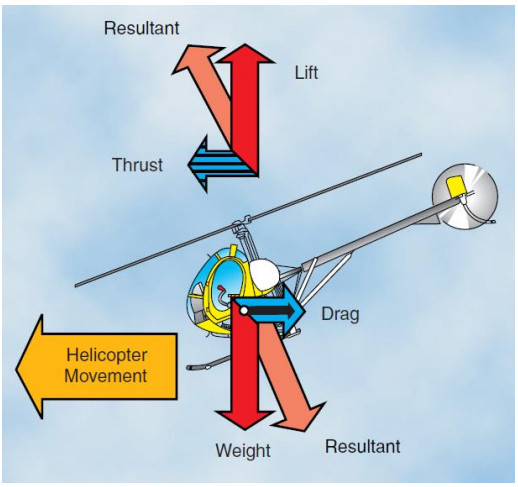

Figure 4-1 Free Body Diagram of Helicopter in Forward Flight

Attitude (pitch angle) of helicopter is required to be changed using cyclic control by pilot to change speed of helicopter because of the flight characteristics of helicopters. Dynamic pressure is directly proportional to square of free stream velocity. Therefore, aerodynamic forces are directly proportional to square of free stream velocity. Equation related to drag force are given below.

$$q_\infty = \frac{1}{2}\rho_{air}V_\infty^2 \tag{4.1}$$

$$F_D = q_\infty C_D A \tag{4.2}$$

$$F_D = \frac{1}{2}\rho_{air} V_\infty^2 C_D A \tag{4.3}$$

Flight at higher airspeed requires higher thrust force. If weight is assumed constant, then required lift force is constant in level flight. Therefore, resultant aerodynamic force ($\vec{F}_R$) produced by rotor system need to be increased using collective control and diverted to direction of motion using cyclic control for higher airspeed by changing pitch angle of helicopter while maintaining required lift force.

4.1 Impact Scenario

Statistical data shows that the bird strike incidents of helicopters usually end up with striking of bird to windshield. Higher forward speed increases impact pressure and impact forces on windshield.

Figure 4-2 Helicopter on Ground

Pitch angle is the one of the parameters affecting magnitude of airspeed of helicopter. It is required to decrease pitch angle (nose down motion) of helicopter while applying more power for higher forward speeds.

Figure 4-3 Helicopter in Forward Flight

While helicopters fly at higher airspeed, birds strike not only with higher speed but also with steeper angle. Therefore, compared to fixed wing aircrafts, impact force and impact pressure increase much more with increase of airspeed. In this thesis work, bird strike analyses were done with differend forward speeds, and pitch angles of helicopter to investigate effect of forward speed and pitch angle.

Figure 4-4 Helicopter just Before Bird Strike

After the airspeed and required pitch angle of helicopter in level flight were estimated, impact angles for different airspeeds of helicopter were defined. Helicopter pitch angles and impact angles for forward speeds were shown in Table 5. Positive and negative pitch angles define pitch up (nose up) and pitch down (nose down) of helicopter, respectively. Impact angle defines an angle between windshield surface and strike direction.

Table 5 Impact Scenario

Airspeed of Helicopter [knots]	Pitch Angle of Helicopter [Degrees]	Impact Angle [Degrees]
80	2°	27°
85	1°	28°
102	-1°	30°
110	-2°	31°
120	-3°	32°

5 EQUATION OF STATE

Equation of state is a relationship of state variables of a material such as fluids, mixtures of fluids, solids, and the interior of stars. It describes the behavior and state of material under a given set of physical conditions. EOS usually consist of pressure, volume, temperature, or internal energy. Linear EOS, Polynomial EOS, Tabulated EOS and Gruneisen EOS are types of equation of state used in bird modeling. In bird strike problems, it is used to describe the pressure-density relationship in the bird medium.

Linear EOS is the simplest EOS. In linear EOS, pressure (P) is function of the bulk modulus (K) of material, current density (ρ) of medium and reference density (ρ_0) of medium.

$$P = K\left(\frac{\rho}{\rho_0} - 1\right) \tag{5.1}$$

In polynomial EOS, pressure consists of internal energy, change in energy during impact, and coefficients. The most used polynomial EOS for bird strike problem is polynomial of degree three [15] as shown in Equation (5.2). It corresponds to a hydrodynamic, isotropic, and non-viscous constitutive law.

$$P = C_0 + C_1\mu + C_2\mu^2 + C_3\mu^3 + (C_4 + C_5\mu + C_6\mu^2)E_i \tag{5.2}$$

where E_i is internal energy and change in density during impact is given in Equation 5.3.

$$\mu = \frac{\rho}{\rho_0} - 1 \tag{5.3}$$

From C_0 to C_6 are function of the speed of sound in the medium (c_0), reference density of the medium (ρ_0) and experimental constant (k). If initial equilibrium pressure is known and negligible, the values of C_0 to C_6 are shown in Equations (5.4 - 5.8).

$$C_1 = \rho_0 {c_0}^2 \tag{5.4}$$

$$C_3 = (k-1)(3k-1)C_1 \tag{5.5}$$

$$C_0 = C_4 = C_5 = C_6 = 0 \tag{5.6}$$

for compression $(\mu > 0)$;

$$C_2 = (2k - 1)C_1 \tag{5.7}$$

for tension $(\mu < 0)$;

$$C_2 = 0 \tag{5.8}$$

Experimental constant k for polynomial EOS of water equals to 2 [16].

Gruneisen EOS is used to describe a relationship between the propagation velocity of a shock (v_s) and velocity of particle (v_p). The v_s-v_p curve is given in Equation (5.9).

$$v_s = C_0 + S_1 v_p + S_2 \left(\frac{v_p}{v_s}\right) v_p + S_3 \left(\frac{v_p}{v_s}\right)^2 v_p \tag{5.9}$$

where S1, S2 and S3 are the coefficients of the slope of the v_s-v_p curve.

Gruneisen EOS with cubic shock velocity-particle velocity defines pressure for materials for compression $(\mu > 0)$ as

$$P = \frac{\rho_0 C^2 \mu \left[1 + \left(1 - \frac{\gamma_0}{2}\right)\mu - \frac{a_{Corr}}{2}\mu^2\right]}{\left[1 - (S_1 - 1)\mu - S_2 \frac{\mu^2}{\mu + 1} - S_3 \frac{\mu^3}{\mu + 1}\right]^2} + (\gamma_0 + a_{Corr}\mu)E \tag{5.10}$$

and for tension $(\mu < 0)$ as

$$P = \rho_0 C^2 \mu + (\gamma_0 + a_{Corr}\mu)E \tag{5.11}$$

where C is the intercept of the v_s-v_p curve given in Equation (5.9); γ_0 is the Gruneisen coefficient; a_{Corr} is the first order correction; ρ_0 is reference density of the medium; and μ change in density given as Equation (5.3). In this thesis work, Gruneisen EOS parameters for water are $C = 1480$, $S_1 = 1.92$, $S_2 = 0$, $S_3 = 0$, and $\gamma_0 = 0.1$ [17, 18].

6 EXPLICIT FINITE ELEMENT METHOD

Selection of an appropriate method is important step for reality of bird strike simulation and accuracy of analysis result. Bird strike problems are high speed dynamics problems, and solution of bird strike problems requires small time steps to obtain more accurate results. Therefore, explicit finite element methods are more suitable for bird strike problems. Each method has both advantages and disadvantages not only in general but also in problem specific. Bird strike problems are the fluid structure interaction problems, and excessive material deformation is observed as a result. Therefore, method should be selected according to requirements of problem. In this section, the methods required to be taken for modeling a bird strike problem were presented in detail. Lagrangian, ALE and SPH methods were chosen to be compared.

6.1 Lagrangian Method

In the Lagrangian method, individual nodes of mesh are attached to material particle. Nodes represent particles of material. Nodes follow material deformation and mesh deforms with material. Therefore, traceability of material deformation can be done simply, and Lagrangian method makes it easy to track small deformations of free surfaces and interfaces between different materials.

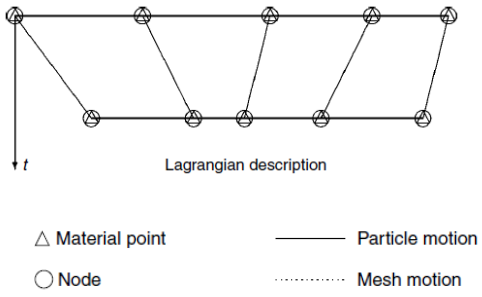

Figure 6-1 Lagrangian Method Description [19]

Lagrangian method is usually used in solid mechanics. In a bird strike analysis, bird model has fluid material behavior, and excessive deformation is observed under high-speed impact condition. Excessive deformation of material increases computation time. Lagrangian method requires time step estimation and several techniques for accurate result in excessive deformation problems. In literature, it was stated about time step that “time step of analysis

must be smaller than the time required for a shock wave to travel through the smallest dimension of the element" [18].

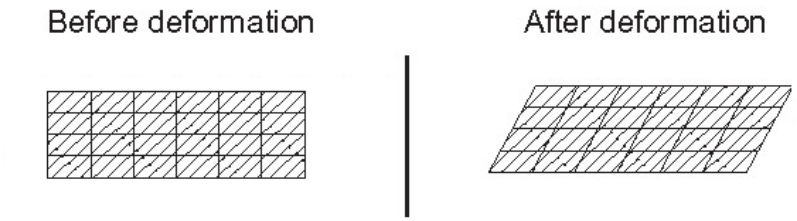

Figure 6-2 Undeformed and Deformed Element in Lagrangian Method [18]

For excessive deformation condition, Lagrangian method requires application of some techniques which are element removement, local mass scale, simplification of small strain, adaptive remeshing, and smaller time step techniques. However, application of techniques increases the analysis time. Element removing is one of the techniques used to avoid excessive deformation conditions of element. The element whose effective strain are higher than predefined critical failure strain of material is removed to avoid numerical instabilities. Each element has mass and energy because of conservation of mass and energy. Removing lots of elements cause unrealistic results, such as lower contact force, fluctuation in pressure and fluctuation in contact force on target surface. In the bird strike analysis, target surface is in contact with highly deformed elements. Therefore, element removing technique could cause incorrect analysis results. Another technique used for excessive deformation conditions is adaptive remeshing technique. In this technique, remeshing is applied to the areas where distorted elements are located on it. Disadvantages of adaptive remeshing technique is increase of analysis time and it is not practical for complex geometries. Also, remeshing operation requires experience of analysis or advanced remapping algorithms because of the complexity of operation. In small strain simplification technique, distorted elements are neglected by not updating Jacobean matrix at each time step. Local mass scaling is another technique used to avoid inaccuracy of result caused by distorted element. In this technique, mass of element is used to calculate nodal and non-elementary time step. Masses of distorted elements which are local masses are increased and time step is kept constant. Disadvantage of mass scaling technique is the increase of final mass which is not suitable for bird strike analysis [18].

6.2 Eulerian Method

Eulerian method is described in this section for better understanding of ALE method. Nodes of Eulerian mesh are fixed in space where the materials are located. Because of fixed mesh nodes, mesh is not affected by material deformation. In other words, mesh nodes do not follow material deformation. Material deformation occurs with transfer of material through cells of mesh.

Mesh cells of Eulerian method should be defined comprehensively to cover materials all along the analysis. At the initial condition, some of the mesh cells contain material and rest of the mesh cells contains space where probable locations of material during deformation.

Fixed mesh of Eulerian method provides advantages to various problems according to problem type. In the fluid dynamics problems, boundary conditions are known if analysis is carried out using fluid restricted by fix objects for example wall and pipe. Therefore, probable location of deforming fluid material during solution is known. Mesh boundary can easily be defined in such problems.

However, high deformation of material is observed in bird strike problems. Therefore, fixed Eulerian mesh takes disadvantage. Because of high deformation of fluid, mesh should be defined to large area. Wider mesh domain increases computation time of analysis. Therefore, Eulerian method is not efficient, and it is expensive for bird strike problems. Difficult tracking of material history is the other disadvantage of Eulerian method. Stress and strain tensors should be transferred between cells for improve material history tracking.

Truncation error of the Taylor series approximation causes numerical dissipation and numerical dispersion in low order differencing scheme-based Eulerian solvers. High order differencing scheme minimizes numerical error. Hence, high order differencing scheme-based Eulerian solvers have less numerical error. On the other hand, use of high order differencing scheme-based Eulerian solvers increase computation time.

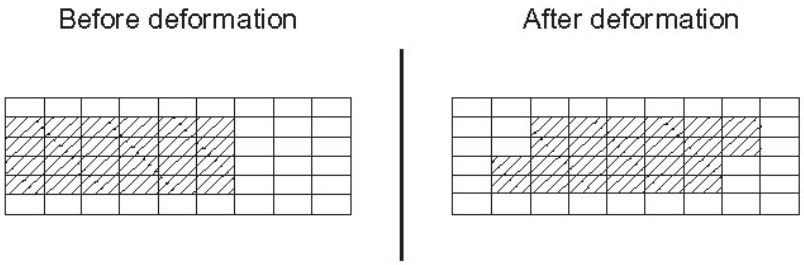

Figure 6-3 Undeformed and Deformed Element in Eulerian Method [18]

6.3 Arbitrary Lagrangian – Eulerian Method

ALE method is a combination of Lagrangian method and Eulerian method. Purpose of ALE method is to combine the advantages of both Lagrangian method and Eulerian method while minimizing disadvantages of them.

In this thesis work LS-DYNA was used for explicit problem because it gives opportunity to work with ALE domains which include two different types of fluid in mesh domain, such as bird material and air. Fluid material was modelled in Eulerian mesh, and impact surface was modelled as Lagrangian mesh. ALE coupling algorithm provides the bird material, which is in Eulerian mesh, an ability to apply load onto Lagrangian surface.

Location of fluid material is evaluated by comparing it with position of Eulerian mesh for each time step. Time step of ALE method consists of three phases which are called Lagrangian phase, smoothing phase, and Eulerian phase, respectively.

The Lagrangian phase is also known as material phase. Material deforms in the Lagrangian phase just like a Lagrangian method. Fluid material which is in material configuration deforms to spatial configuration by neglecting convective effects. Beside of Lagrangian solution, undesirable high distortion of the spatial discretization may be observed on nodal and quadrature points.

In the smoothing phase high distortion of the spatial discretization is minimized by remeshing. New relocated mesh is developed by mesh smoothing algorithm. The smoothing phase is used between Lagrangian phase and Eulerian phase to obtain the mesh velocity.

The last phase is the Eulerian phase which is also known as convection phase. In the convection phase, convective terms are considered with data transferring of solution which was obtained in Lagrangian phase.

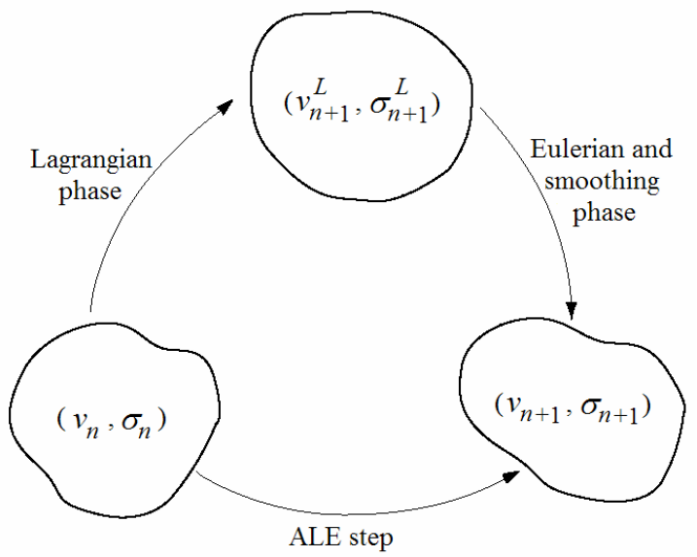

Figure 6-4 Phases of ALE Time Step [20]

ALE method has some advantages, disadvantages, and similarities compared to Eulerian method and Lagrangian method. Like Eulerian method, fluid particles are able to move between cells. Also, similar to Lagrangian method, mesh follows the material deformation. Different than the Eulerian method and Lagrangian method, transportation of fluid particles between mesh cells and deformation of background mesh in accordance with the deformation of the fluid material occur at the same time.

In ALE method, Element distortion occurs less than does in Lagrangian method. In case of observing the mesh distortions, ALE method overcomes with material distortions better than Lagrangian method does, with the help of smoothing phase. Pressure profile result of ALE method is smoother than pressure profile result of Lagrangian method. [21]. Negative element volume and tangling may be observed rarely. Compared to Eulerian method, ALE method has smaller grid structure size and more accurate contact modeling.

ALE background mesh moves with average velocity of fluid particles and deforms in accordance with the deformation of the fluid. One of the disadvantages of ALE method is that increase of mesh size negatively effects the accuracy of results. The other two

disadvantages are element distortion causing negative volume and filtration of some portion of dynamic loading in Lagrangian and Eulerian interaction [18]. Disadvantages can be minimized using finer mesh.

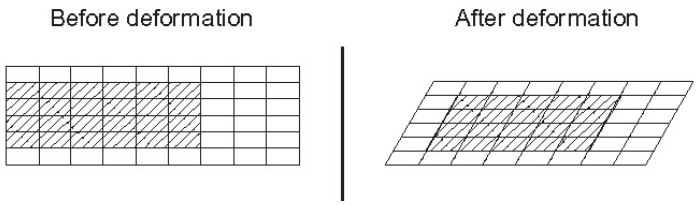

Figure 6-5 Undeformed and Deformed Element in ALE Method [18]

6.4 Smoothed Particle Hydrodynamics

Smoothed Particle Hydrodynamics (SPH) method was developed in the late 1970s by Monaghan for astrophysics problems [22]. Main difference between SPH method and the other methods used in this thesis work is methodology of discretization of material model. Instead of mesh, fluid material is modelled as separate moving particles as shown in Figure 6-6. Also, it is not required to represent void space using additional elements. Therefore, issues associated with element distortions are not observed, and computational time decreases.

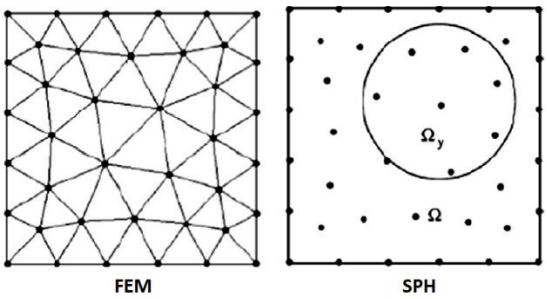

Figure 6-6 Discretization of FEM and SPH [22]

In SPH method, fluid particles are in interact with neighbor particles, and particles represent an interpolation point where all the properties of fluid are known, such as volume, mass, velocity, pressure. Particle interaction is computed by using interpolation. Kernel function is used as interpolation function for interpolation points.

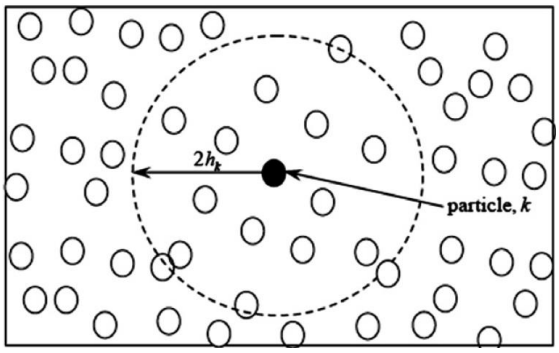

Figure 6-7 Domain of the Sphere in the SPH Method [22]

Each particle has its own smoothing length. Main purpose of smoothing length is to keep optimum number of particles in interaction with defined particle for continuum. Interaction occurs in sphere shaped support domain whose radius is twice of smoothing length as shown in Figure 6-7. Therefore, smoothing length of particle is not constant value, and it changes within time. Variable smoothing length avoids material compression and material expansion. Smoothing length increases while particles diverge from each other. Conversely, smoothing length decreases while particles come closer to each other. Material compression causes longer solution time of problem and material expansion causes numerical fracture.

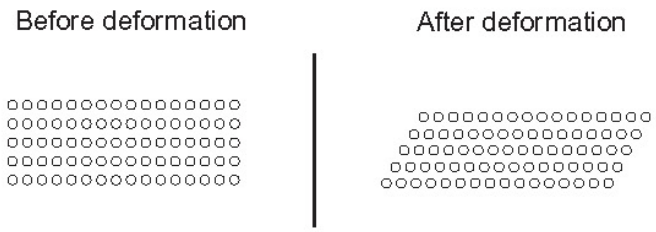

Figure 6-8 Undeformed and Deformed Element in SPH Method [18]

6.5 Comparison of Methods

Each method has advantages and disadvantages according to problem type. In the bird strike problems, excessive deformation of bird model is observed after impact. In this section, advantages and disadvantages of Lagrangian method, Eulerian method, ALE method, and SPH method are compared.

Advantages of Lagrangian method are listed below.

- Easy tracking of the both the small deformations and time-history of material particles because nodes of mesh are attached to material particle and mesh deforms with material.
- Ease of defining boundary conditions because boundary nodes are defined on material surface.
- Simpler modeling
- Lower computational cost

Disadvantages of Lagrangian method for material under excessive deformation are listed below.

- Requirement of smaller time steps and new time step estimation.
- Requirement of additional technique (element removement, local mass-scaling, small-strain simplifications, adaptive remeshing or smaller time step which are increases solution time) for accurate result.

Advantages of Eulerian method are listed below.

- No mesh distortion is observed.
- Larger time steps can be used.

Disadvantages of Eulerian method for material under excessive deformation are listed below.

- Requirement of defining wider mesh domain which increases computational time.
- Difficulty of material history tracking. It is required to transfer stress and strain tensors between cells for improve material history tracking.
- Requirement of high order differencing scheme-based Eulerian solver which is increasing solution time, to overcome numerical dispersion and numerical dissipation.

ALE method has advantages of both Lagrangian method and Eulerian method. Therefore, advantages are compared to Lagrangian method and Eulerian method, and listed below.

- ALE method overcomes element distortions better with the help of smoothing phase compared to Lagrangian method.

- ALE method has smoother pressure profile result compared to Lagrangian method.
- Contact modeling of ALE method is more accurate compared to the Eulerian method [18].
- Compared to Eulerian method, ALE method captures material boundary better because mesh deforms with material.

Disadvantages of ALE method for material under excessive deformation are listed below.

- Mesh size increases with excessive deformation of material and increase of mesh size effects the accuracy of results negatively.
- Negative volume could be observed because of element distortion.

Advantages of SPH method are listed below.

- Particles are used instead of mesh.
- Requires less element compared to Eulerian method.
- Issues associated with element distortions are not observed.
- Useful for high-speed fluid structure interaction problems.
- Simple tracking the deformations of material particles.

Disadvantages of SPH method for material under excessive deformation are listed below.

- Accuracy decreases at sharp surfaces.
- Parallel computing is required.
- Requires higher CPU power. Parallel processing is used on solver computer which is equipped with multi core processors. Therefore, computational cost is higher.

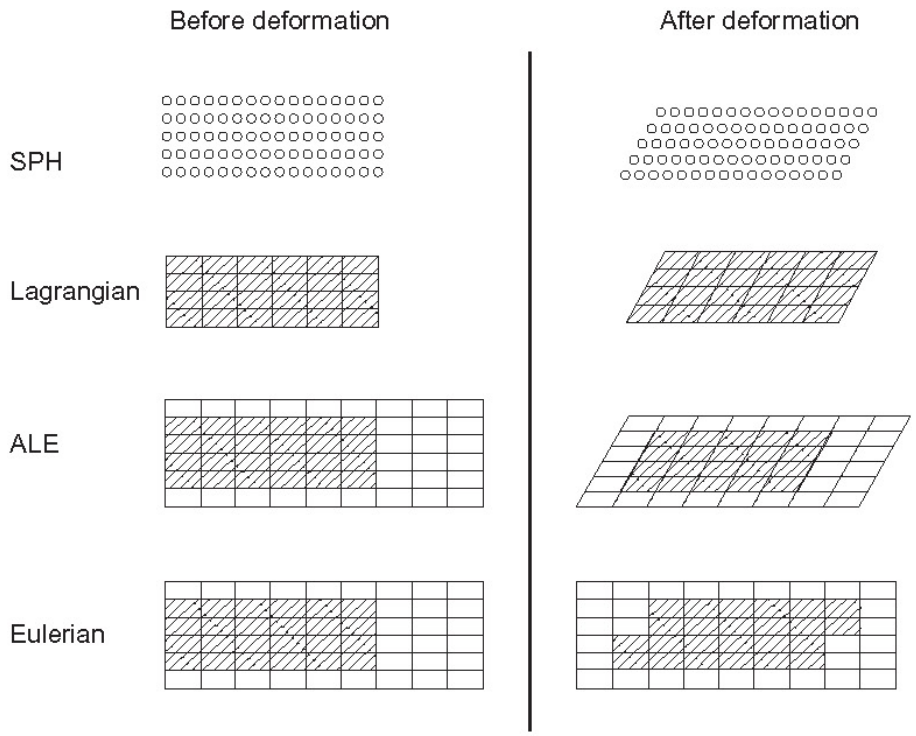

Figure 6-9 Element Deformation (SPH, Lagrangian, ALE and Eulerian) [18]

7 MODELING OF ANALYSIS SETUP

7.1 Physical Properties of Bird Model

Bird strike requirements are defined at European Aviation Safety Agency (EASA) publication of easy access rules for large rotorcraft certification specifications “CS 29.631 Birdstrike” and Federal Aviation Administration - Department of Transportation “14 CFR § 29.631 - Bird strike”. Bird strike requirement for rotorcrafts are stated as “The rotorcraft must be designed to assure capability of continued safe flight and landing (for Category A) or safe landing (for Category B) after impact with a 1 kg bird, when the velocity of the rotorcraft (relative to the bird along the flight path of the rotorcraft) is equal to V_{NE} or V_H (whichever is the lesser) at altitudes up to 8000 feet” [1, 2]. Category A helicopters are defined as multi-engined helicopters that provide continued safe flight or rejected takeoff in the event of engine failure. Category B helicopters are defined as single-engined helicopters or multi-engined helicopters that does not provide Category A requirements. They do not provide continued safe flight in the event of engine failure, landing is required.

Geometric shape of a bird model affects the analysis results. Commonly used three bird geometries in bird strike analysis and tests are cylindrical model, cylindrical model with hemispherical ends, and ellipsoidal model. In this thesis all of them were used for analysis and each of them has specific identifier name. Cylindrical bird shape was called Bird Shape 1. Cylindrical bird shape with hemispherical ends was called Bird Shape 2. Ellipsoidal bird shape was called Bird Shape 3.

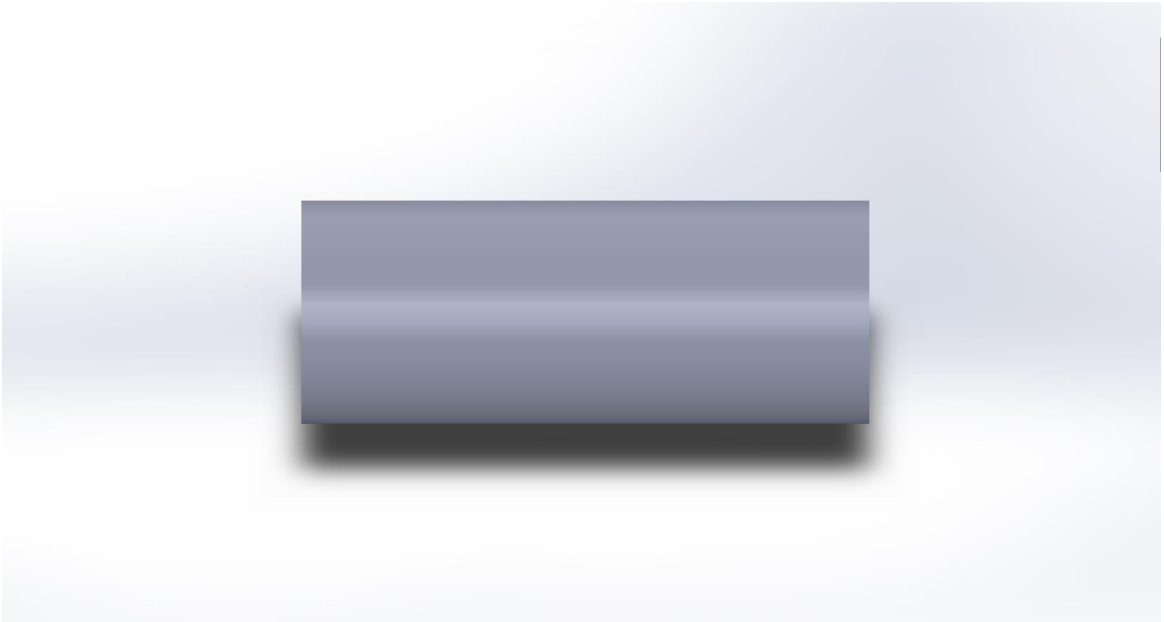

Figure 7-1 Bird Shape 1 - View 1

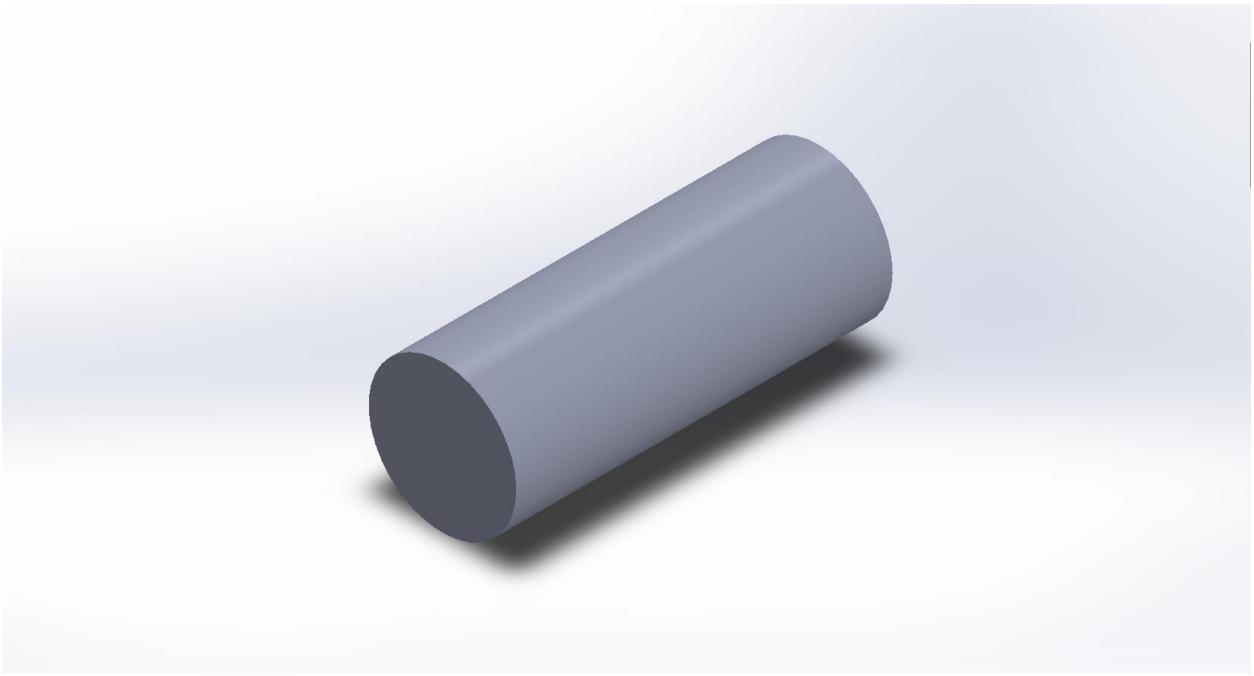

Figure 7-2 Bird Shape 1 - View 2

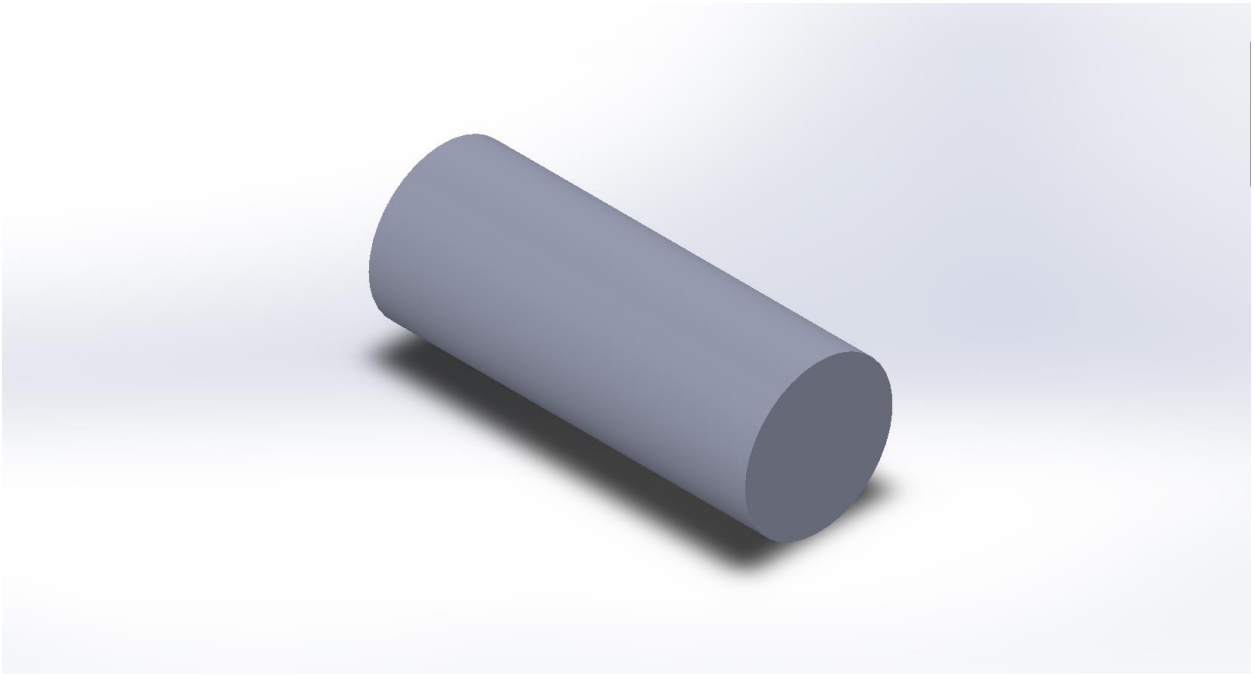

Figure 7-3 Bird Shape 1 – View 3

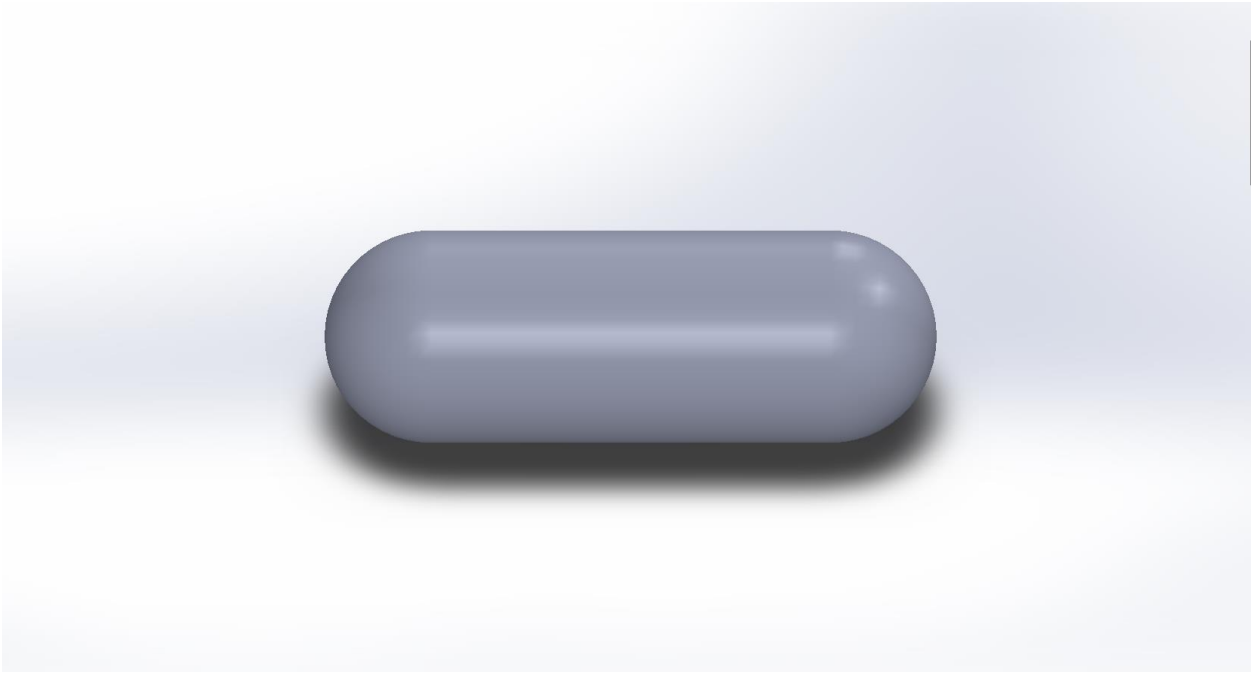

Figure 7-4 Bird Shape 2 – View 1

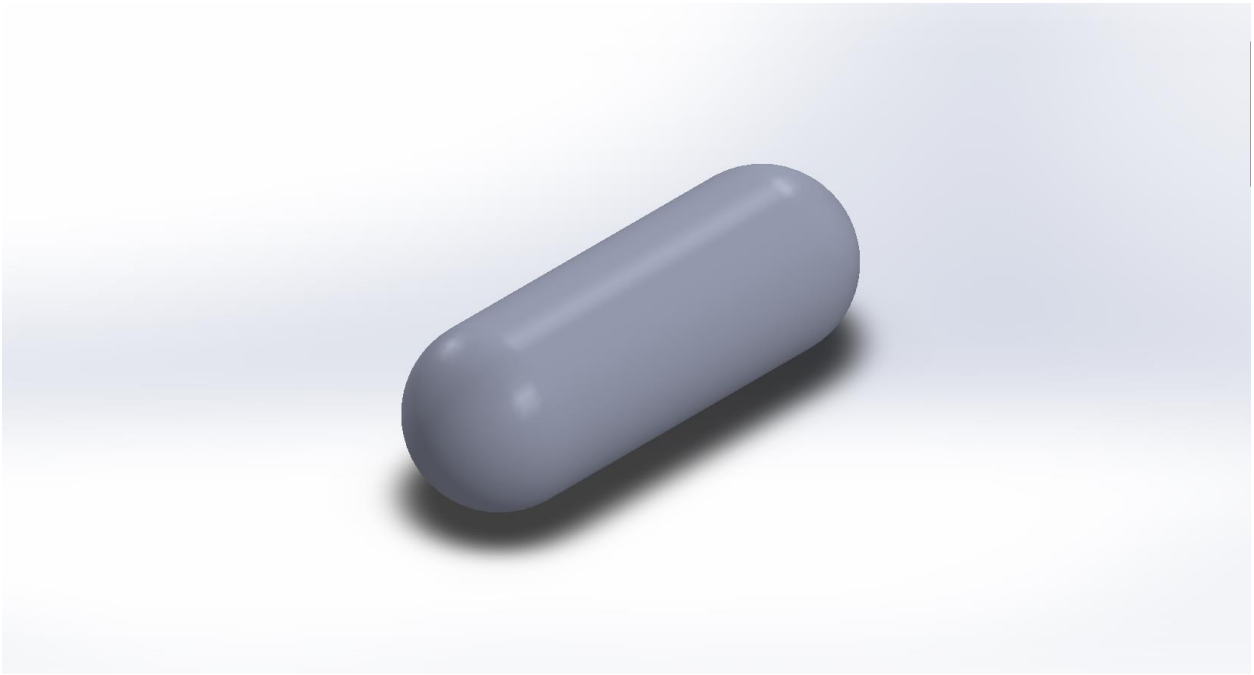

Figure 7-5 Bird Shape 2 – View 2

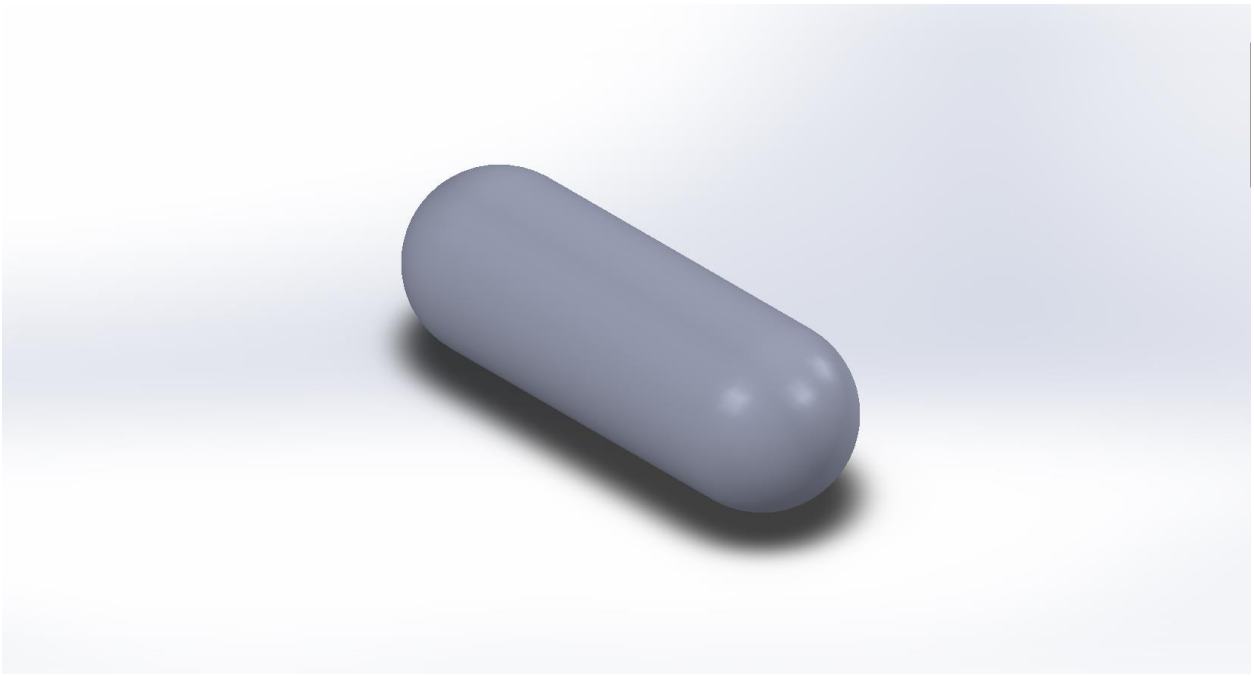

Figure 7-6 Bird Shape 2 – View 3

Figure 7-7 Bird Shape 3 – View 1

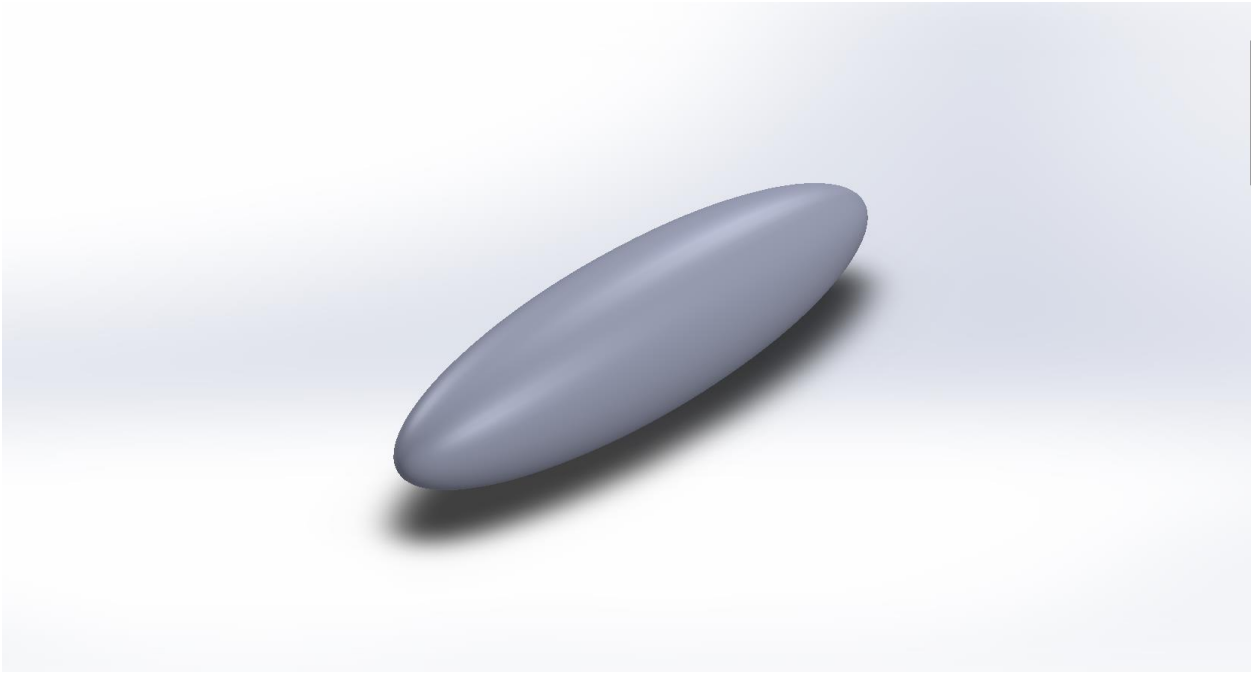

Figure 7-8 Bird Shape 3 – View 2

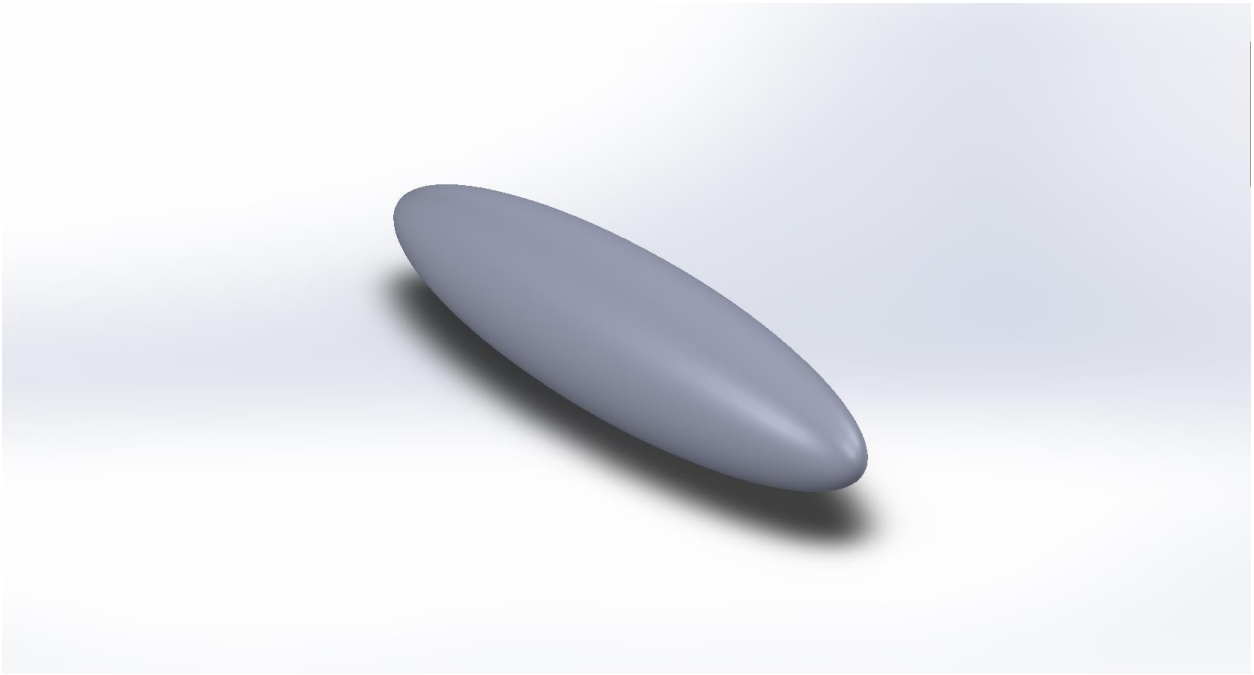

Figure 7-9 Bird Shape 3 – View 3

Material properties of bird model also affect the analysis result. Density of a bird used for bird strike tests could be between $900\ kg/m^3$ and $1060\ kg/m^3$ [23]. Database of over 100 species of birds were used to assess relationship between mass and density for plucked birds. Following empirical formulas derived in literature were used to obtain physical properties of bird models [24, 25]. For the following eleven equations, units of density, mass, and diameter are kg/m^3, kg, and meter (m), respectively. Density and cross section diameter of bird model are the function of mass.

$$\rho_{bird} = 959 - 63 \log_{10} m_{bird} \tag{7.1}$$

$$D_{bird} = 0.0804\ (m_{bird})^{0.335} \tag{7.2}$$

Following three equations were used to determine volume, density, and length of the cylindrical shaped bird geometry.

$$V_{bird} = \pi \frac{D_{bird}^2}{4} L_{bird} \tag{7.3}$$

$$\rho_{bird} = \frac{m_{bird}}{V_{bird}} = \frac{m_{bird}}{\pi \frac{D_{bird}^2}{4} L_{bird}} \tag{7.4}$$

$$L_{bird} = \frac{4m_{bird}}{\pi \rho_{bird} D_{bird}^2} \tag{7.5}$$

Following three equations were used to determine volume, density, and length of the cylindrical shaped bird geometry with hemispherical ends.

$$V_{bird} = \frac{4}{3}\pi \frac{D_{bird}^3}{8} + \pi \frac{D_{bird}^2}{4} (L_{bird} - D_{bird}) = \pi D_{bird}^2 \left(\frac{D_{bird}}{6} + \frac{(L_{bird} - D_{bird})}{4} \right) \tag{7.6}$$

$$\rho_{bird} = \frac{m_{bird}}{V_{bird}} = \frac{m_{bird}}{\pi D_{bird}^2 \left(\frac{D_{bird}}{6} + \frac{(L_{bird} - D_{bird})}{4} \right)} \quad (7.7)$$

$$L_{bird} = 4 \left(\frac{m_{bird}}{\pi \rho_{bird} D_{bird}^2} - \frac{D_{bird}}{6} \right) + D_{bird} \quad (7.8)$$

Following three equations were used to determine volume, density, and length of the ellipsoidal shaped bird geometry.

$$V_{bird} = \frac{\pi D_{bird}^2 L_{bird}}{6} \quad (7.9)$$

$$\rho_{bird} = \frac{m_{bird}}{V_{bird}} = \frac{6 m_{bird}}{\pi D_{bird}^2 L_{bird}} \quad (7.10)$$

$$L_{bird} = \frac{6 m_{bird}}{\pi D_{bird}^2 \rho_{bird}} \quad (7.11)$$

Material and geometric properties of 0.9 kg and 1 kg bird models of different geometry are calculated for previous analysis.

Table 6 Properties of Bird Models

Bird Model	Mass (kg)	Density (kg/m^3)	Diameter (m)	Volume (m^3)	Length (m)
Cylindrical	0.9	961.883	0.07761	0.000936	0.19777
Cylindrical with Hemispherical Ends					0.22365
Spherical					0.29667
Cylindrical	1	959	0.08040	0.001043	0.20539
Cylindrical with Hemispherical Ends					0.23219
Spherical					0.30809

7.2 Comparison of Methods and Bird Shapes

In this part of the thesis work, combinations of bird models and methods were compared. Lagrangian, SPH and ALE methods were used with three different bird shapes. Bird impactors striking to rigid plate were modelled in LS-DYNA by implementing methods. Combination of three methods and three bird shapes were used for modeling the impactor bird. Analyses were repeated twice using different element numbers for each of Lagrangian and ALE bird models; and twice using different particle numbers of SPH bird models for observing effect of element and particle number. Therefore, eighteen different combinations were analyzed and compared not only with each other but also with literature. At the end of the comparison part, one of the combinations were chosen for following analyses.

Dimensional properties of bird model effects the analysis results. Diameter, density, and dimensions of bird models were calculated as a function of mass. In this section, analyses were done for 0.9 kg bird which is closer to 1 kg bird. According to Table 7, a duck with 0.9 kg mass and 86 m/s relative velocity creates 4.4 tons (≃ 4.31E+04 Newton) impact force on the impact surface. In the Table 7, bird and aircraft assumed to fly in opposite directions, and speed of a bird was defined as 14m/s.

Table 7 Physical Parameters Associated with Bird Strikes on Aircraft [24]

Bird Size	**Small**	**Medium small**	**Small medium**	**Large medium**	**Medium large**	**Large**
Typical Species	Starling	Cattle Egret	Eastern Curlew	Duck	Ibis	Pelican
Weight (kg)	0.085	0.300	0.700	0.900	1.800	5.000
Diameter (m)	0.035	0.054	0.071	0.078	0.098	0.138
Density (gm/cc)	1.026	0.992	0.969	0.962	0.943	0.915
Aircraft Speed 140kts (FAR 23.775 & FAR 33.77)						
Impact Speed (m/s)	58-86	58-86	58-86	58-86	58-86	58-86
Impact Force (tonnes)	0.1-0.9	0.3-2.1	0.4-3.7	0.5-4.4	0.8-6.9	1.6-13.7

Aircraft Speed 250 kts						
Impact Speed (m/s)	115-143	115-143	115-143	115-143	115-143	115-143
Impact Force (tonnes)	0.4-2.5	1.0-5.8	1.7-10.2	2.0-12.0	3.2-19.0	6.0-38.0
Aircraft Speed 350 kts (FAR 25.775 & FAR 25.571)						
Impact Speed (m/s)	166-194	166-194	166-194	166-194	166-194	166-194
Impact Force (tonnes)	0.9-4.6	2.1-10.7	3.6-18.8	4.3-22.3	6.7-35.3	13-70

Strike Models 1 to Strike Model 18 were modelled with 86.0222222 m/s initial velocity of impactor bird striking to fixed rigid square plate. Impact trajectory of impactors were perpendicular to surface. Dimensions and density of 0.9 kg bird models which were listed in Table 6 were compared with reference dimensions. Dimension and density properties of impactor bird shapes of strike models for 0.9 kg mass were listed in Table 8.

Table 8 Properties of 0.9 kg Bird

0.9 kg Bird Model Properties	Reference [24]	Bird Shape 1	Bird Shape 2	Bird Shape 3
Length (m)	-	0.19777	0.22365	0.29667
Diameter (m)	0.078	0.07761		
Density (kg/m3)	0.962	961.883		

Strike Model 1 to Strike Model 18 were the combination of bird shape, analysis method and element/particle numbers.

7.2.1 Analysis with Lagrangian Method

In this section, effects of bird shape and element number were investigated using Lagrangian method and three bird shapes. Results showed that, bird shape affects analyses results more than element number of bird model does. Impact forces of Bird Shape 1 were more than thirteen times of reference value. Bird Shape 2 and Bird Shape 3 created reasonable impact

force results. However, results were smaller than reference value. Results were given in Table 9.

Table 9 Lagrangian Results for Different Particle Numbers and Bird Shapes

	Reference [24]	Bird Shape 1		Bird Shape 2		Bird Shape 3	
Analysis Model	-	Strike Model 1	Strike Model 2	Strike Model 3	Strike Model 4	Strike Model 5	Strike Model 6
Element Number (Bird)	-	5752	22336	6283	23437	6254	24043
Impact Force (N)	4.31E+04	6.11E+05	5.84E+05	3.97E+04	3.48E+04	3.22E+04	3.14E+04
Analysis Result	-	Figure 7-10	Figure 7-11	Figure 7-12	Figure 7-13	Figure 7-14	Figure 7-15

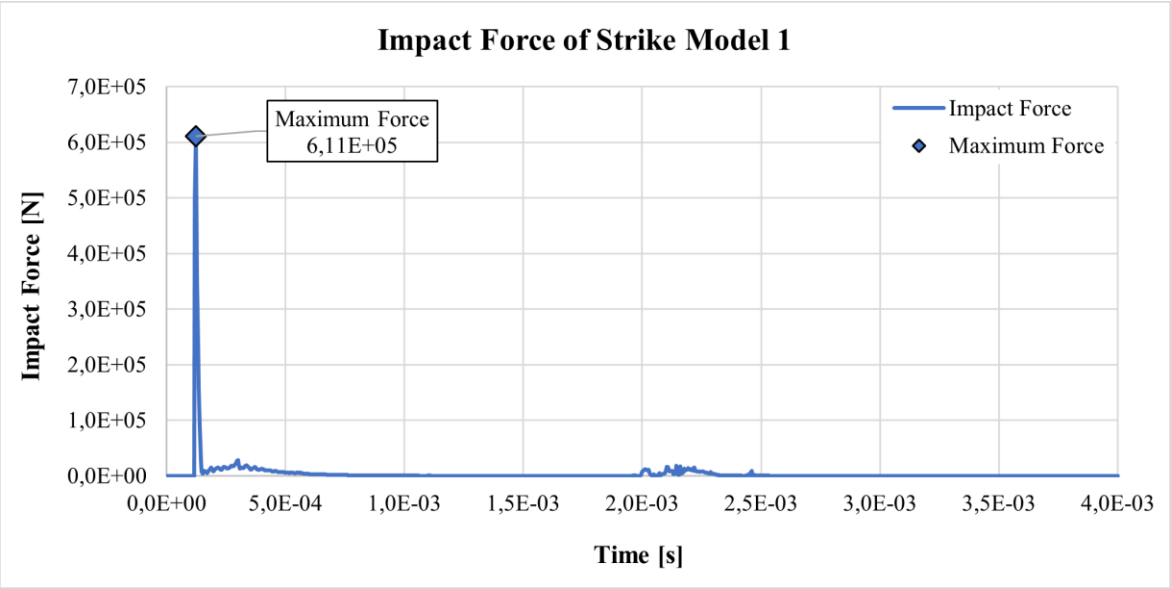

Figure 7-10 Impact Force of Strike Model 1

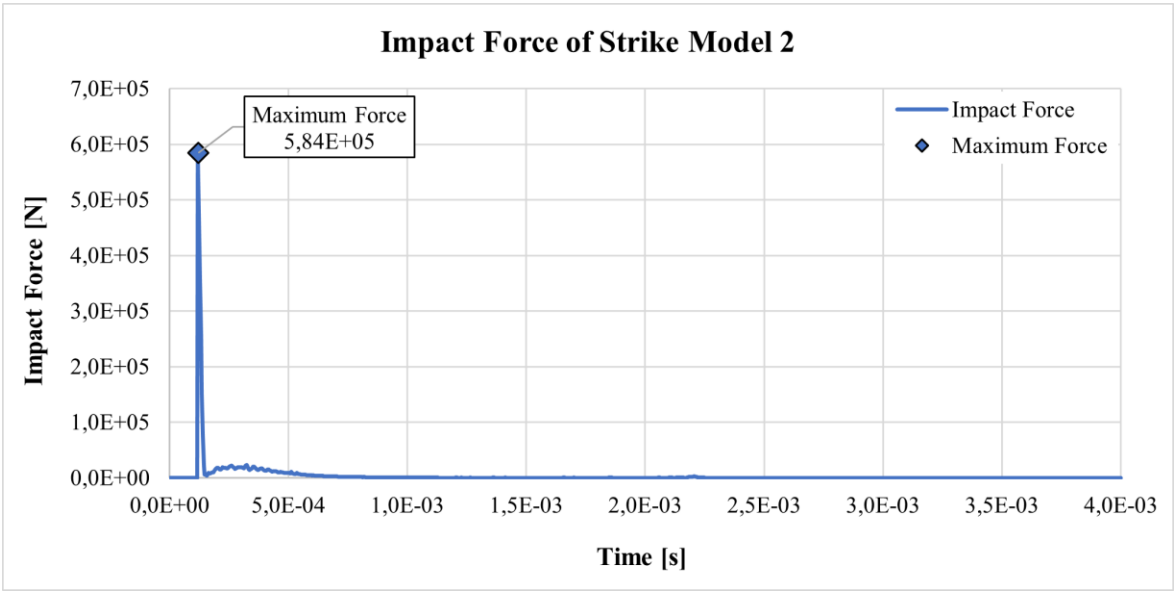

Figure 7-11 Impact Force of Strike Model 2

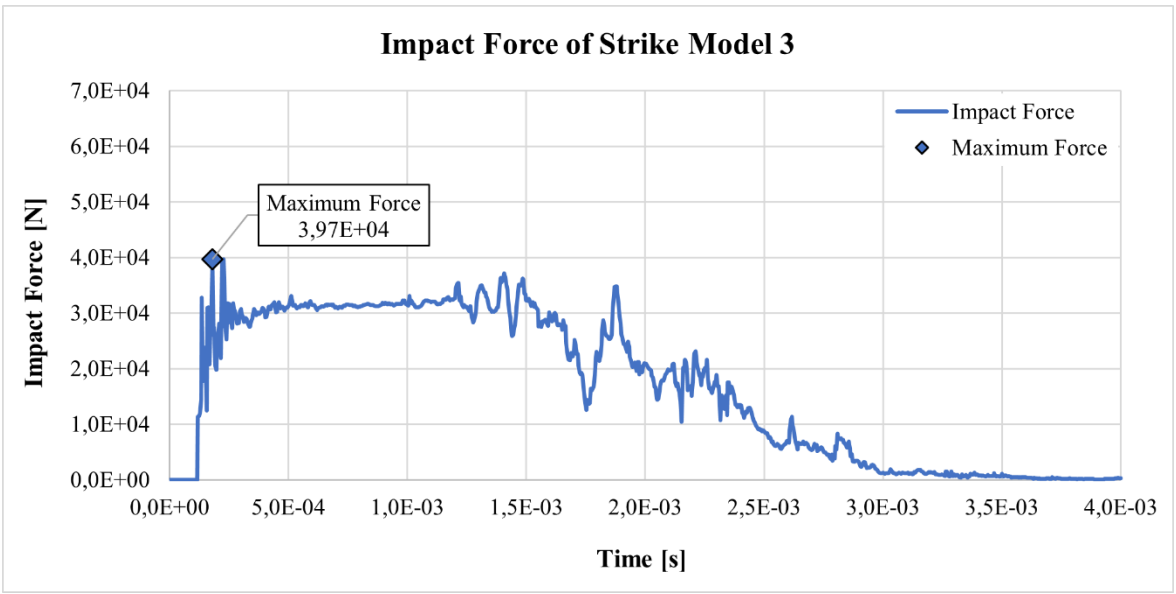

Figure 7-12 Impact Force of Strike Model 3

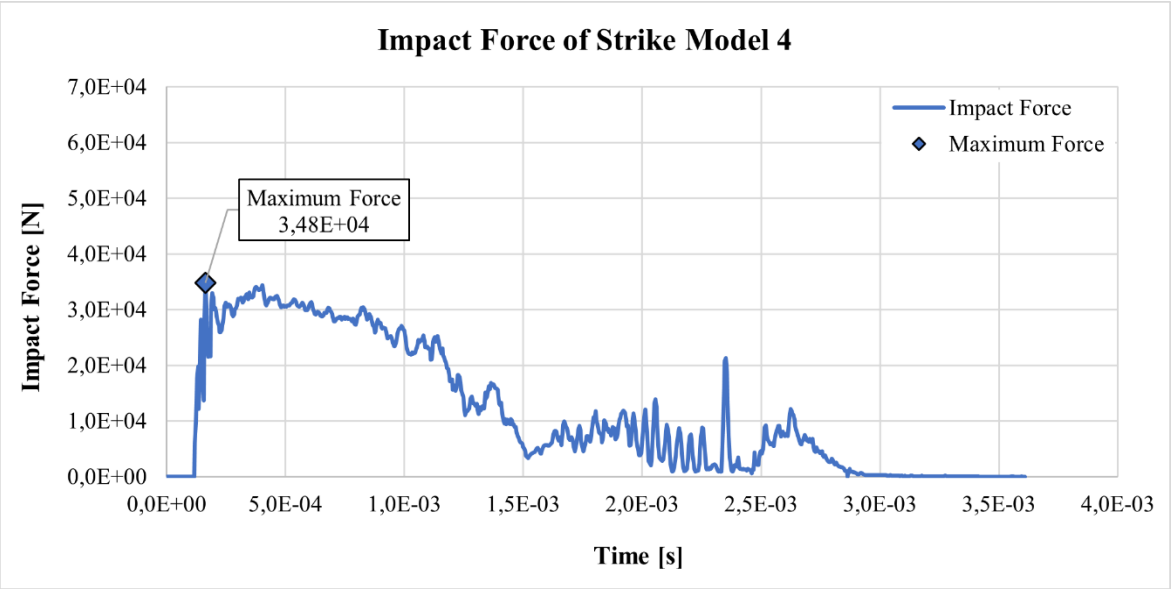

Figure 7-13 Impact Force of Strike Model 4

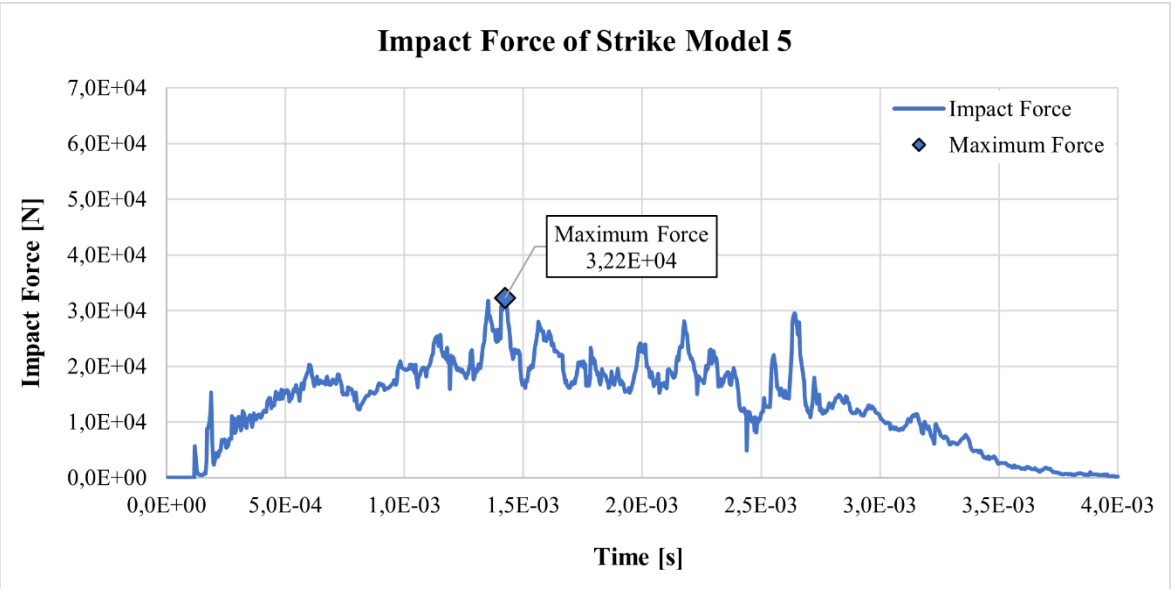

Figure 7-14 Impact Force of Strike Model 5

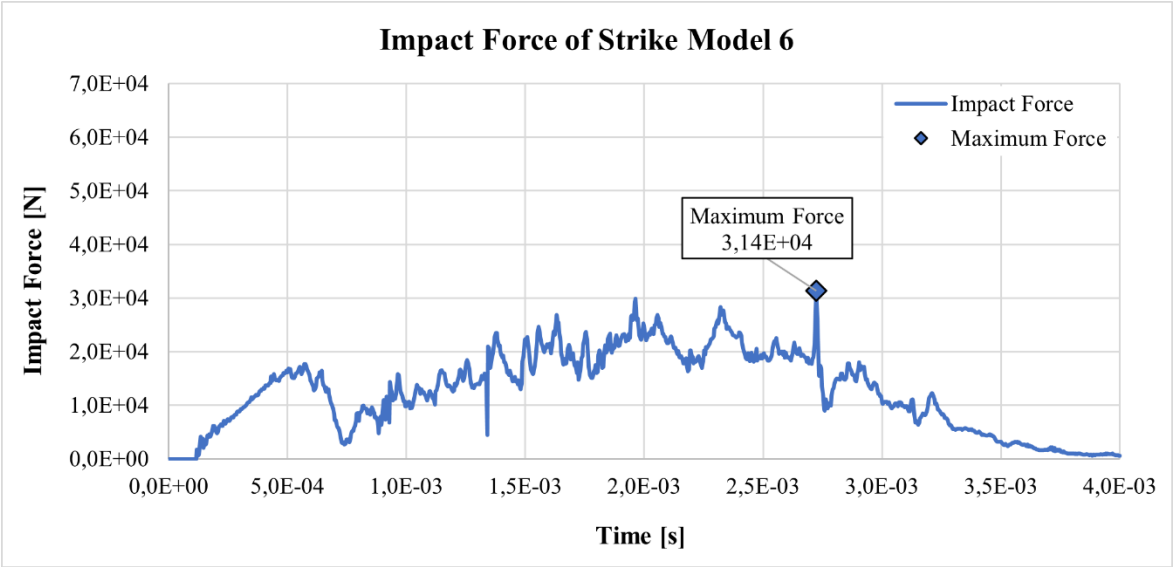

Figure 7-15 Impact Force of Strike Model 6

7.2.2 Analysis with SPH Method

In this section, effect of bird shape and particle number were investigated using SPH method and three bird shapes. Results show that, bird shape affects analyses results more than particle number of bird model does. Impact forces of Bird Shape 1 were more than nine times of reference value, and it is not suitable for analyses. On the other hand, Bird Shape 2 and Bird Shape 3 created reasonable results. However, results of Bird Shape 3 were smaller than reference value. Results of Bird Shape 2 show that bird model with higher particle number gives better results. Results were given in Table 10.

Table 10 SPH Results for Different Particle Number and Bird Shapes

	Reference [24]	Bird Shape 1		Bird Shape 2		Bird Shape 3	
Analysis Model	-	Strike Model 7	Strike Model 8	Strike Model 9	Strike Model 10	Strike Model 11	Strike Model 12
Particles Number (Bird)	-	23151	175288	22945	174630	22855	174819
Impact Force (N)	4.31E+04	3.89E+05	4.01E+05	5.38E+04	4.37E+04	4.07E+04	3.33E+04
Result of Analysis	-	Figure 7-16	Figure 7-17	Figure 7-18	Figure 7-19	Figure 7-20	Figure 7-21

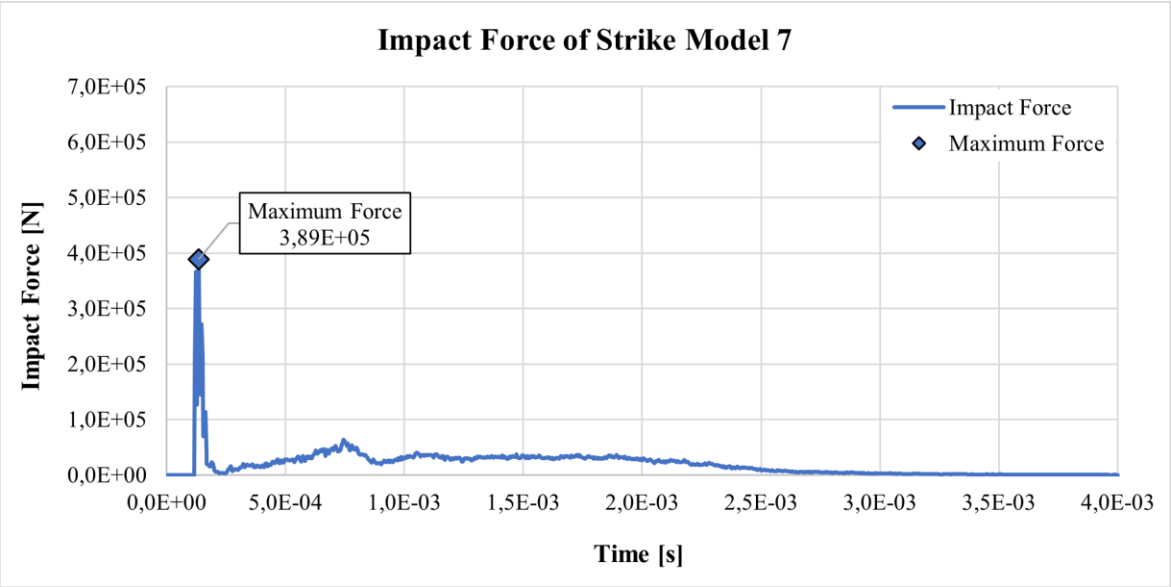

Figure 7-16 Impact Force of Strike Model 7

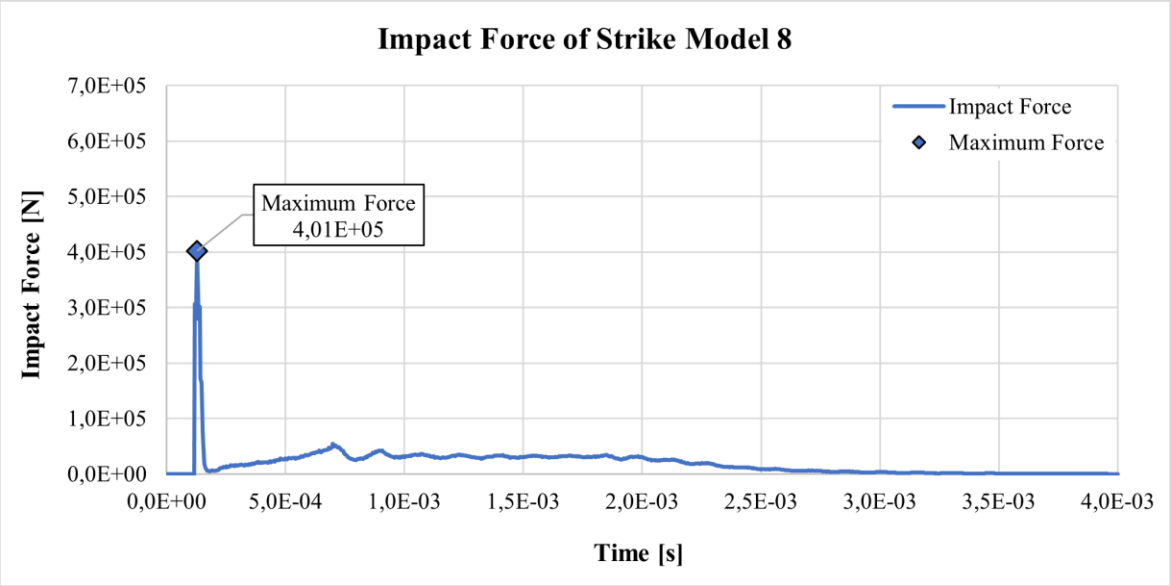

Figure 7-17 Impact Force of Strike Model 8

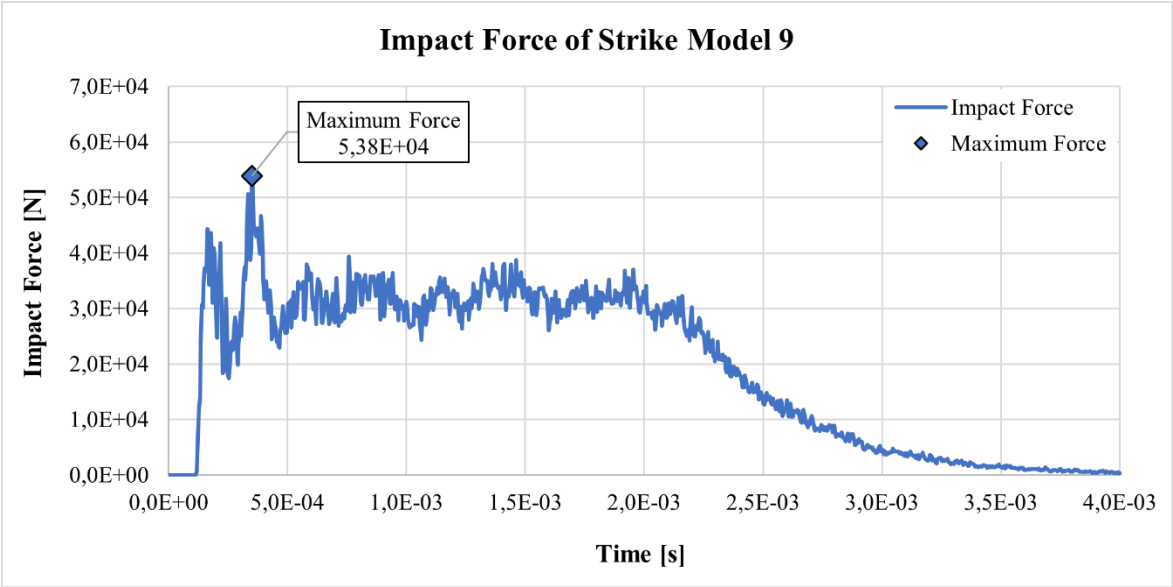

Figure 7-18 Impact Force of Strike Model 9

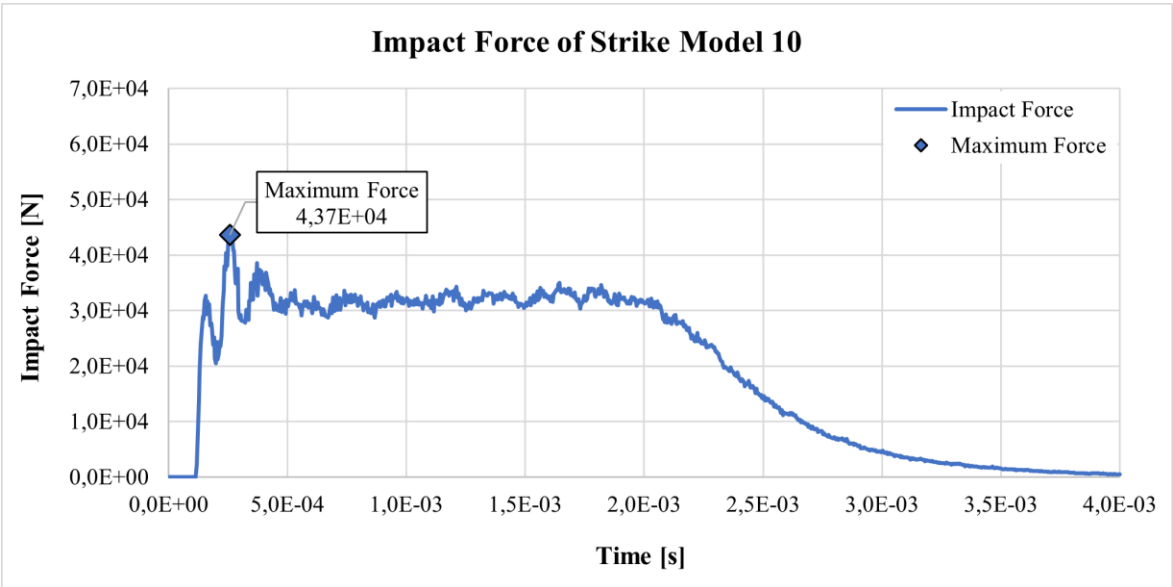

Figure 7-19 Impact Force of Strike Model 10

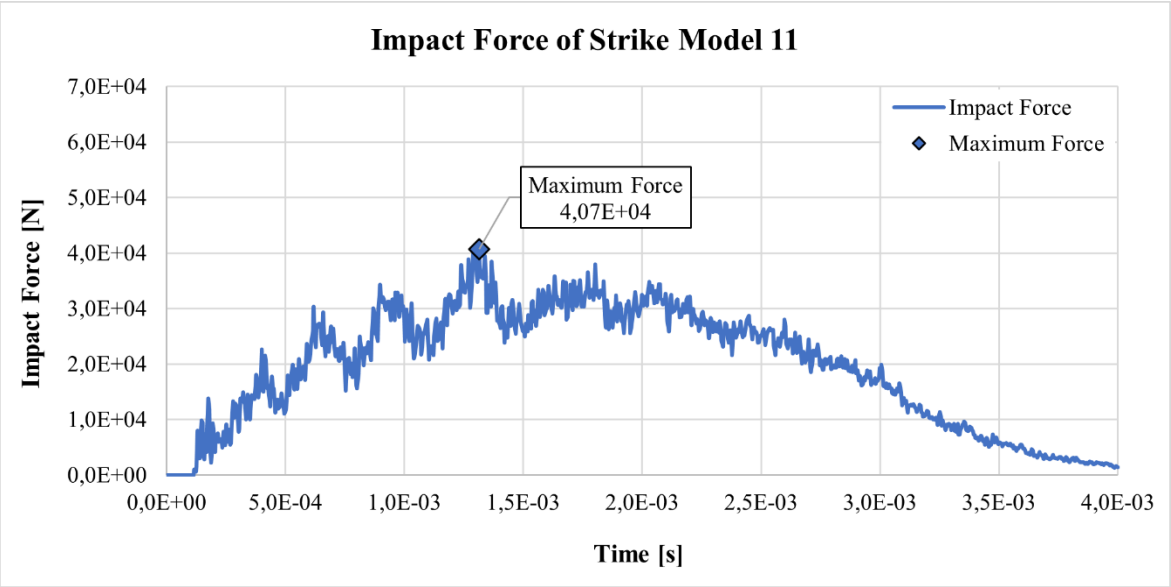

Figure 7-20 Impact Force of Strike Model 11

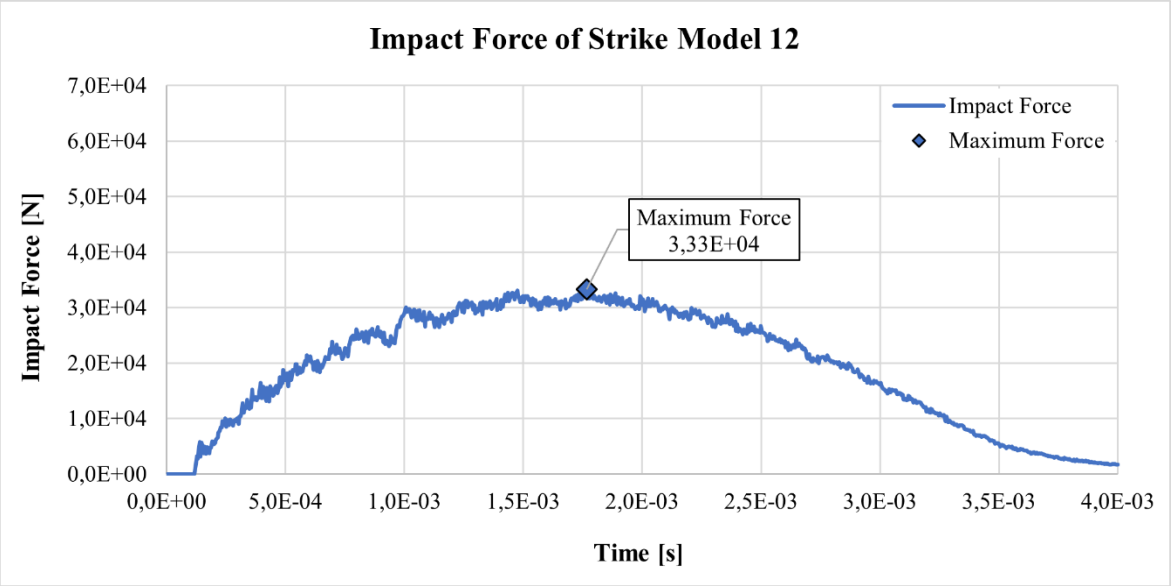

Figure 7-21 Impact Force of Strike Model 12

7.2.3 Analysis with ALE Method

In this section, effects of bird shape and element number were investigated using ALE method and three bird shapes. Extraordinary initial peaks of impact forces were observed just after impact in results of Strike Model 15, Strike Model 17, and Strike Model 18. Therefore, they were ignored, and maximum impact forces were corrected. They were named as "Corrected Impact Force (N)" in Table 11. Results show that, bird shape affects analyses results more than element number of bird model does.

Impact force of Bird Shape 1 was more than eleven times of reference value and it is not suitable for analyses. Impact force of Strike Model 15 was almost twice of the reference value. Results of Strike Model 16, Strike Model 17 and Strike Model 18 were more coherent to the reference value. However, results of them were smaller than the reference value. Results were given in Table 11.

Table 11 ALE Results for Different Particle Numbers and Bird Shapes

	Reference [24]	Bird Shape 1		Bird Shape 2		Bird Shape 3	
Analysis Model	-	Strike Model 13	Strike Model 14	Strike Model 15	Strike Model 16	Strike Model 17	Strike Model 18
Element Number (Bird)	-	143	1342	145	1333	359	2873
Element Number (Enclosure)	-	1672	13999	1912	16124	4204	37222
Number Element (Impact Surface)	-	17956					
Impact Force (N)	4.31E+04	2.89E+06	5.17E+05	2.12E+05	4.21E+04	4.89E+04	6.91E+04
Corrected Impact Force (N)	-	-	-	8.61E+04	-	3.76E+04	3.63E+04
Analysis Result	-	Figure 7-22	Figure 7-23	Figure 7-24	Figure 7-25	Figure 7-26	Figure 7-27

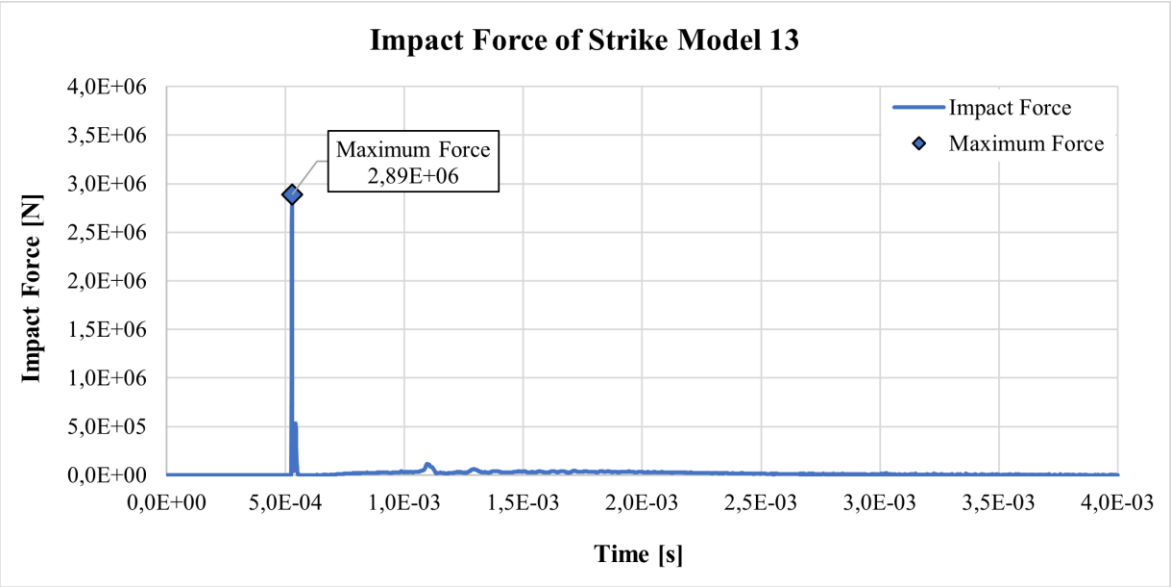

Figure 7-22 Impact Force of Strike Model 13

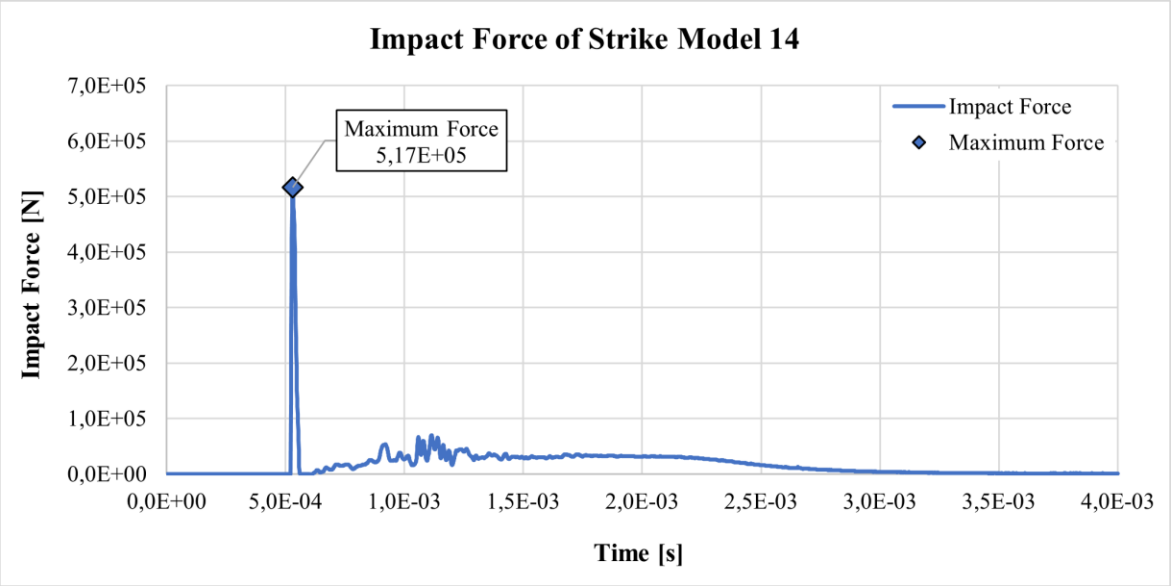

Figure 7-23 Impact Force of Strike Model 14

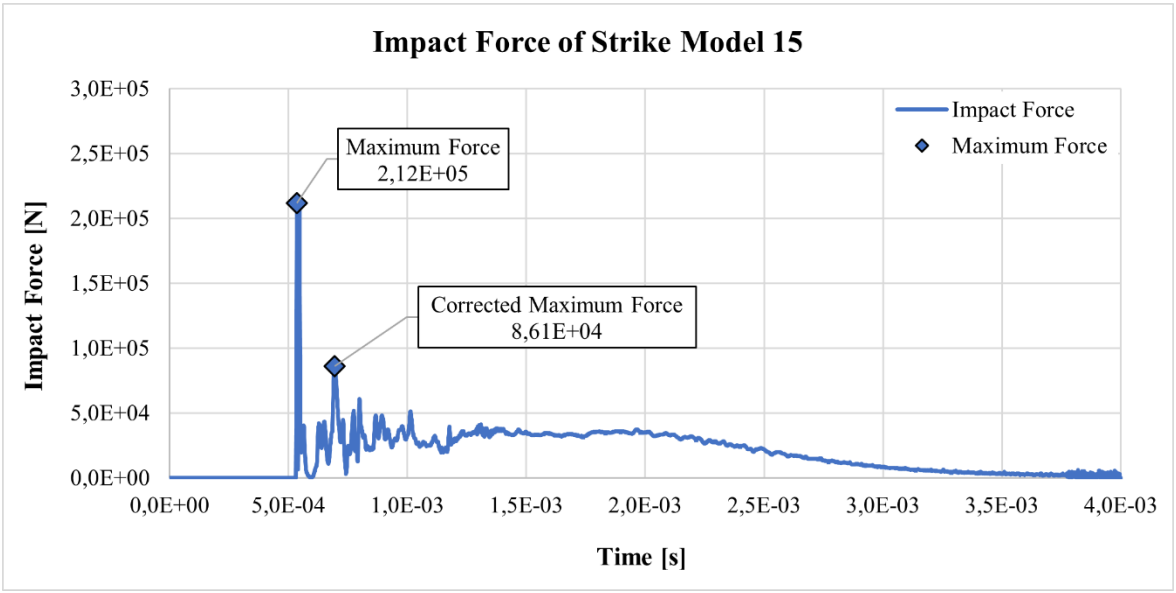

Figure 7-24 Impact Force of Strike Model 15

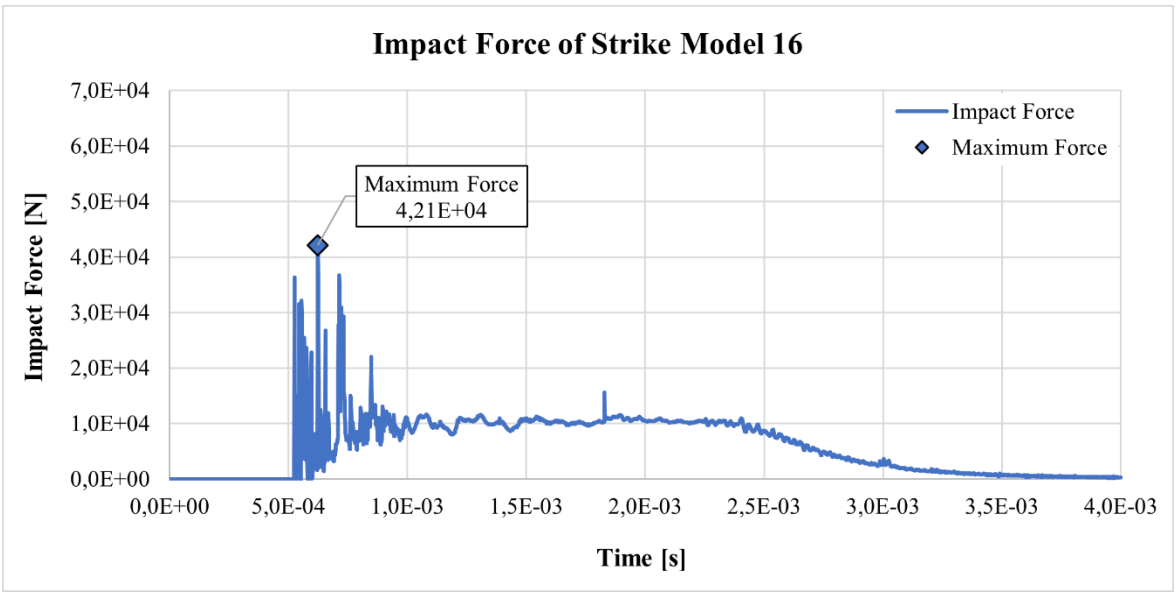

Figure 7-25 Impact Force of Strike Model 16

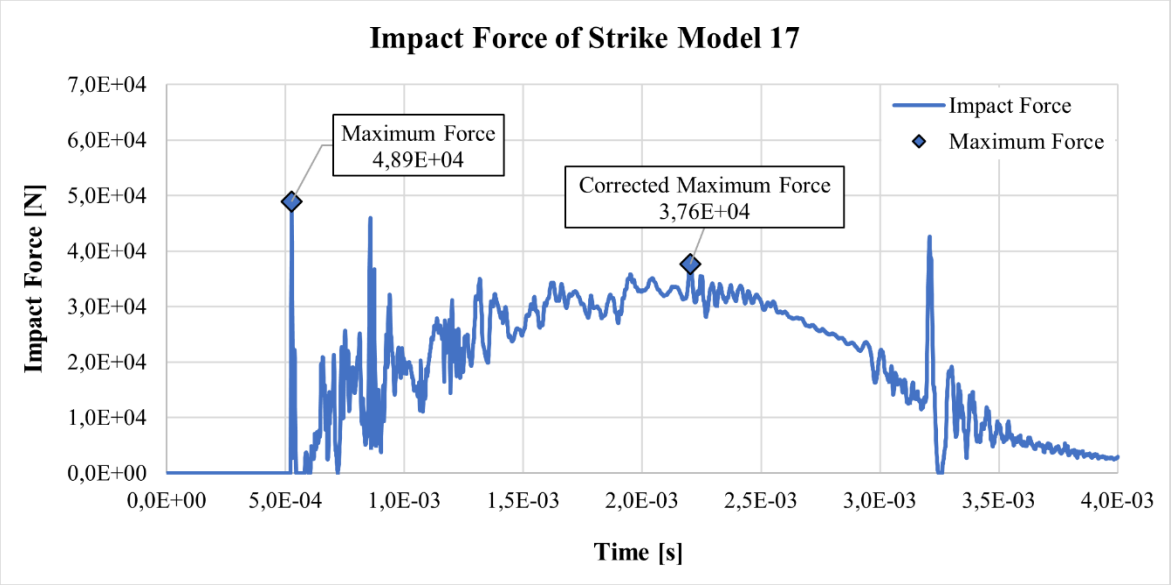

Figure 7-26 Impact Force of Strike Model 17

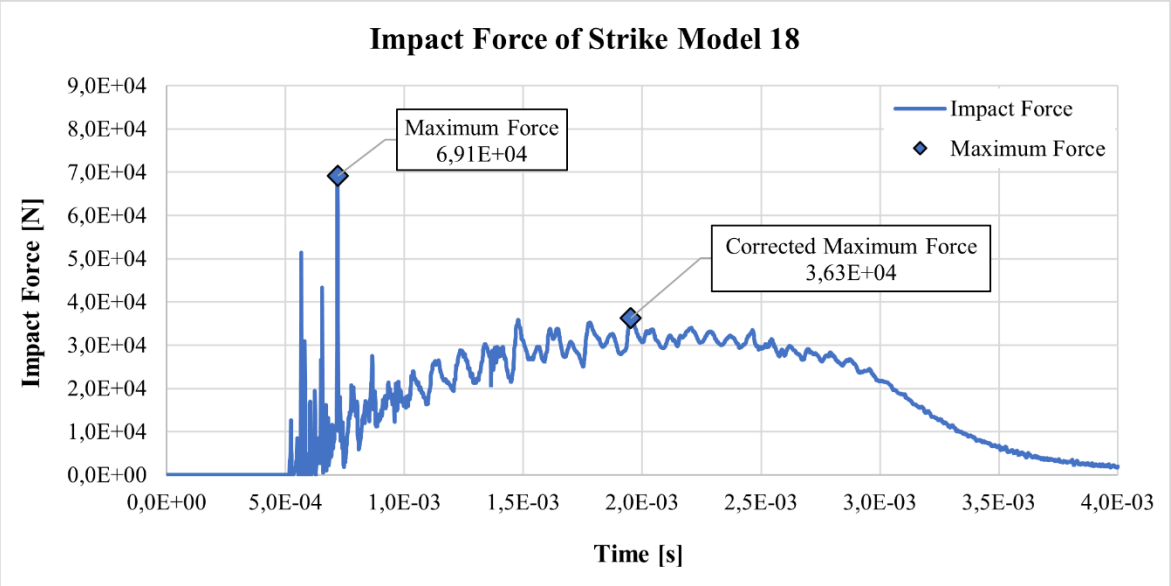

Figure 7-27 Impact Force of Strike Model 18

7.2.4 Comparison of Bird Shape – Analysis Method Combinations

All analysis results of Strike Model 1 to Strike Model 18 show that shape of bird model affects results more than number of elements and number of particles. It was seen that; force trends did not change depending on number of elements and number of particles. However, shape of the impactor bird and method type change trend and value of impact force. Therefore, analysis method and impactor shape are important parameters for accuracy of result. In this section analysis methods were compared for each of the three bird shapes.

In the Table 12, analysis results of Bird Shape 1 were displayed together. Results show that Bird Shape 1 did not create realistic impact forces, and it is not suitable for bird strike analyses.

Table 12 Result Comparison Using Bird Shape 1

Bird Shape 1	Reference [24]	Lagrangian		SPH		ALE	
Analysis Model	-	Strike Model 1	Strike Model 2	Strike Model 7	Strike Model 8	Strike Model 13	Strike Model 14
Impact Force (N)	4.31E+04	6.11E+05	5.84E+05	3.89E+05	4.01E+05	2.89E+06	5.17E+05
Analysis Result	-	Figure 7-10	Figure 7-11	Figure 7-16	Figure 7-17	Figure 7-22	Figure 7-23
Related Table	Table 7	Table 9		Table 10		Table 11	

In the Table 13, analysis results of Bird Shape 2 were displayed together. Results show that Bird Shape 2 creates reasonable impact forces. Impact forces of Lagrangian and ALE methods were less than the reference value. However, impact force of SPH method was higher than reference impact force. Analyses result of Strike Model 8 was the closest to reference impact force value.

Table 13 Result Comparison Using Bird Shape 2

Bird Shape 2	Reference [24]	Lagrangian		SPH		ALE	
Analysis Model	-	Strike Model 3	Strike Model 4	Strike Model 9	Strike Model 10	Strike Model 15	Strike Model 16
Impact Force (N)	4.31E+04	3.97E+04	3.48E+04	5.38E+04	4.37E+04	2.12E+05	4.21E+04
Analysis Result	-	Figure 7-12	Figure 7-13	Figure 7-18	Figure 7-19	Figure 7-24	Figure 7-25
Related Table	Table 7	Table 9		Table 10		Table 11	

In the Table 14, analysis results of Bird Shape 3 were displayed together. Results show that Bird Shape 3 creates reasonable impact forces. However, all the impact forces are less than reference value.

Table 14 Result Comparison Using Bird Shape 3

Bird Shape 3	Reference Data [24]	Lagrangian		SPH		ALE	
Analysis Model	-	Strike Model 5	Strike Model 6	Strike Model 11	Strike Model 12	Strike Model 17	Strike Model 18
Impact Force (N)	4.31E+04	3.22E+04	3.14E+04	4.07E+04	3.33E+04	4.89E+04	6.91E+04
Corrected Impact Force (N)	-	-	-	-	-	3.76E+04	3.63E+04
Result of Analysis	-	Figure 7-14	Figure 7-15	Figure 7-20	Figure 7-21	Figure 7-26	Figure 7-27
Related Table	Table 7	Table 9		Table 10		Table 11	

According to Table 12, Table 13 and Table 14, Bird Shape 1 is not suitable for any analysis method because of unrealistic analysis results. Bird Shape 2 and Bird Shape 3 created reasonable impact forces that was close to reference value. However, only the impact force of Strike Model 10, combination of Bird Shape 2 and SPH method, was higher than reference value, and it was the closest to reference impact force value. Therefore, Strike Model 10 was the most reasonable Bird Shape - Method combination to become safe side and going to be used for future analyses.

7.3 Proof of Analysis Model

In this section, Strike Model 10 was compared with previous experimental studies. Therefore, shape and dimensions of impact surface; density and dimensions of impactor bird were modified suitably in accordance with the reference experimental study and bird strike requirement for rotorcraft.

In the experimental study of Wilbeck, 76.2 cm diameter and 10.16 cm thick circular plate was used [26]. Bird strike requirement for rotorcrafts are stated as "The rotorcraft must be designed to assure capability of continued safe flight and landing (for Category A) or safe landing (for Category B) after impact with a 1 kg bird, when the velocity of the rotorcraft (relative to the bird along the flight path of the rotorcraft) is equal to V_{NE} or V_H (whichever is the lesser) at altitudes up to 8 000 feet" [1, 2]. Therefore, it is required to proof Strike Model 10 for 1 kg bird and circular plate. Density, diameter, and length of 1 kg impactor were calculated using Equation (7.1), Equation (7.2) and Equation (7.8), respectively. They were listed in Table 15. Impact surface was modelled 10.16 cm thick circular plate with 76.2 cm diameter.

Table 15 Properties of 1kg Cylindrical Bird Model with Hemispherical Ends

1 kg Bird Model Properties (Cylindrical Model with Hemispherical Ends)	
Length (m)	0.23219
Diameter (m)	0.08040
Density (kg/m3)	959

After modification of Strike Model 10 for 1 kg bird and circular plate, new strike model was created as Strike Model 19 to simulate Wilbeck's experimental study. Also, Strike Model 20 was created to show effect of impact surface shape. Differences of Strike Models were listed in Table 16.

Table 16 Differences of Strike Models

	Strike Model 10	Strike Model 19			Strike Model 20		
Impact Surface	Square Plate	Circular Plate			Square Plate		
Impact Speed (m/s)	86.0222222	116	197	253	116	197	253

Strike simulations of Strike Model 19 and Strike Model 20 for impact speeds of 116 m/s were shown in Figure 7-28 and Figure 7-29, respectively.

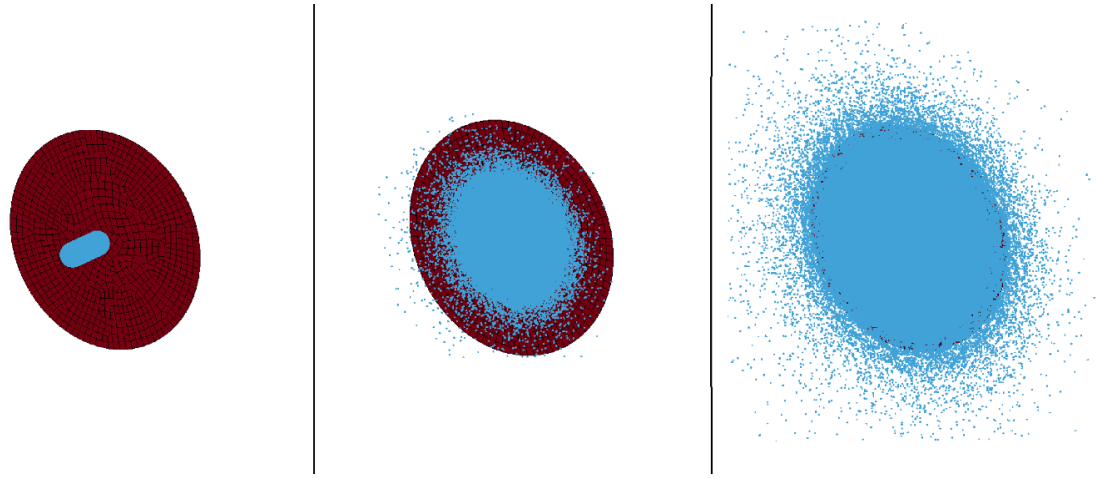

Figure 7-28 Strike Simulation of Strike Model 19 (116 m/s)

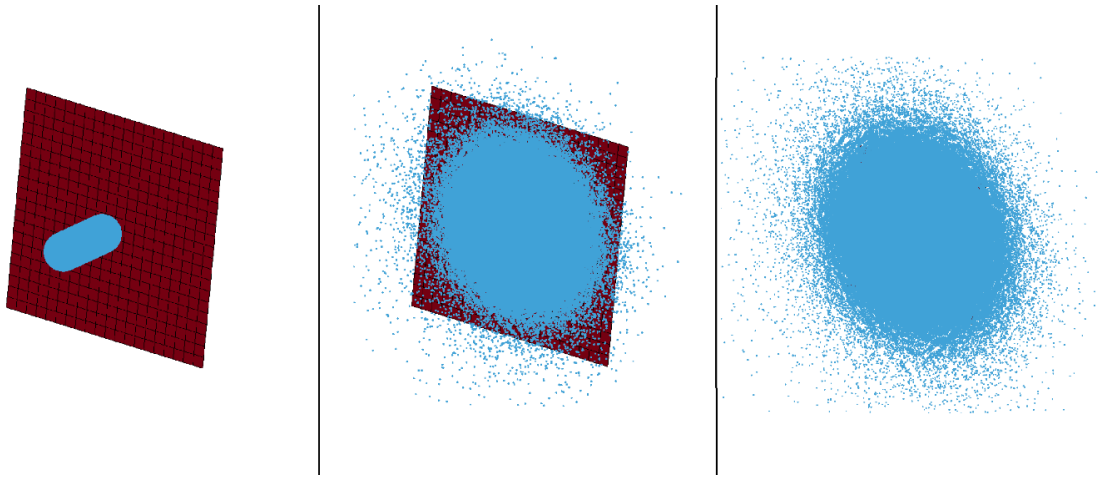

Figure 7-29 Strike Simulation of Strike Model 20 (116 m/s)

Figure 7-30 and Figure 7-31 show that impact forces of circular and square impact surfaces are close to each other. Both Strike Model 19 and Strike Model 20 are suitable for impact force analyses.

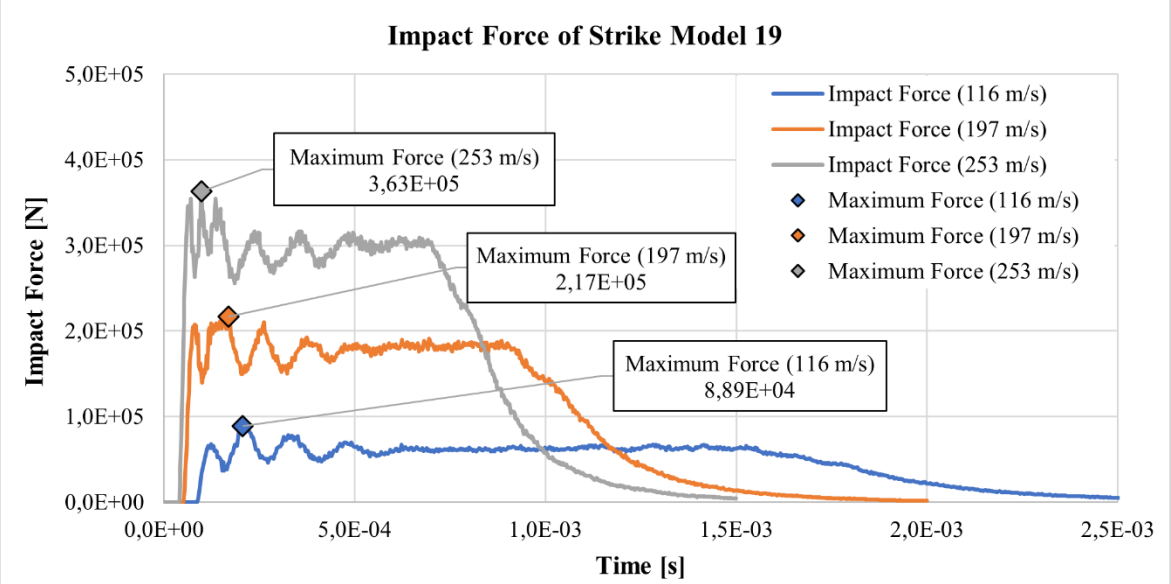

Figure 7-30 Impact Force of Strike Model 19

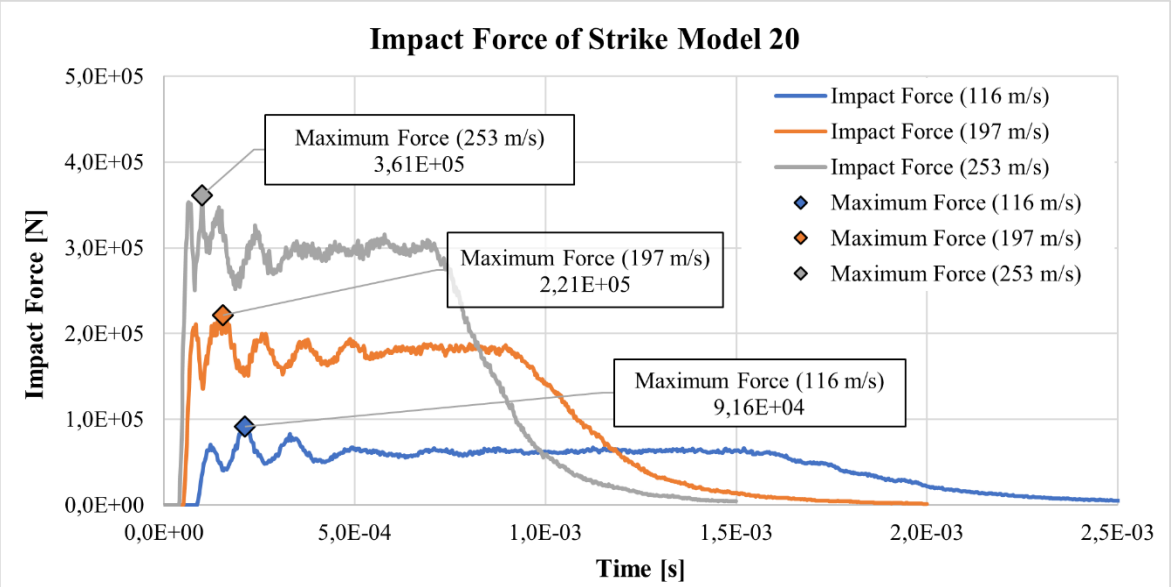

Figure 7-31 Impact Force of Strike Model 20

Figure 7-32 and Figure 7-33 show that trend of impact pressures measured on surfaces are similar to each other. However, magnitudes change according to shape of impact surfaces.

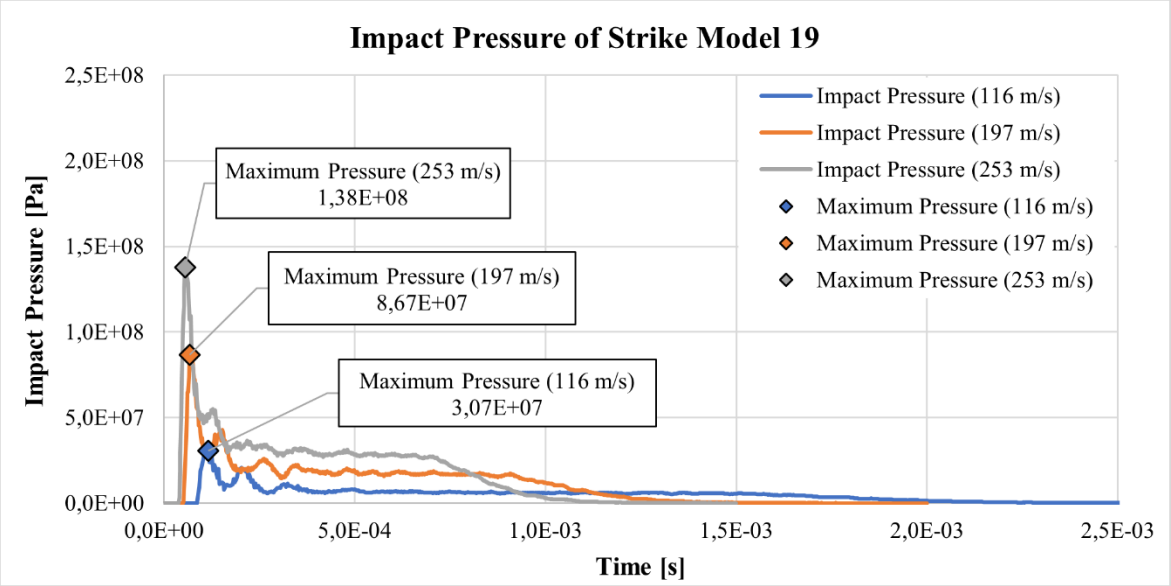

Figure 7-32 Impact Pressure of Strike Model 19

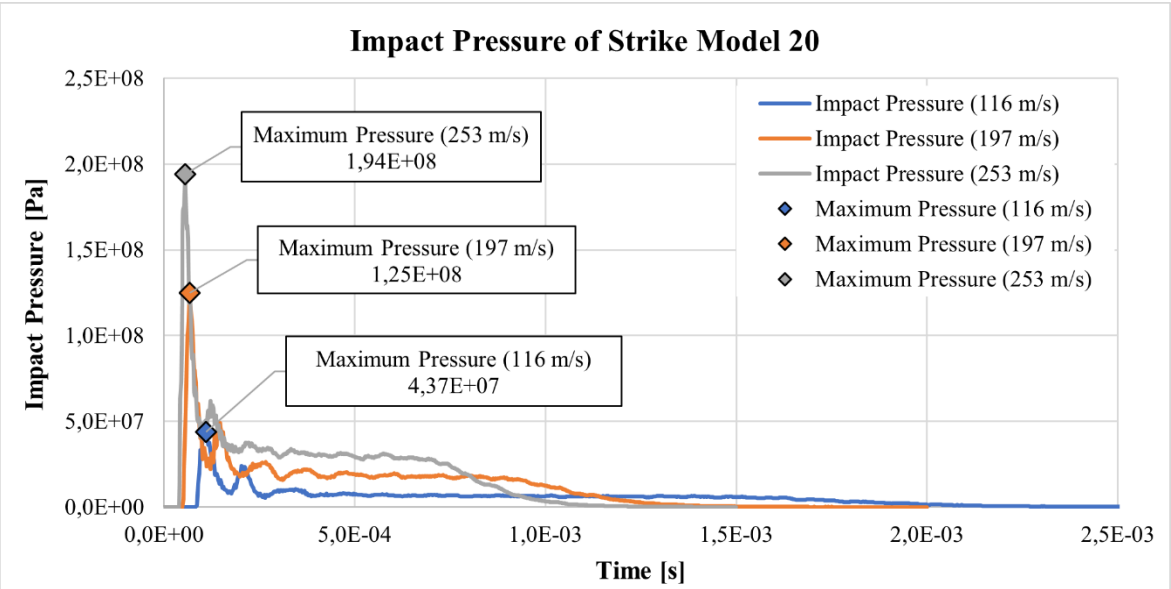

Figure 7-33 Impact Pressure of Strike Model 20

Hugoniot pressure and stagnation pressure of the Wilbeck's experimental data, Strike Model 19 and Strike Model 20 were compared with each other, and results were shown in Figure 7-34 and Figure 7-35, respectively. Hugoniot pressure of Strike Model 19 and Strike Model 20 were inside the result data set of Wilbeck's experiment [26, 27], and they were close to second order polynomial trend lines of data set of Wilbeck's experiment. Also, stagnation pressure of both Strike Model 19 and Strike Model 20 were between theoretical stagnation pressure curve given in Equation (7.12) and second order polynomial trend lines of data set of Wilbeck's experiment [27]. Therefore, both Strike Model 19 and Strike Model 20 are suitable for impact pressure analyses. The only difference between Strike Model 19 and Strike Model 20 is the shape of impact surfaces.

$$P_{stagnation} = \frac{1}{2}\rho_{impactor}V_{impact}^2 \qquad (7.12)$$

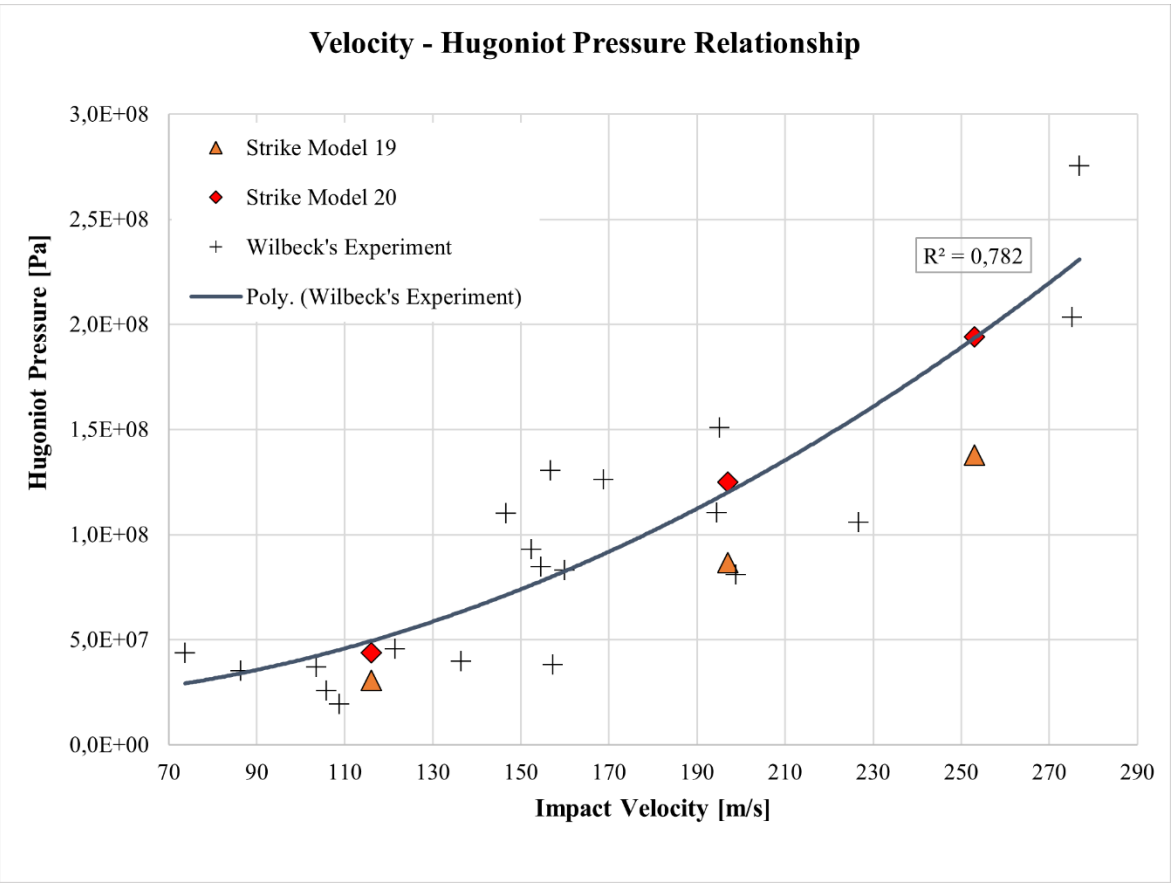

Figure 7-34 Hugoniot Pressure Comparison

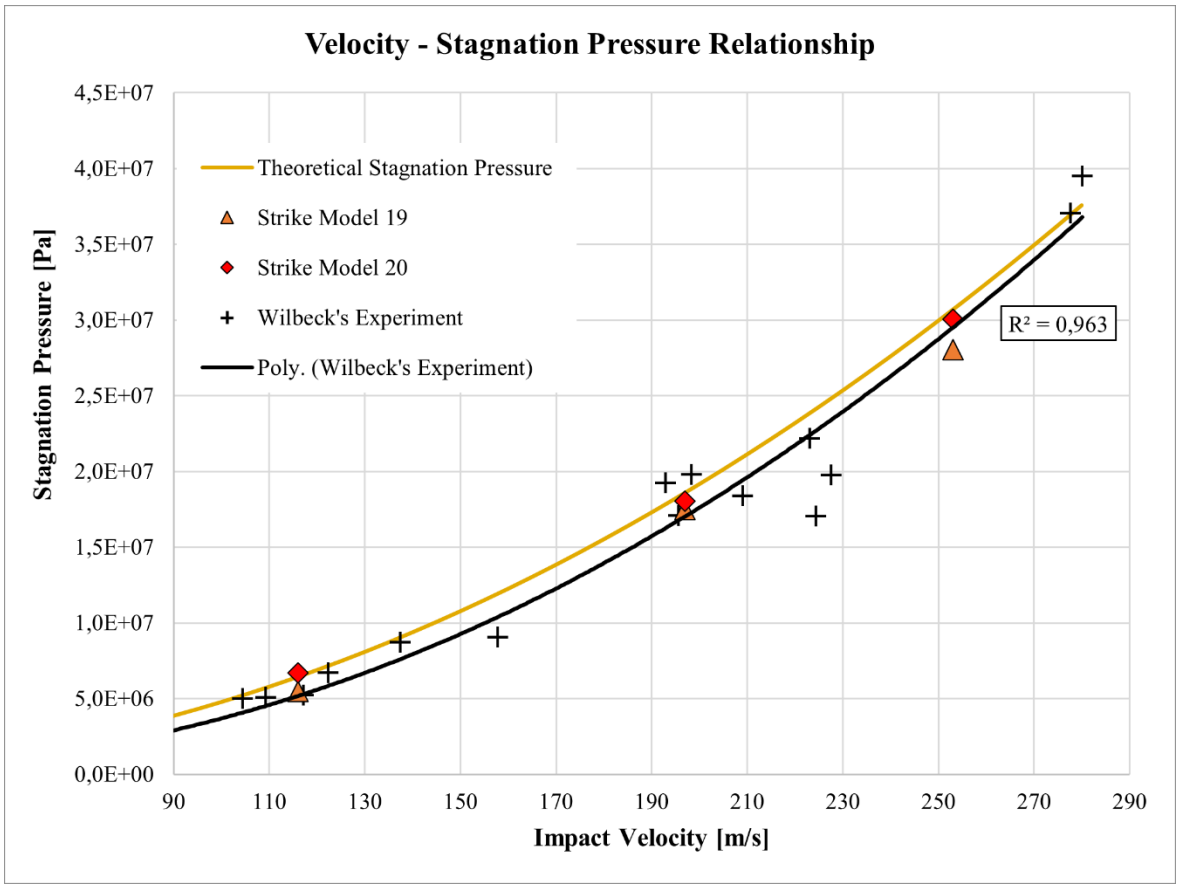

Figure 7-35 Stagnation Pressure Comparison

8 HELICOPTER STRIKE

In this section of thesis work, impact scenario was defined for both excluding effect of pitch change and including effect of pitch change. Helicopter airspeed changes in accordance with helicopter pitch angle. In other words, impact pressure and forces not only change with respect to speed of helicopter but also change with impact angle. Analysis model named "Strike Model 21" was used to investigate the effect of impact speed excluding pitch change, and "Strike Model 22" was used to investigate effect of impact speed including pitch change.

Impact surface was 5 mm thick trapezoid shaped windshield, and dimensions of it was given in Figure 8-1.

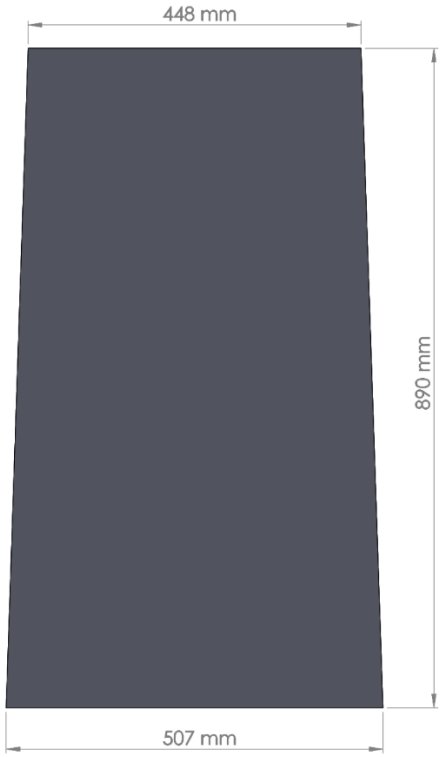

Figure 8-1 Trapezoid Windshield

Helicopter was assumed to move in Z direction and analyses were done according to coordinate system given in Figure 8-2.

Figure 8-2 Impact Direction

8.1 Bird Strike without Effect of Pitch Change

Analyses were done using parameneters given in Table 17 and analysis model was named as Strike Model 21. Impact angle defines an angle between windshield surface and strike direction. Analysis results of Strike Model 21 would later be used to investigate the effect of pitch change.

Table 17 Impact Scenario of Strike Model 21

Airspeed of Helicopter [knots]	Pitch Angle of Helicopter [Degrees]	Impact Angle [Degrees]
80	2°	27°
85	2°	27°
102	2°	27°
110	2°	27°
120	2°	27°

Following impact pressure tables show impact pressure on windshield surface by time, and maximum impact pressure on windshield surface. Following impact force tables show resultant impact force, component of impact force in X, Y, Z axises; shear force and normal

force components of impact force on windshield by time; and maximum values of them. Following figures show strike simulation and analysis result of Strike Model 21 with 80 knots impact speed.

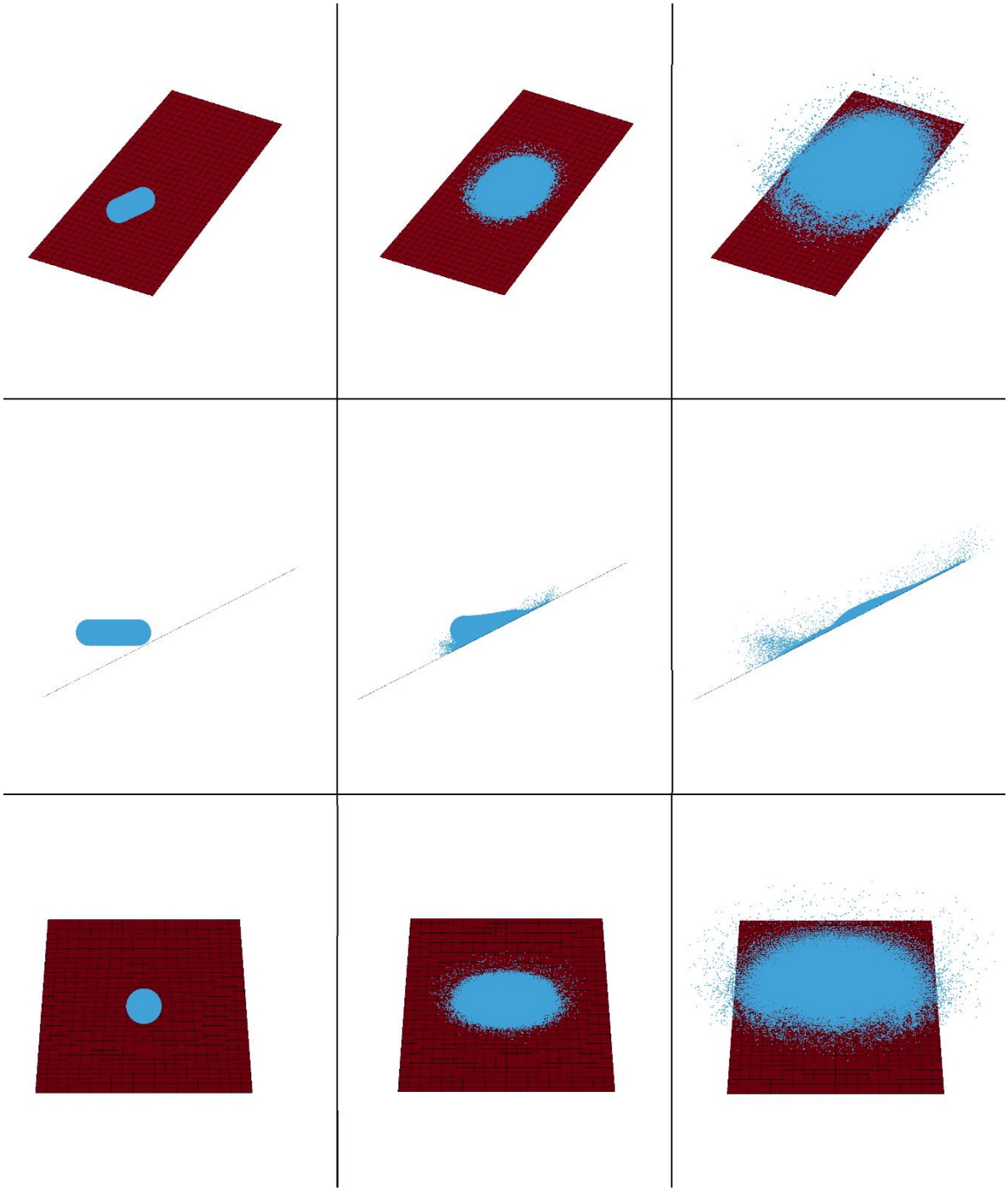

Figure 8-3 Strike Simulation of Strike Model 21 with 80 knots

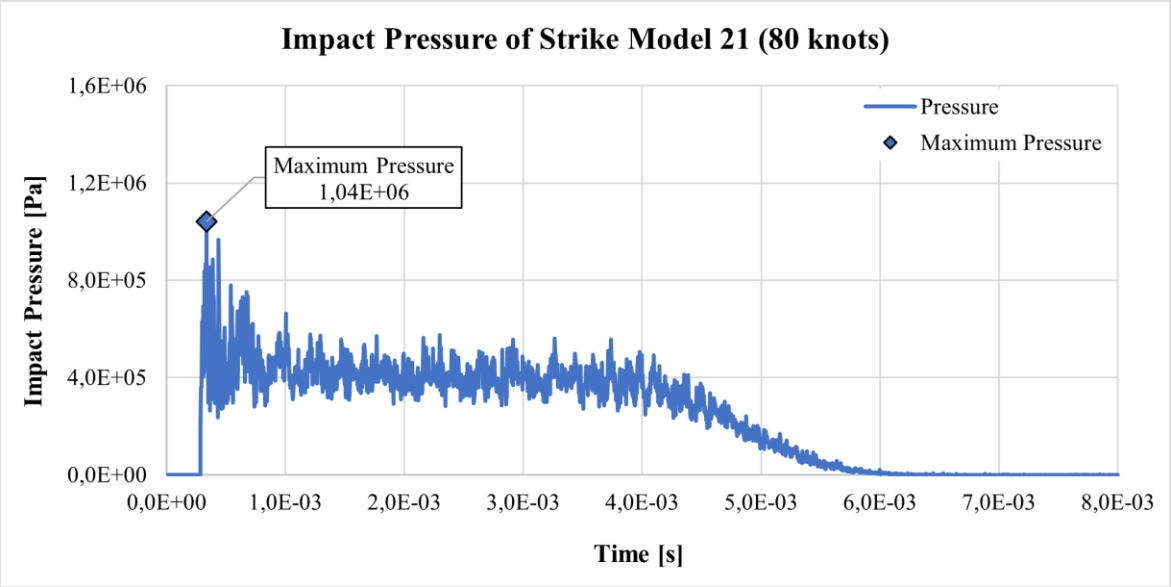

Figure 8-4 Impact Pressure of Strike Model 21 with 80 knots

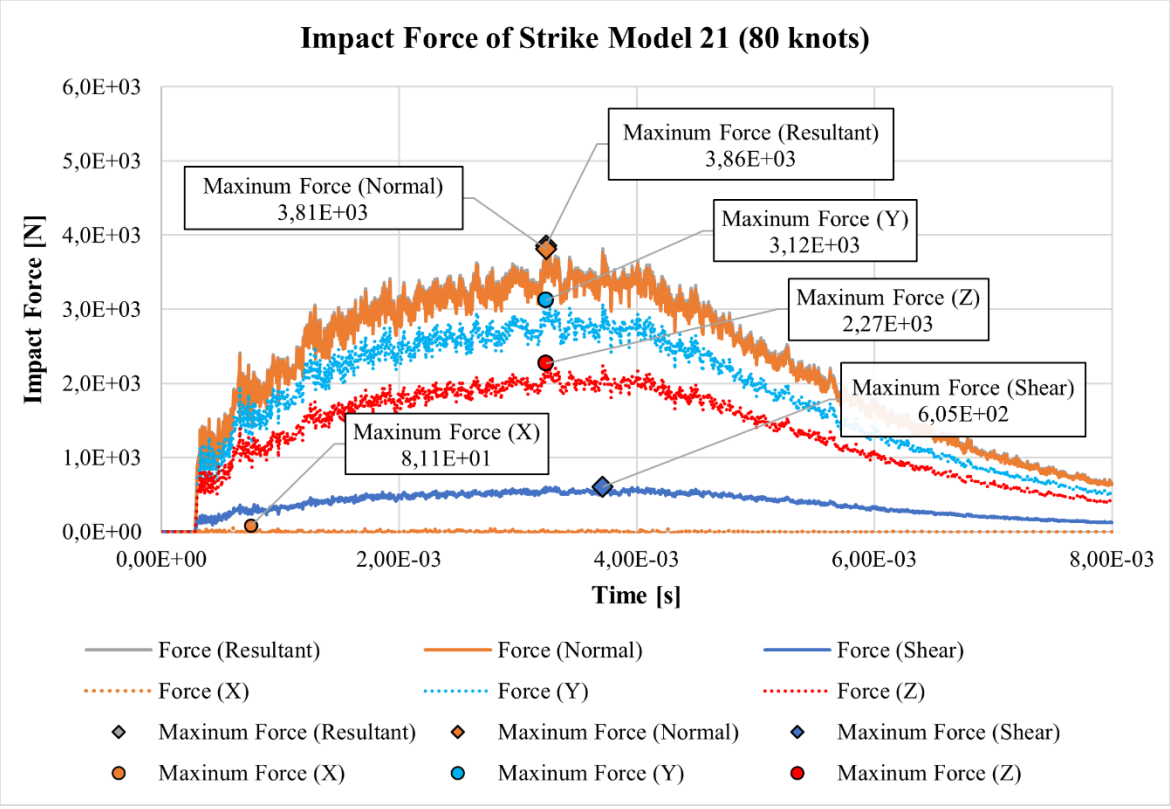

Figure 8-5 Impact Forces of Strike Model 21 with 80 knots

Following figures show strike simulation and analysis result of Strike Model 21 with 85 knots impact speed.

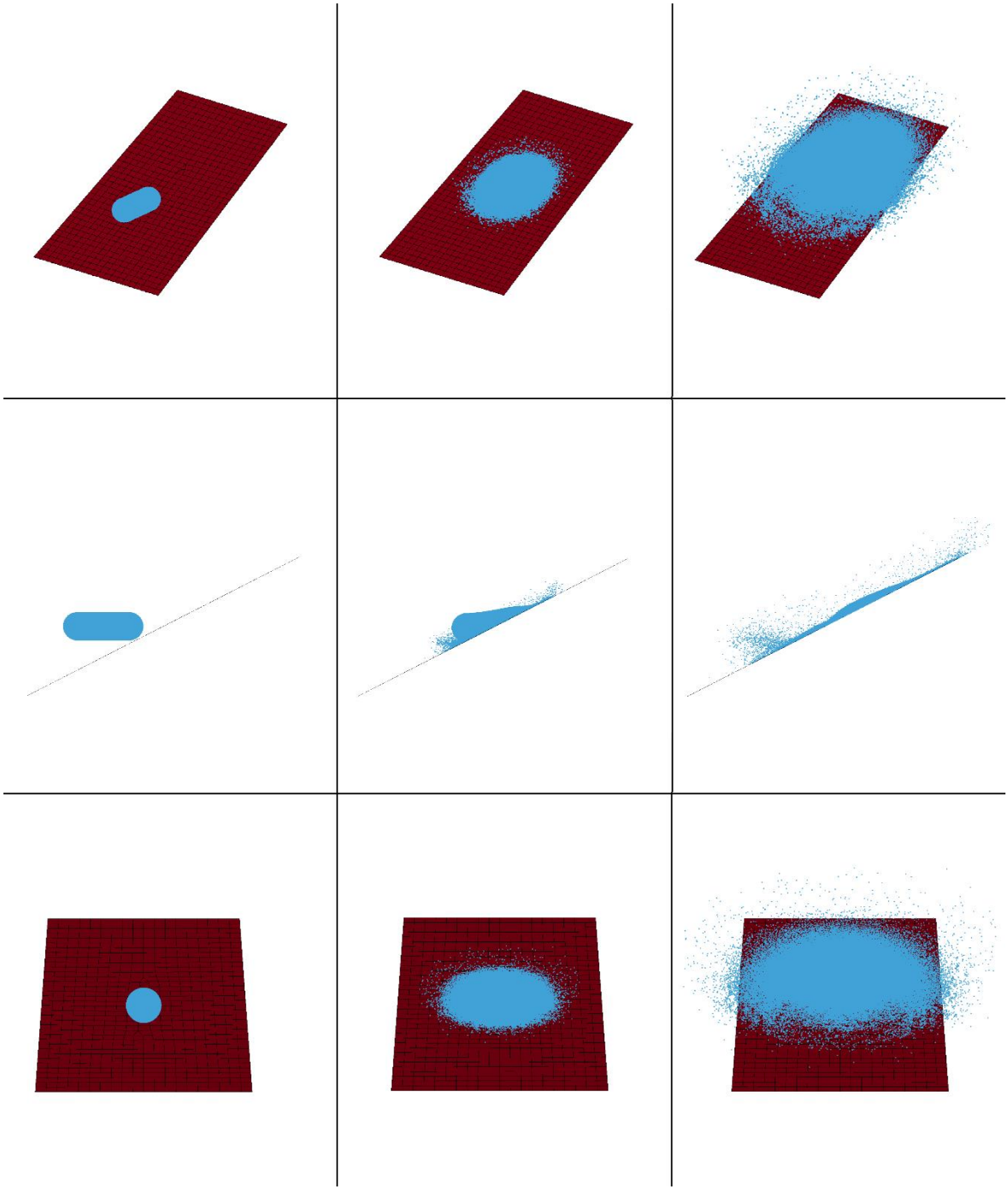

Figure 8-6 Strike Simulation of Strike Model 21 with 85 knots

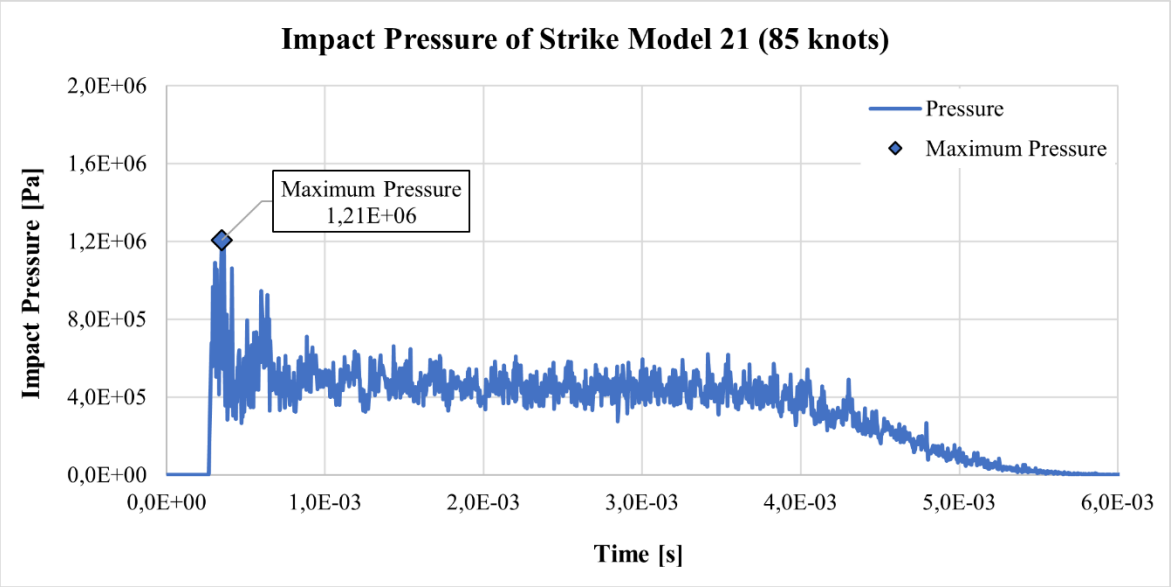

Figure 8-7 Impact Pressure of Strike Model 21 with 85 knots

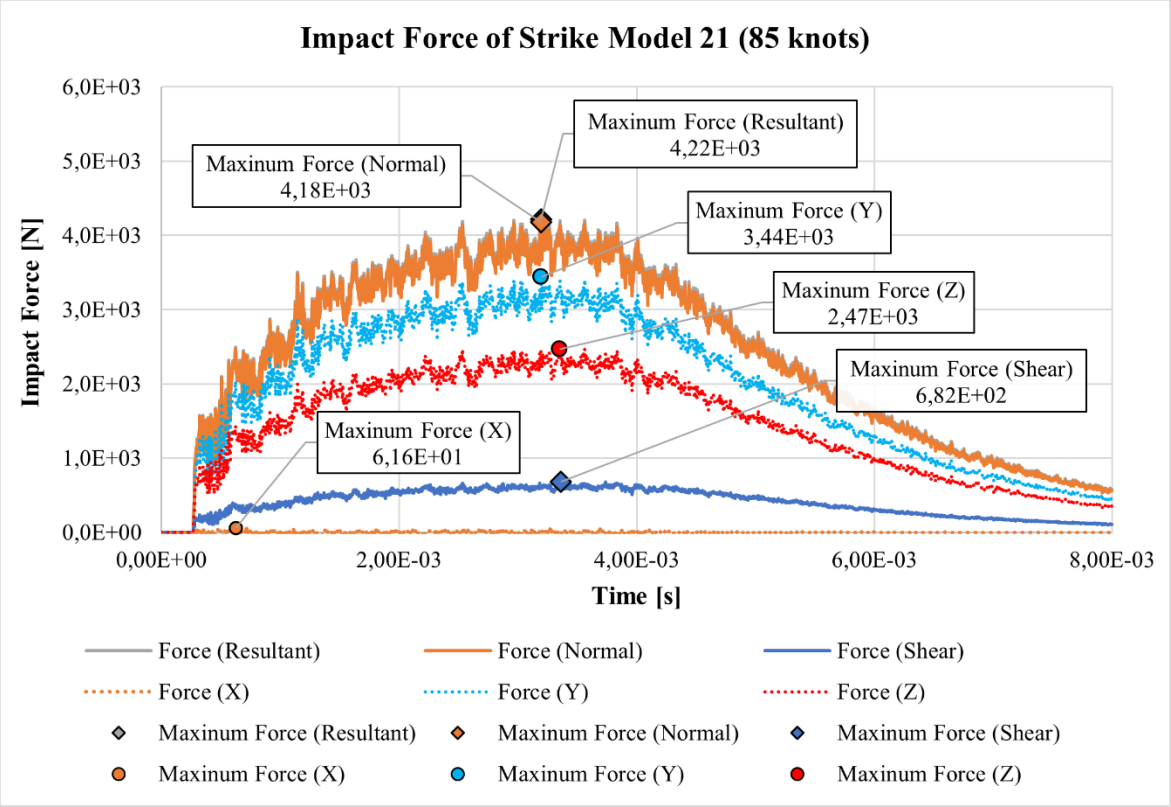

Figure 8-8 Impact Forces of Strike Model 21 with 85 knots

Following figures show strike simulation and analysis result of Strike Model 21 with 102 knots impact speed.

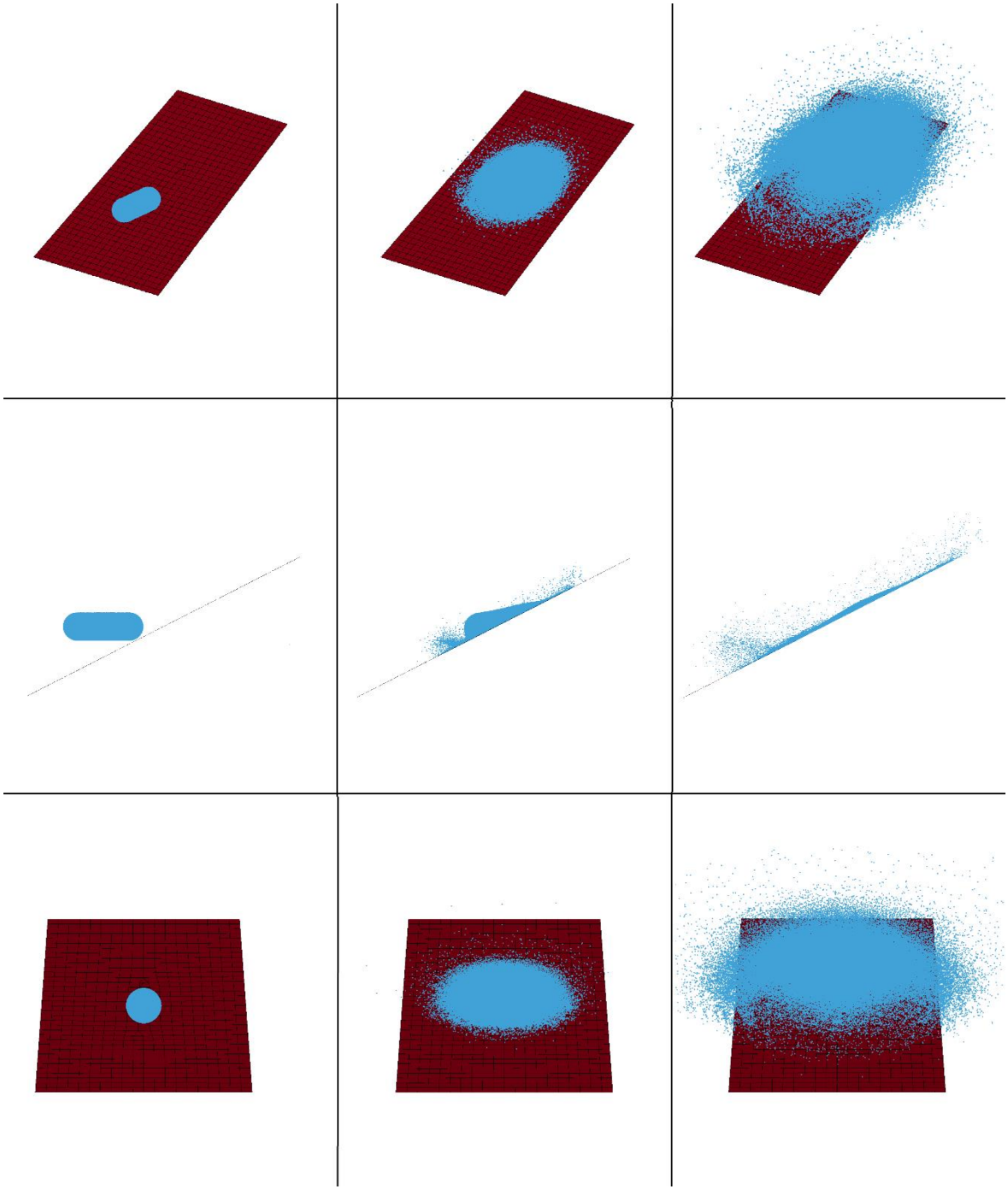

Figure 8-9 Strike Simulation of Strike Model 21 with 102 knots

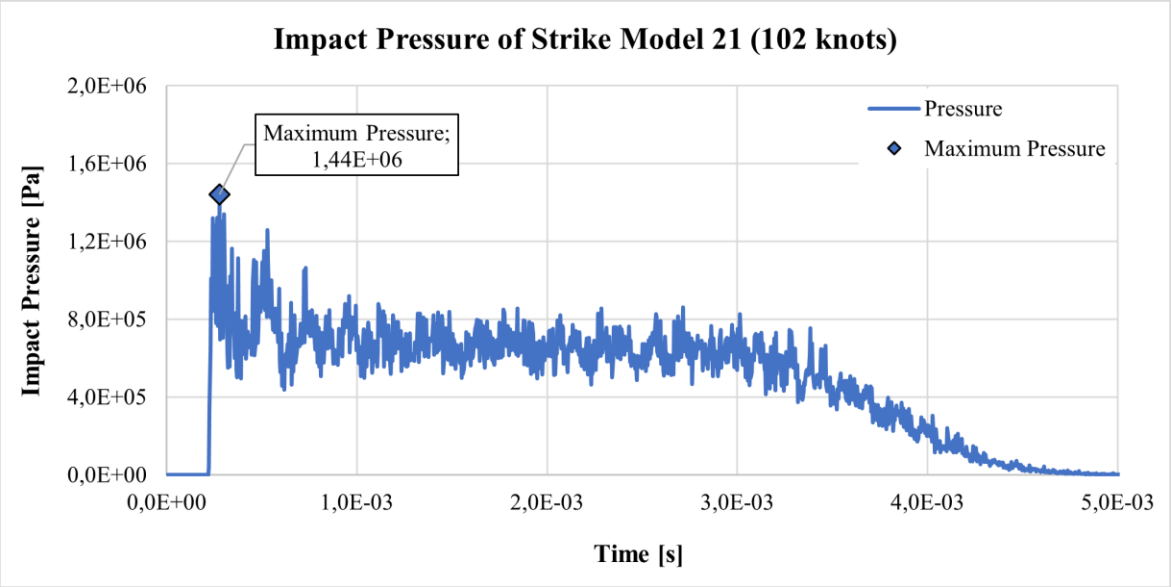

Figure 8-10 Impact Pressure of Strike Model 21 with 102 knots

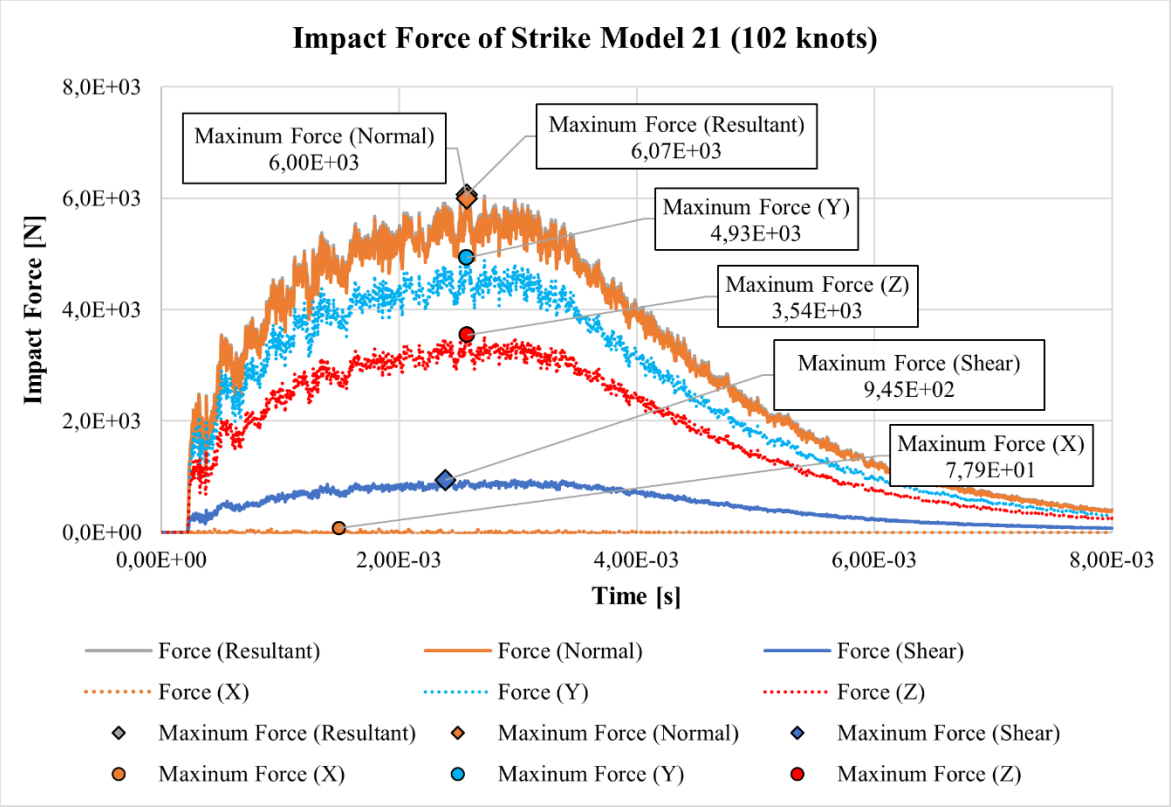

Figure 8-11 Impact Forces of Strike Model 21 with 102 knots

Following figures show strike simulation and analysis result of Strike Model 21 with 110 knots impact speed.

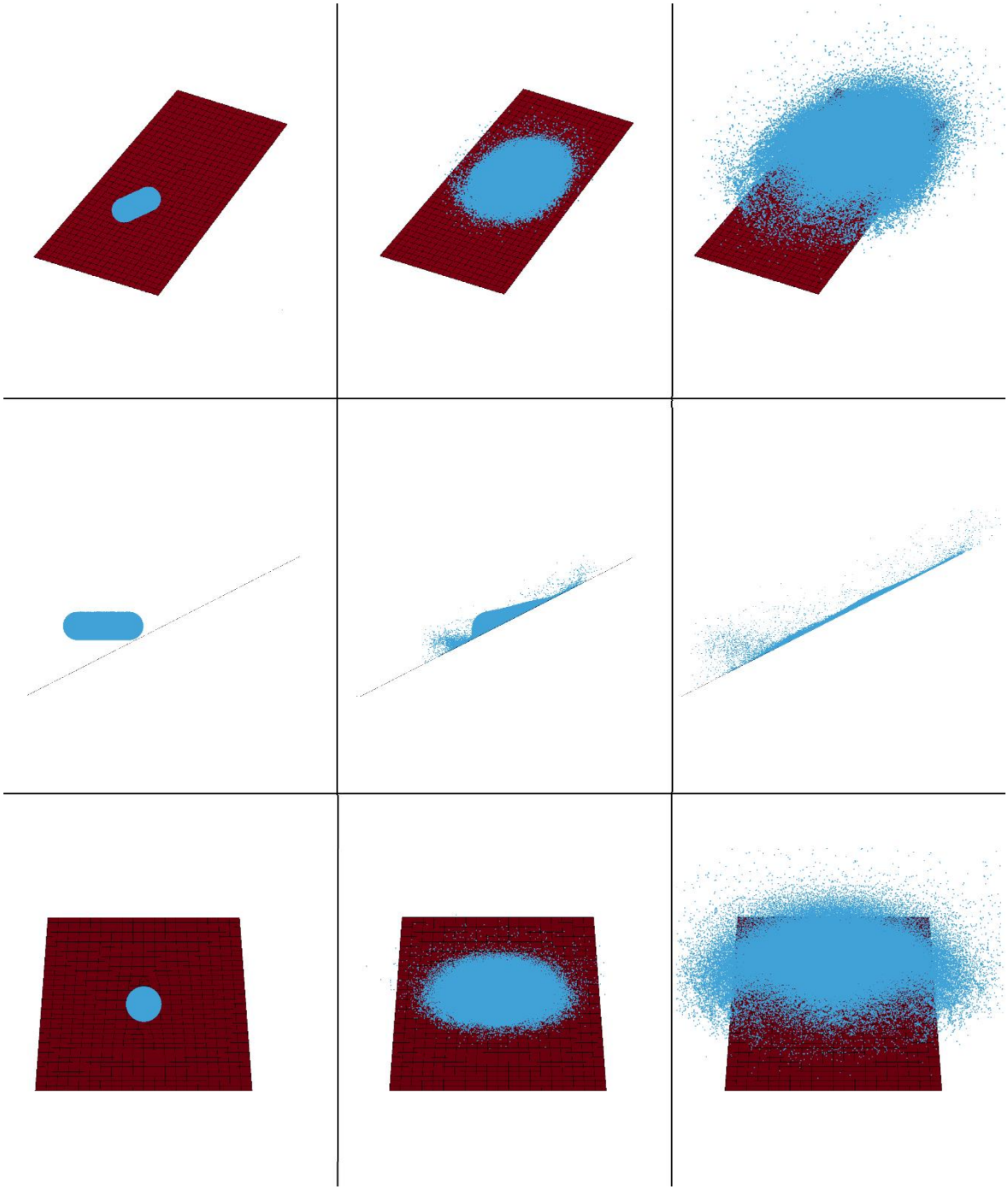

Figure 8-12 Strike Simulation of Strike Model 21 with 110 knots

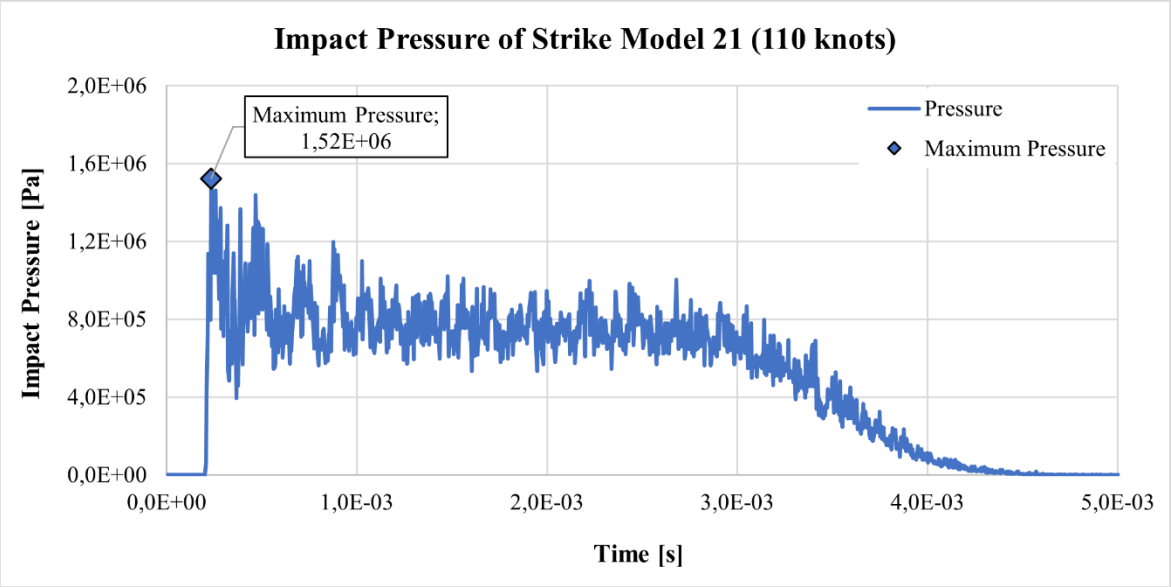

Figure 8-13 Impact Pressure of Strike Model 21 with 110 knots

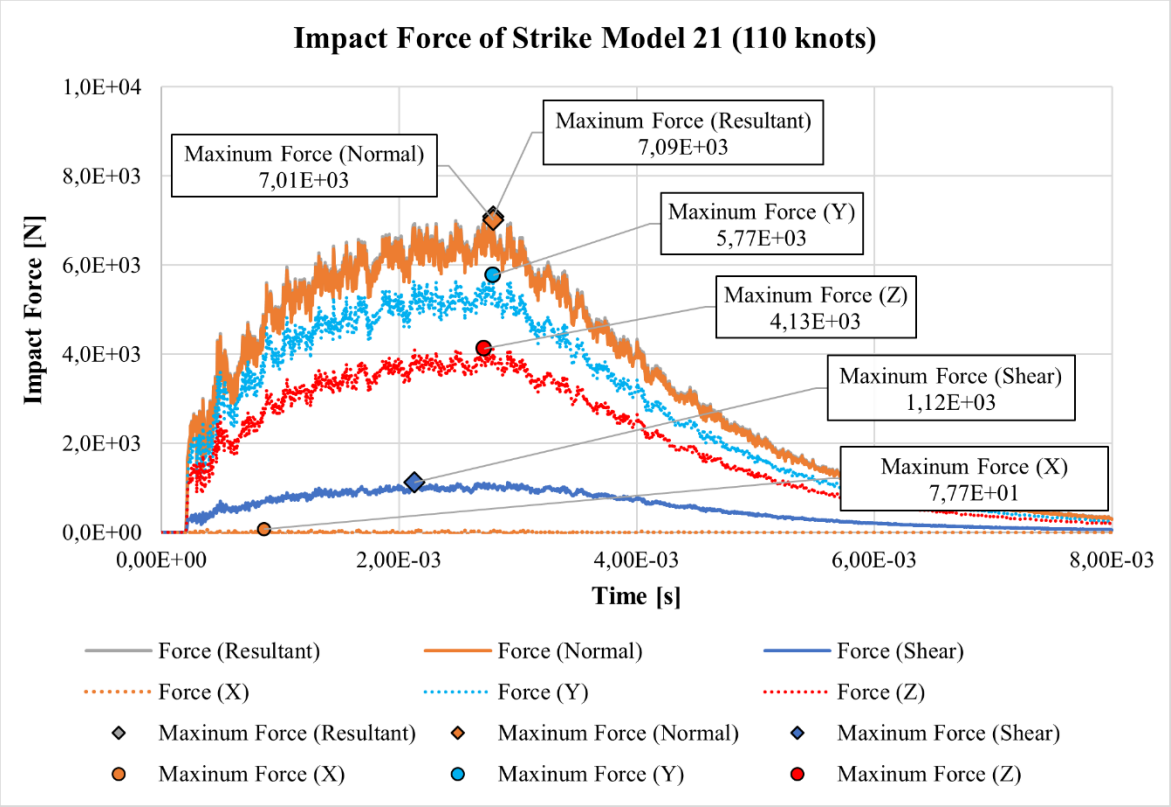

Figure 8-14 Impact Forces of Strike Model 21 with 110 knots

Following figures show strike simulation and analysis result of Strike Model 21 with 120 knots impact speed.

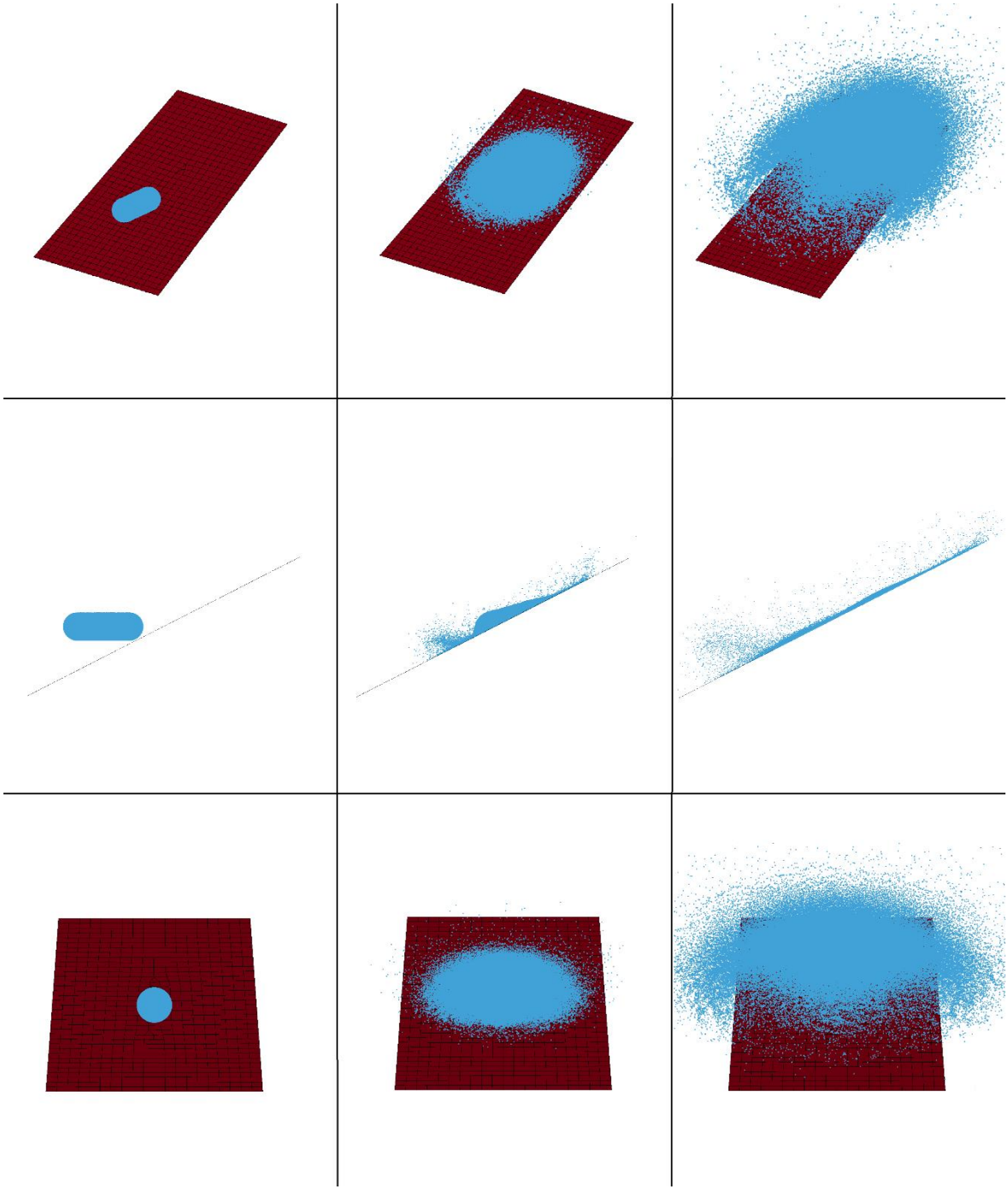

Figure 8-15 Strike Simulation of Strike Model 21 with 120 knots

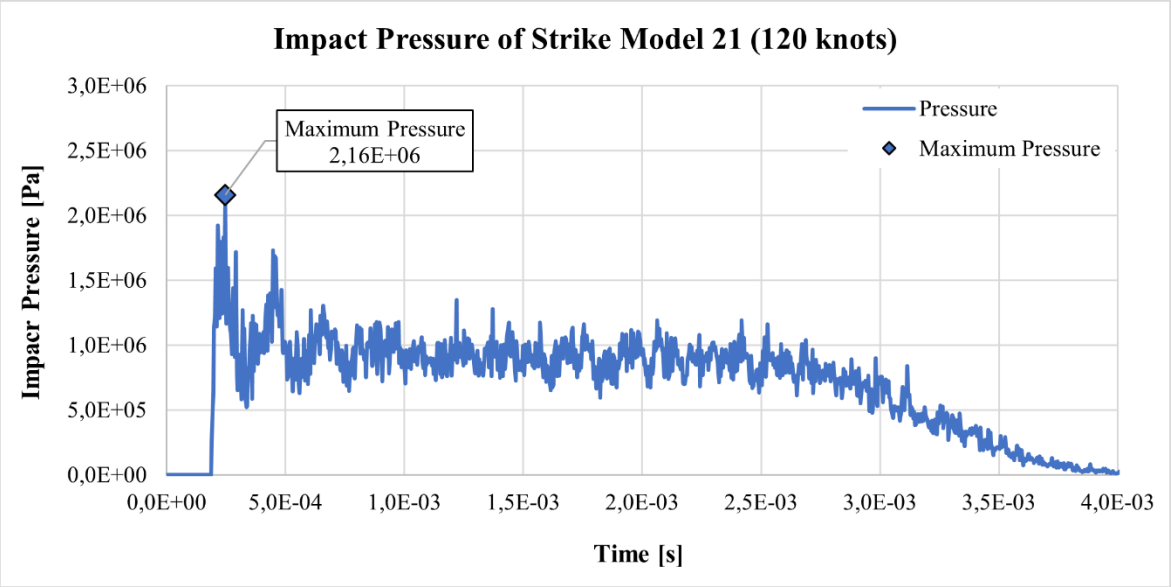

Figure 8-16 Impact Pressure of Strike Model 21 with 120 knots

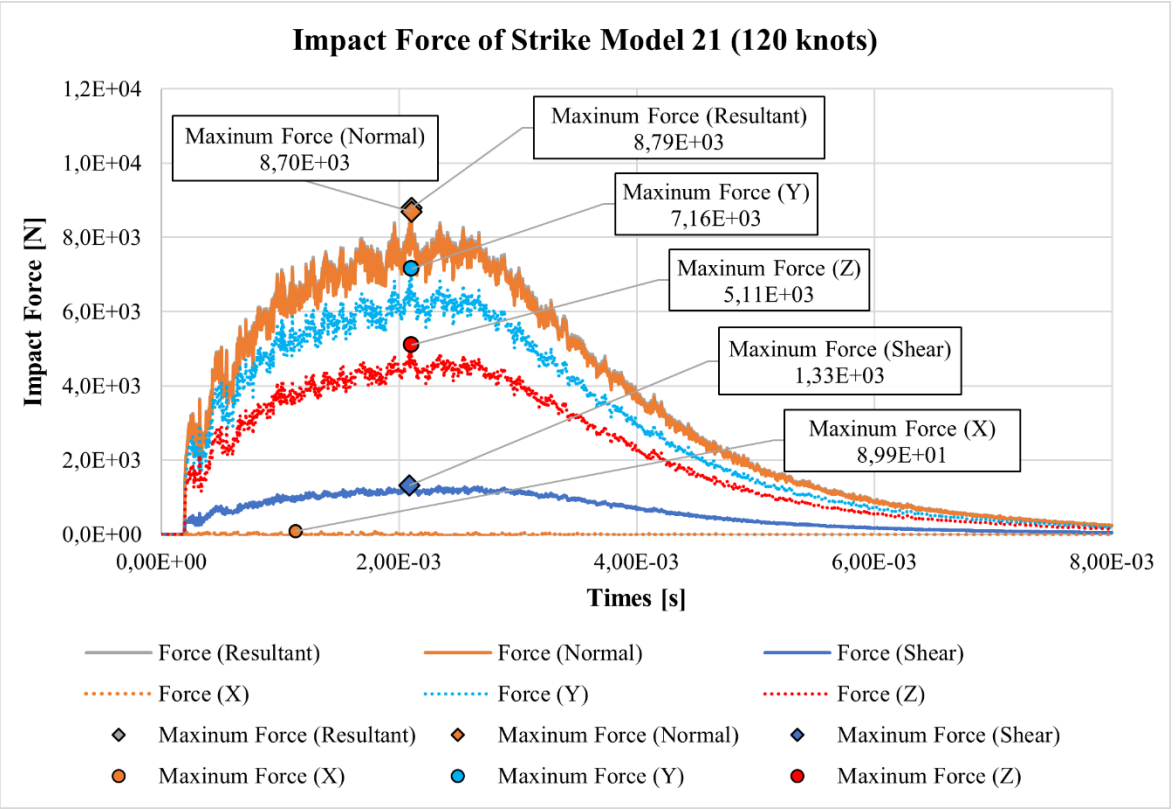

Figure 8-17 Impact Forces of Strike Model 21 with 120 knots

8.2 Bird Strike with Effect of Pitch Change

In this section, analyses were done using parameneters given in Table 18 and analysis model was named as Strike Model 22. Impact angle defines an angle between windshield surface and strike direction. Analysis results of Strike Model 22 would later be compared with Strike Model 21 in conclusion part to investigate the effect of pitch change.

Table 18 Impact Scenario of Strike Model 22

Airspeed of Helicopter [knots]	Pitch Angle of Helicopter [Degrees]	Impact Angle [Degrees]
80	2°	27°
85	1°	28°
102	-1°	30°
110	-2°	31°
120	-3°	32°

Following impact pressure tables show impact pressure on windshield surface by time, and maximum impact pressure on windshield surface. Following impact force tables show resultant impact force, component of impact force in X, Y, Z axises; shear force and normal force components of impact force on windshield by time; and maximum values of them.

Following figures show strike simulation and analysis result of Strike Model 22 with 80 knots impact speed.

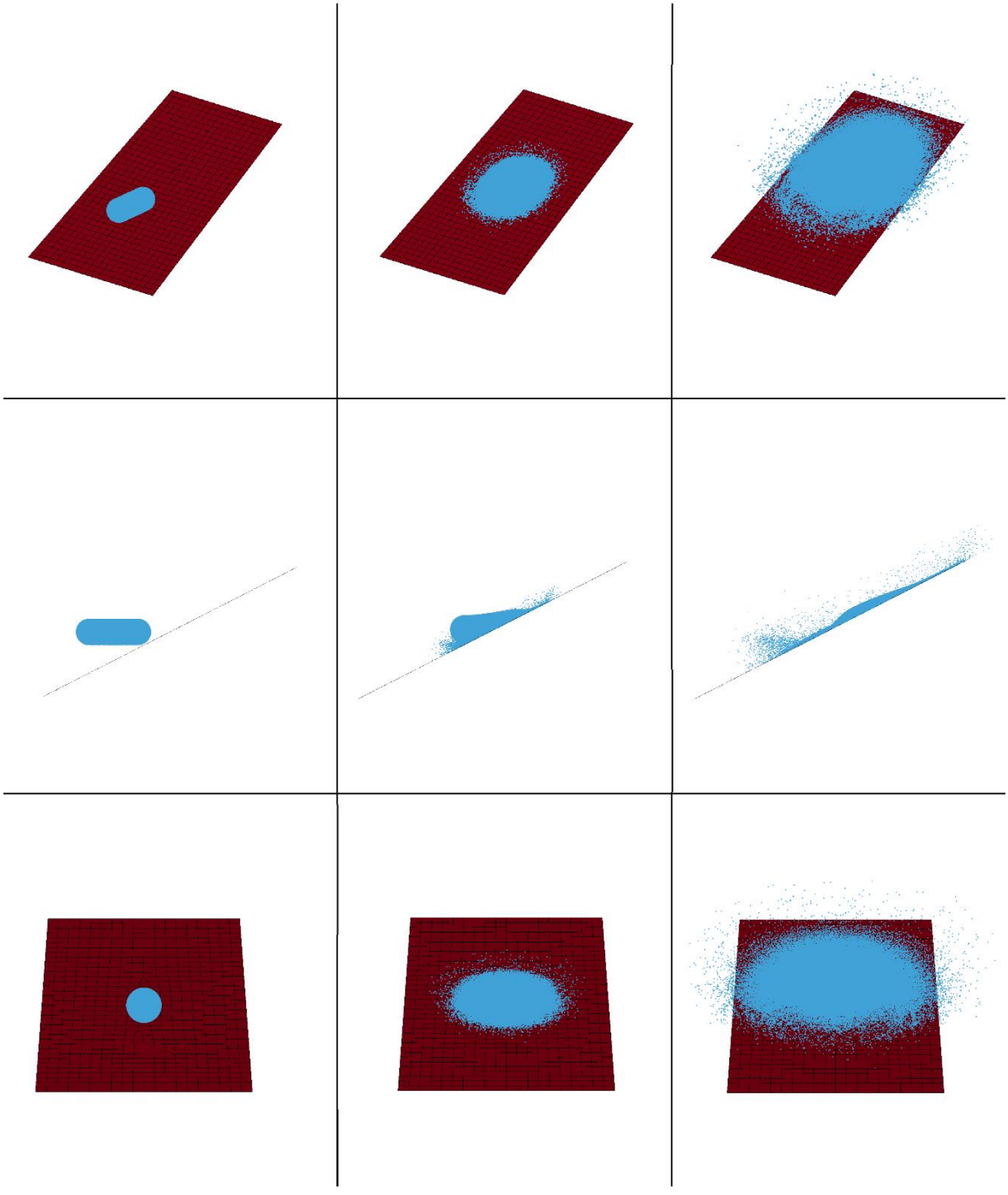

Figure 8-18 Strike Simulation of Strike Model 22 with 80 knots

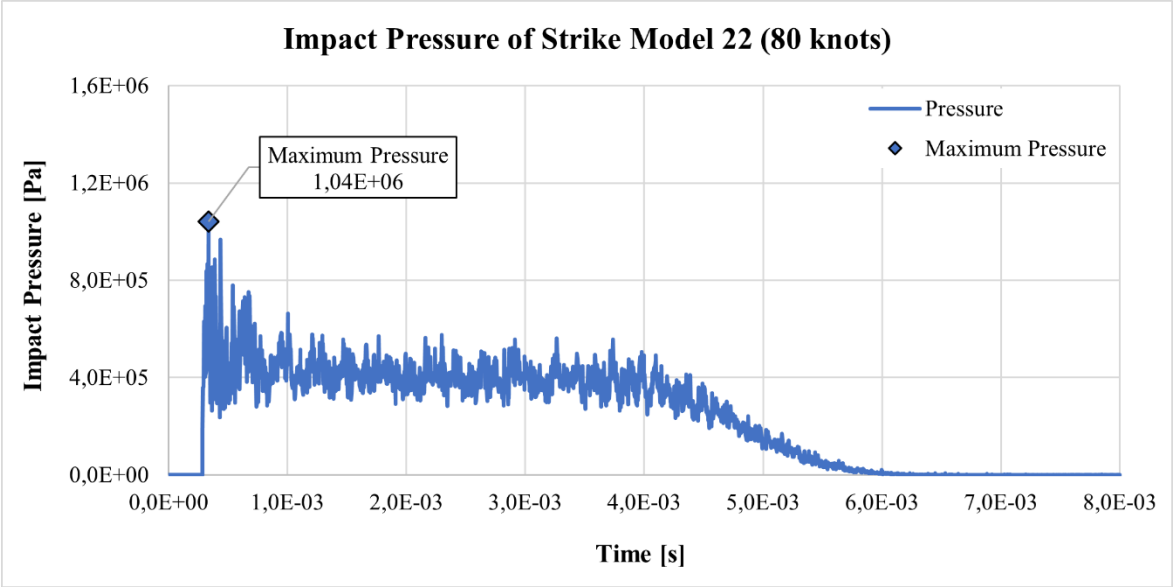

Figure 8-19 Impact Pressure of Strike Model 22 with 80 knots

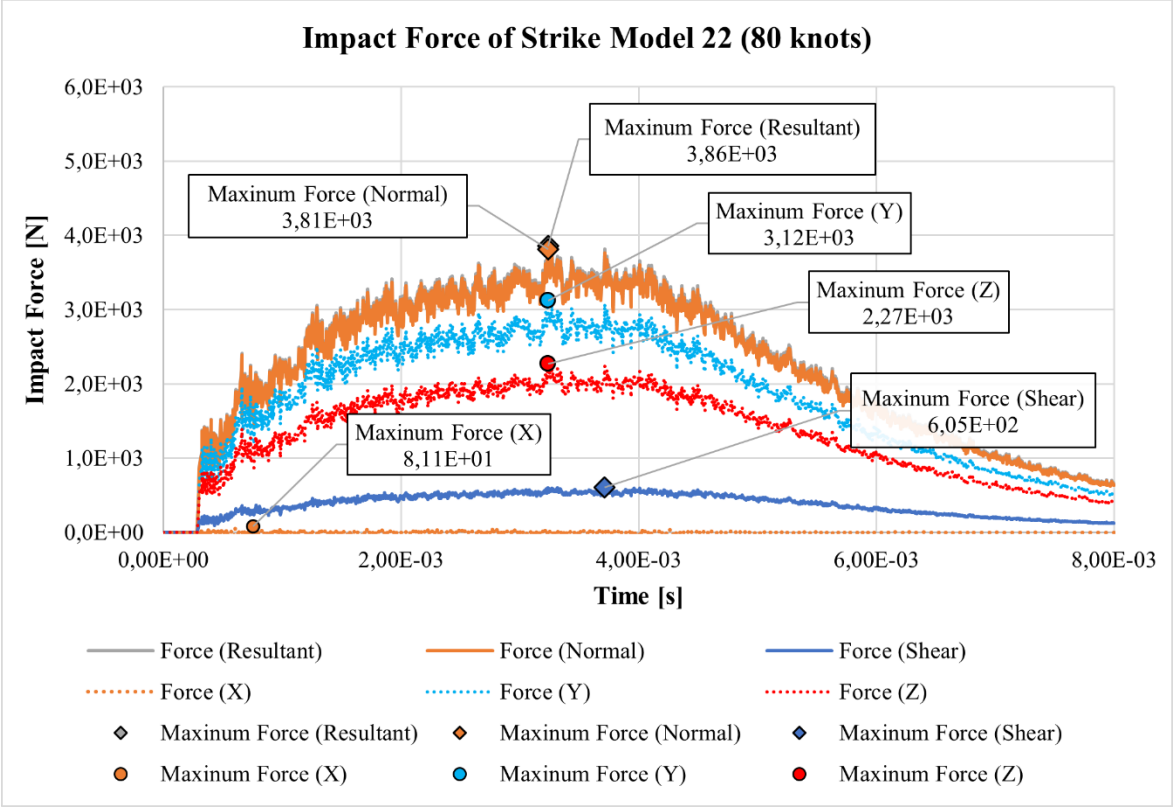

Figure 8-20 Impact Forces of Strike Model 22 with 80 knots

Following figures show strike simulation and analysis result of Strike Model 22 with 85 knots impact speed.

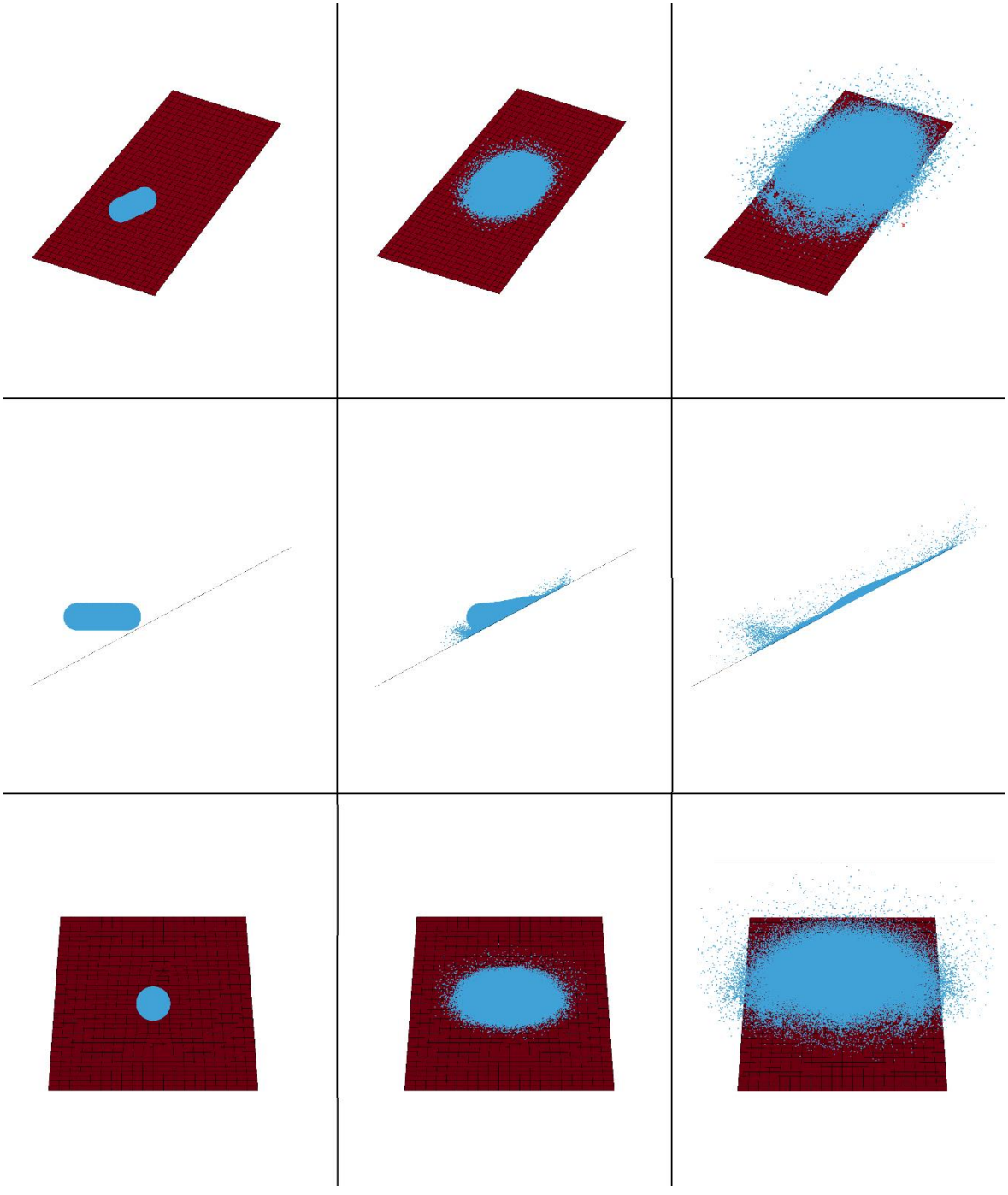

Figure 8-21 Strike Simulation of Strike Model 22 with 85 knots

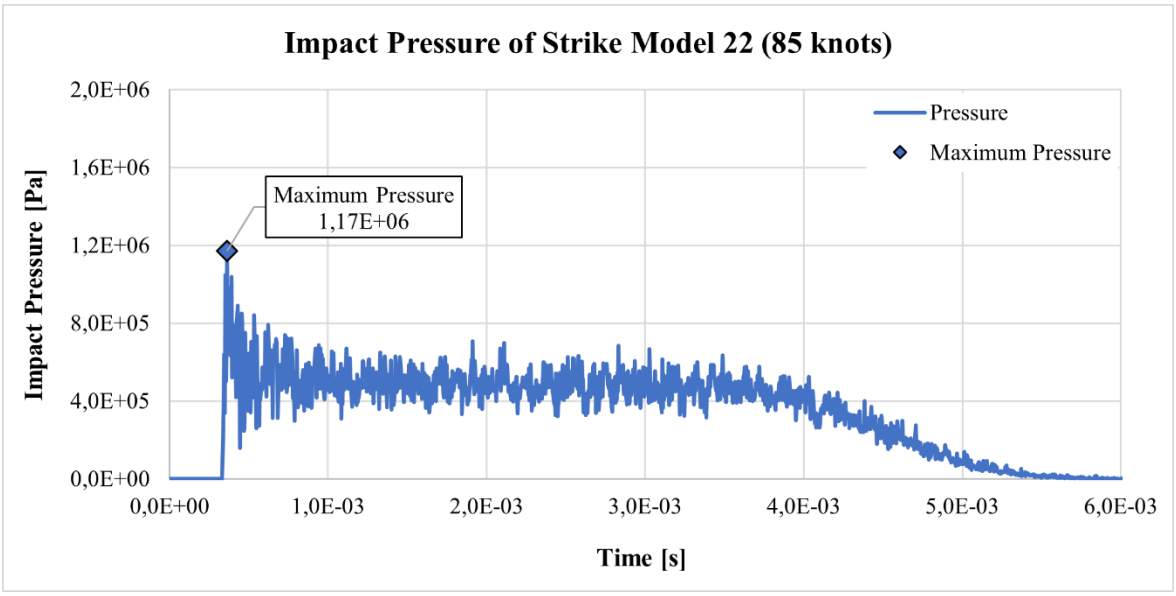

Figure 8-22 Impact Pressure of Strike Model 22 with 85 knots

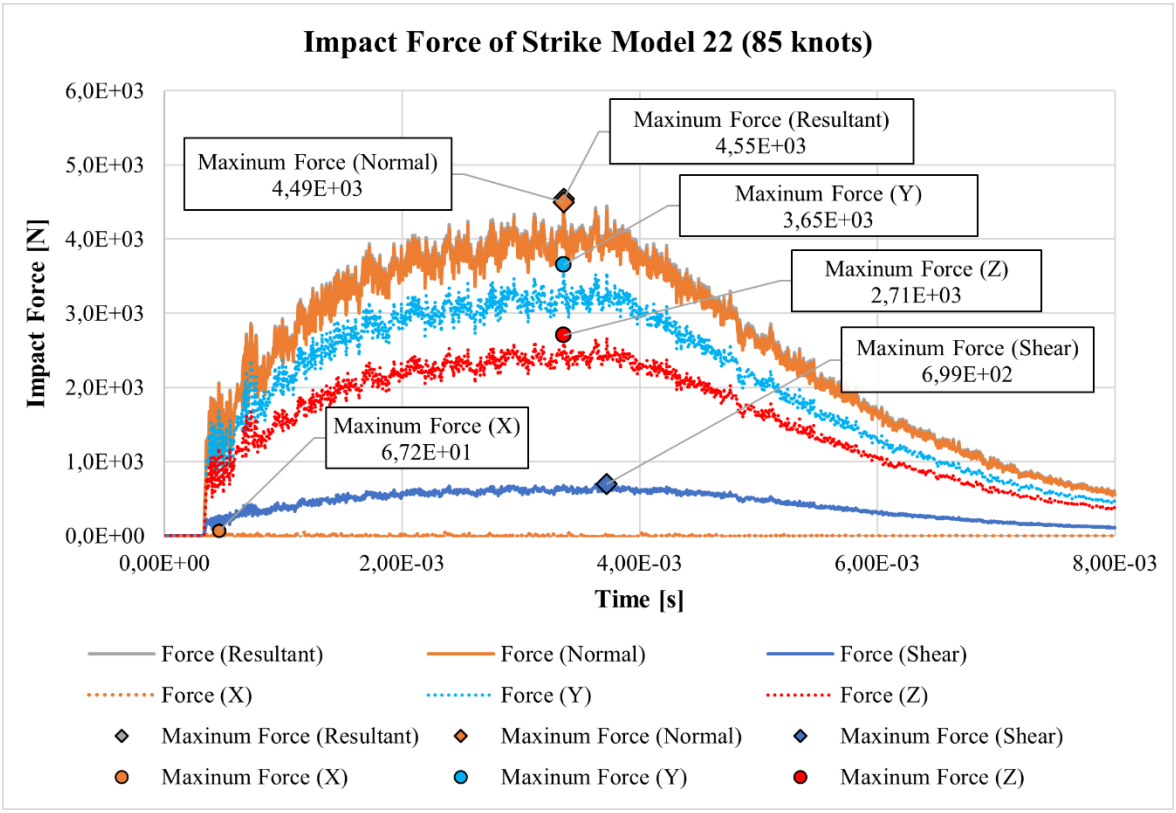

Figure 8-23 Impact Forces of Strike Model 22 with 85 knots

Following figures show strike simulation and analysis result of Strike Model 22 with 102 knots impact speed.

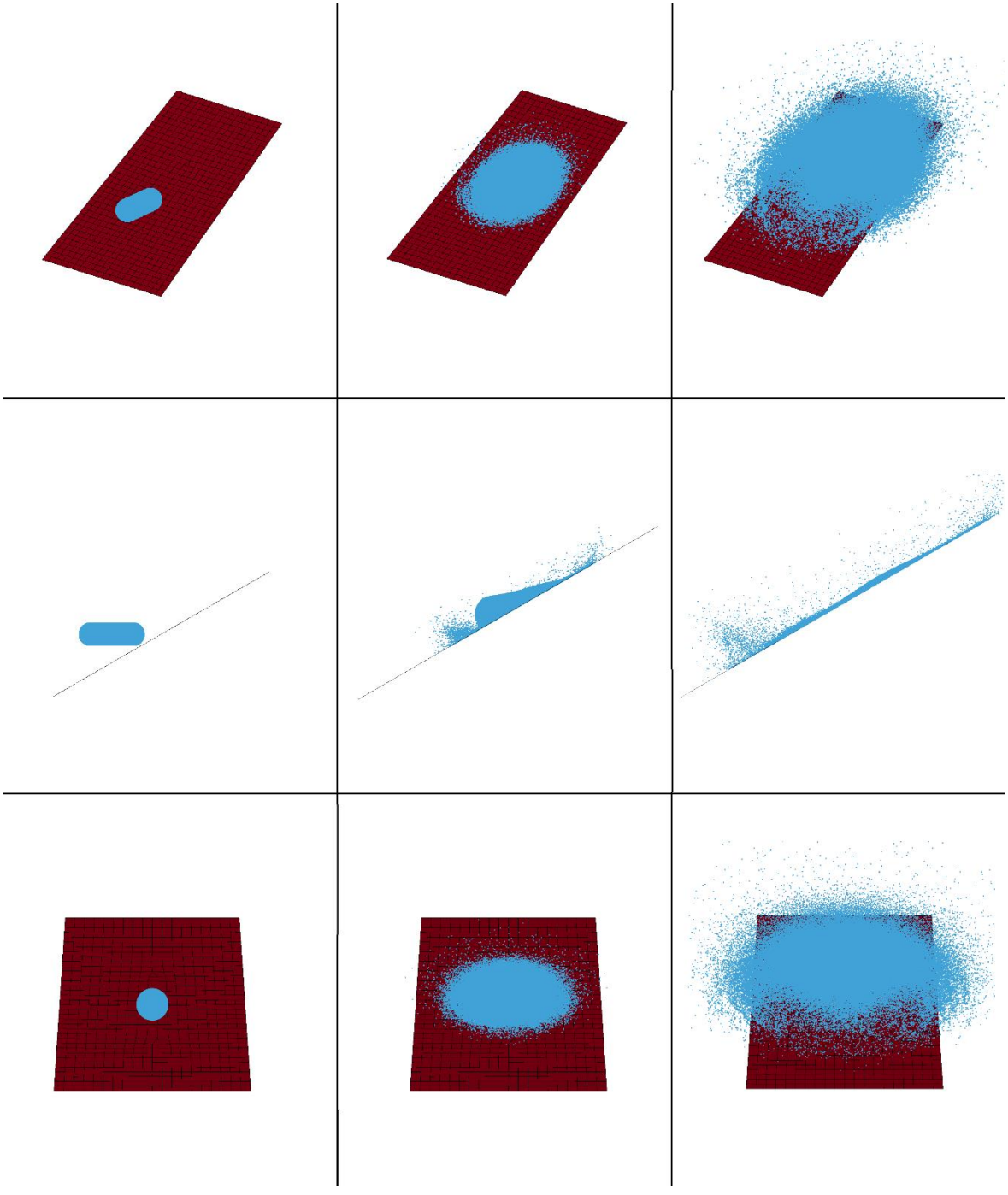

Figure 8-24 Strike Simulation of Strike Model 22 with 102 knots

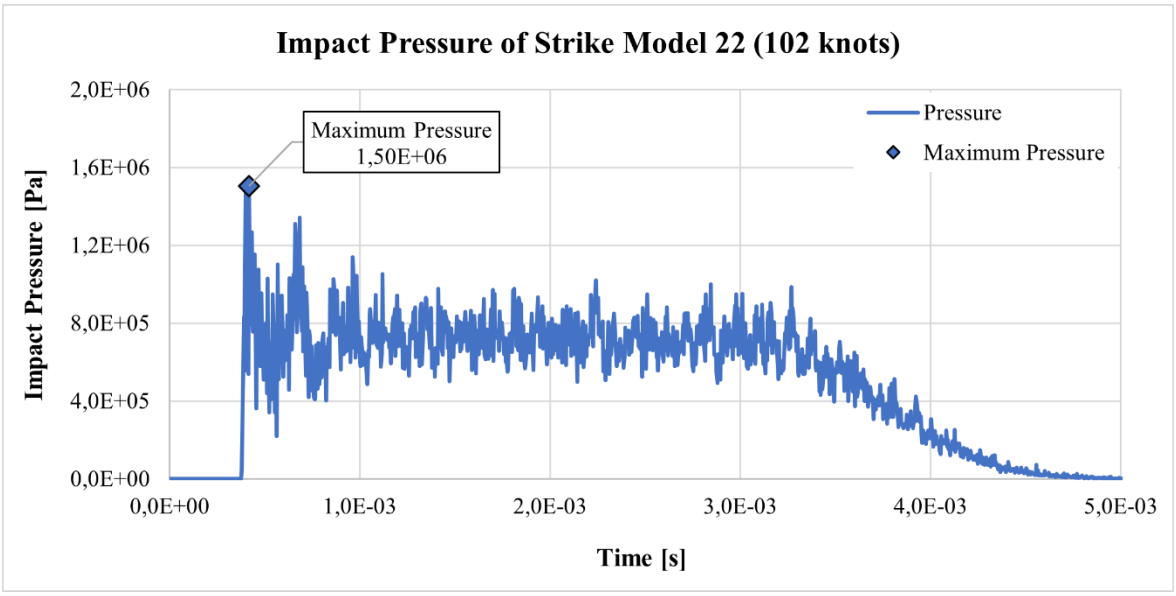

Figure 8-25 Impact Pressure of Strike Model 22 with 102 knots

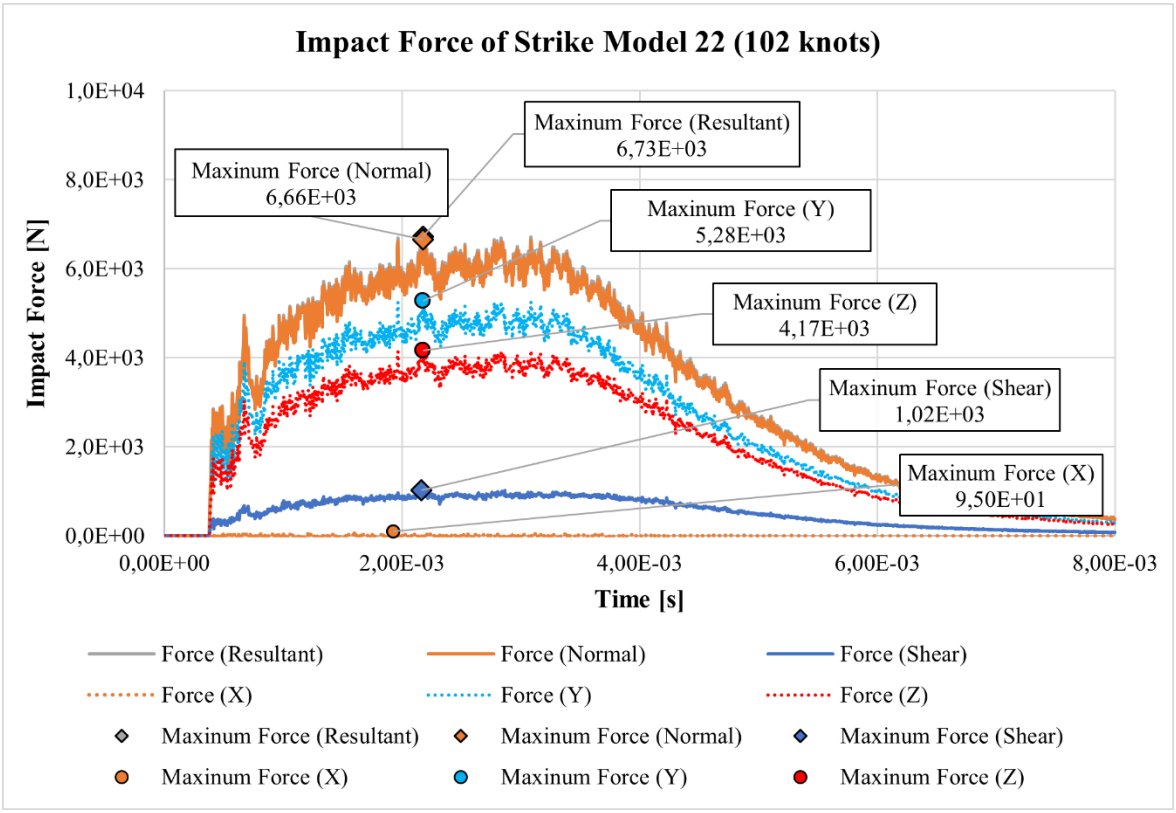

Figure 8-26 Impact Forces of Strike Model 22 with 102 knots

Following figures show strike simulation and analysis result of Strike Model 22 with 110 knots impact speed.

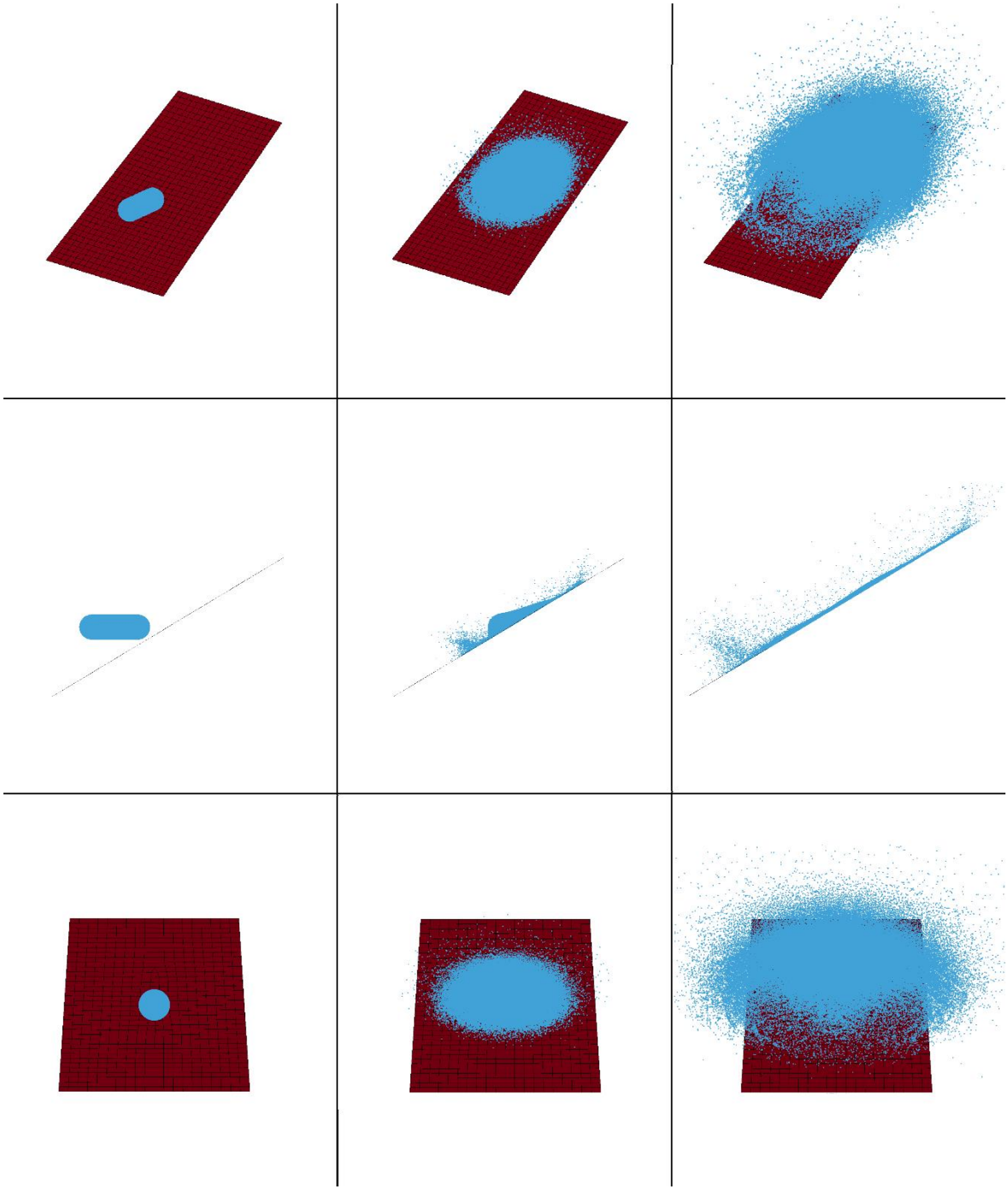

Figure 8-27 Strike Simulation of Strike Model 22 with 110 knots

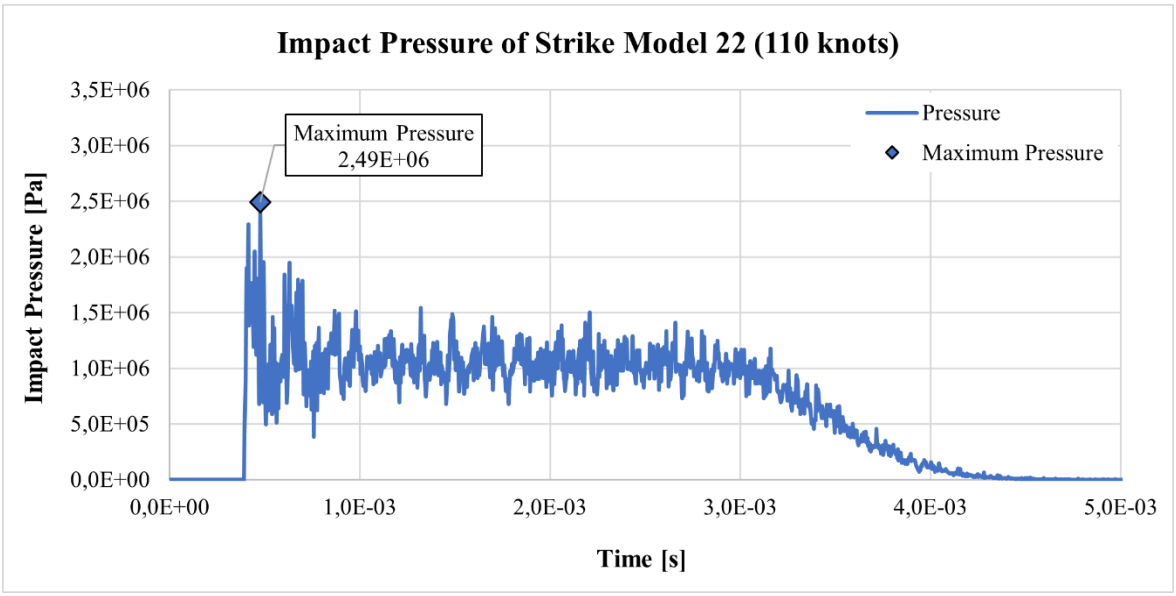

Figure 8-28 Impact Pressure of Strike Model 22 with 110 knots

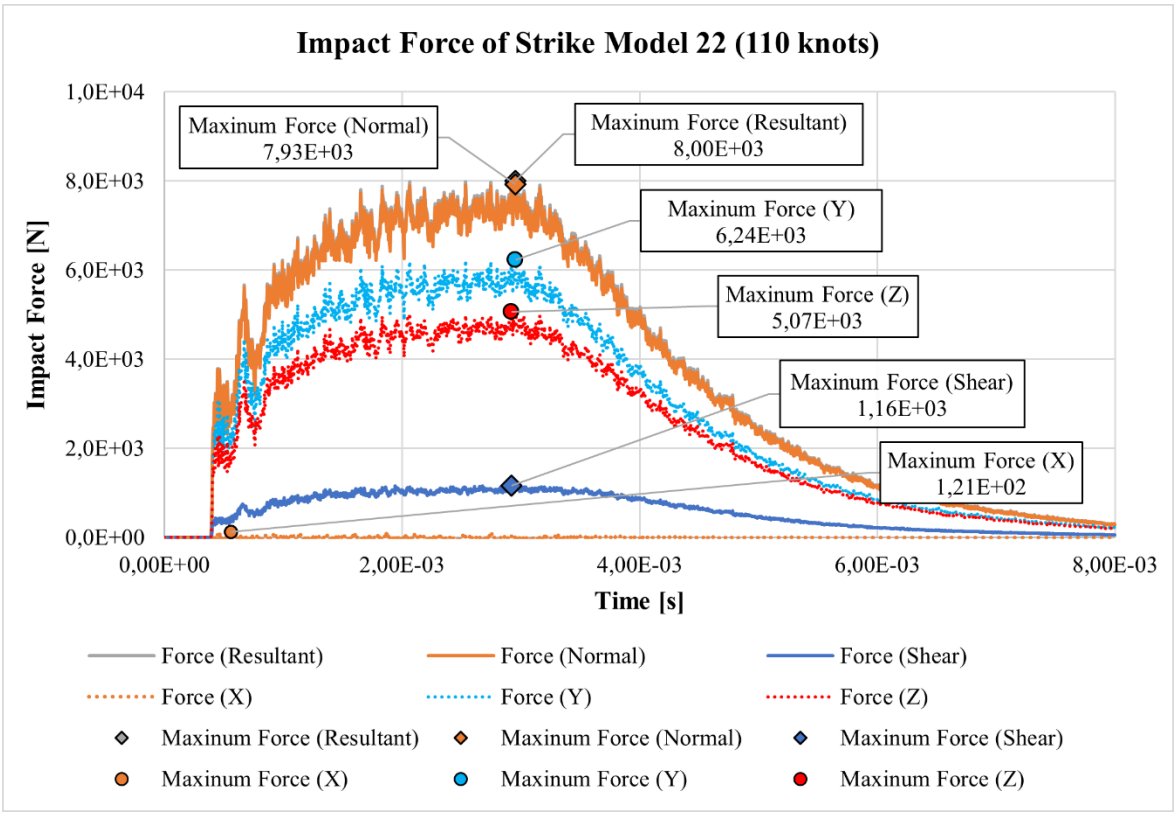

Figure 8-29 Impact Forces of Strike Model 22 with 110 knots

Following figures show strike simulation and analysis result of Strike Model 22 with 120 knots impact speed.

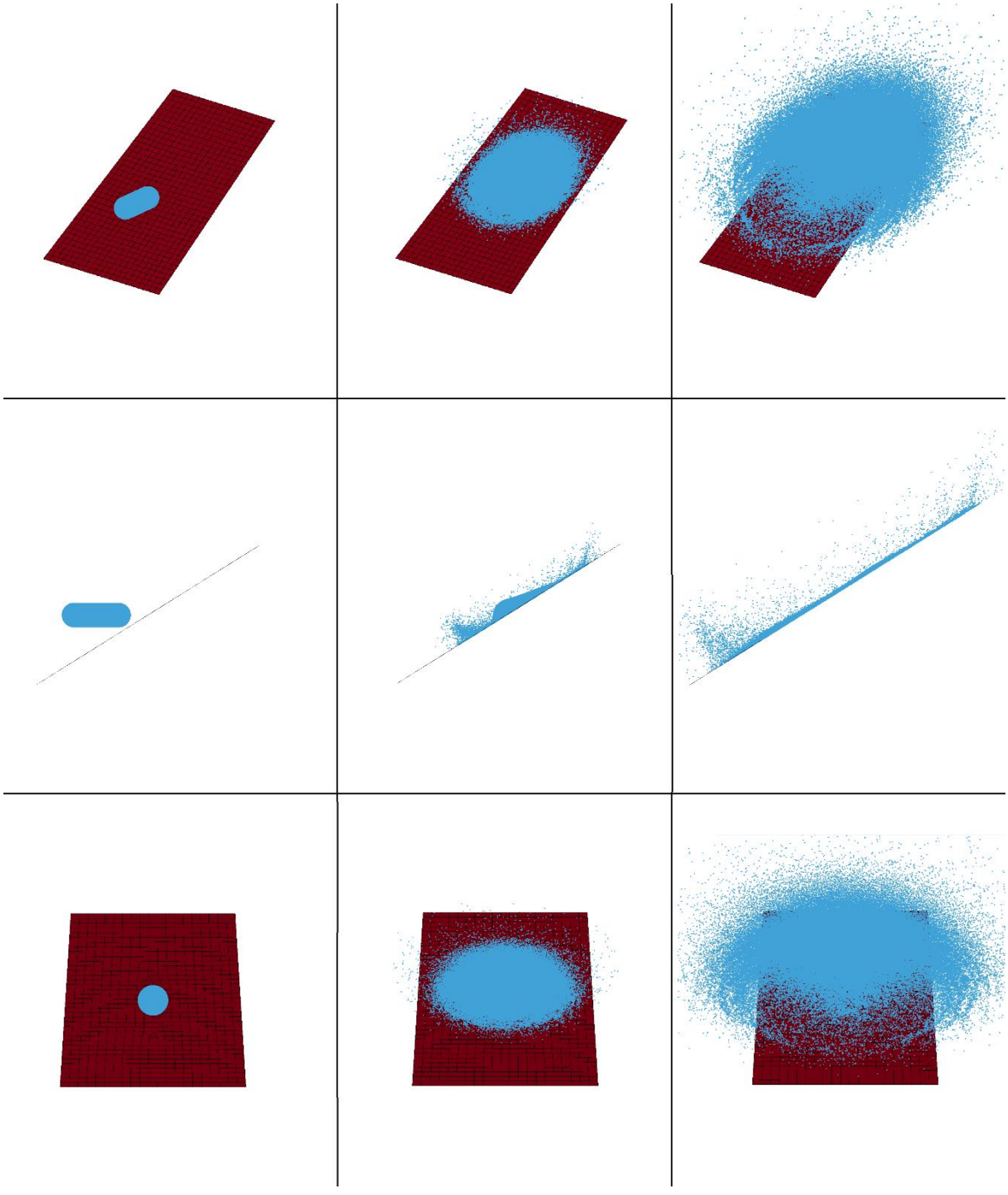

Figure 8-30 Strike Simulation of Strike Model 22 with 120 knots

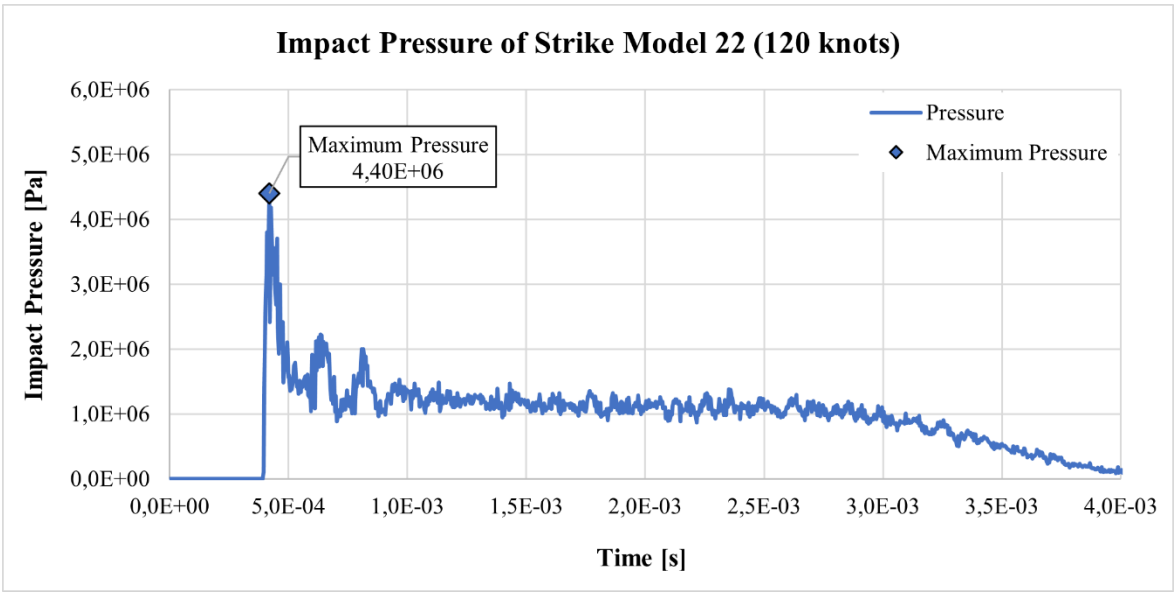

Figure 8-31 Impact Pressure of Strike Model 22 with 120 knots

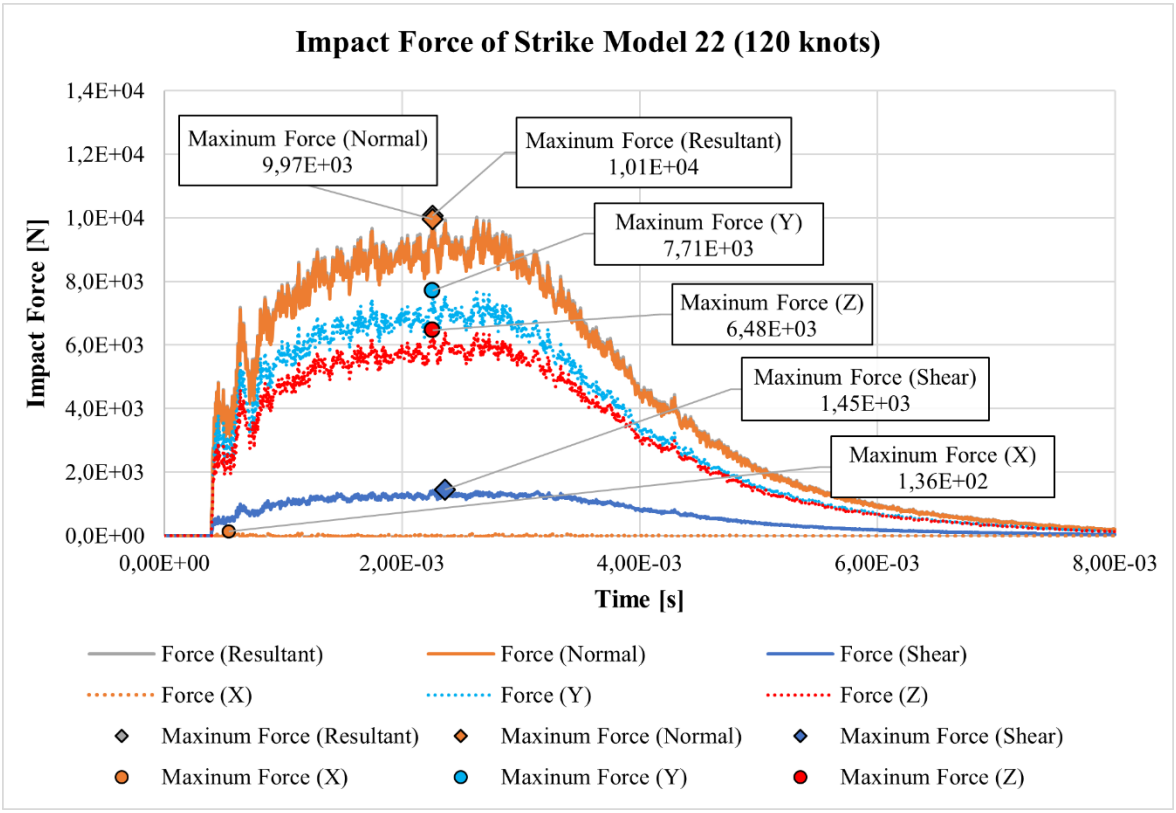

Figure 8-32 Impact Forces of Strike Model 22 with 120 knots

9 CONCLUSION

Bird strike accidents have been important issue since beginning of aviation, and importance of bird strike incidents continues increasing. Bird strike requirements for large rotorcraft are stated that category A rotorcraft must be able to continue safe flight and land safely and category B rotorcraft must be able to land safely after strike of 1 kg bird with relative velocity of aircraft equals to V_{NE} or V_H [1, 2].

Final strike models were created using Bird Shape 2 and SPH method which were chosen as the most reasonable Bird Shape - Method combination after evaluation of eighteen different combinations.

Bird strike incidents effect rotary-wing aircrafts more than fixed-wing aircrafts because effect of bird strike not only changes by impact speed but also changes by impact angle. For higher impact speeds, effect of impact angle can be seen better. Therefore, Strike Model 21 and Strike Model 22 were created as final strike models. Strike Model 22 was created by including pitch change to include the effect of strike angle, and Strike Model 21 was created by excluding pitch change to exclude the effect of strike angle. Results of Strike Model 21 and Strike Model 22 were compared to investigate effect of bird strike to rotary-wing aircraft.

Final analyses were done using both Strike Model 21 and Strike Model 22 for impact speeds of 80, 85, 102, 110 and 120 knots. Maximum values of impact pressures, resultant forces, normal forces were compared.

Maximum impact pressures of bird strike at impact speeds of 80, 85, 102, 110 and 120 knots were shown in Figure 9-1. Second order polynomials trend line was created with coefficient of determination value of 0,9511 by using maximum impact pressure data of Strike Model 21, and third order polynomial trend line was created with coefficient of determination value of 0,9977 by using maximum impact pressure data of Strike Model 22.

Figure 9-1 shows that maximum impact pressure increases exponentially for higher impact speeds. However, increase of maximum impact pressure of Strike Model 22 was significantly higher than increase of maximum impact pressure of Strike Model 21. At the

120 knots impact speed, consisting impact pressure on windshield was 2,155 megapascal if effect of helicopter pitch angle change was not included; and 4,405 megapascal if effect of helicopter pitch angle change was included. According to analyses for 120 knots impact speed, maximum impact pressure increases by 104,4% with including change of helicopter pitch angle.

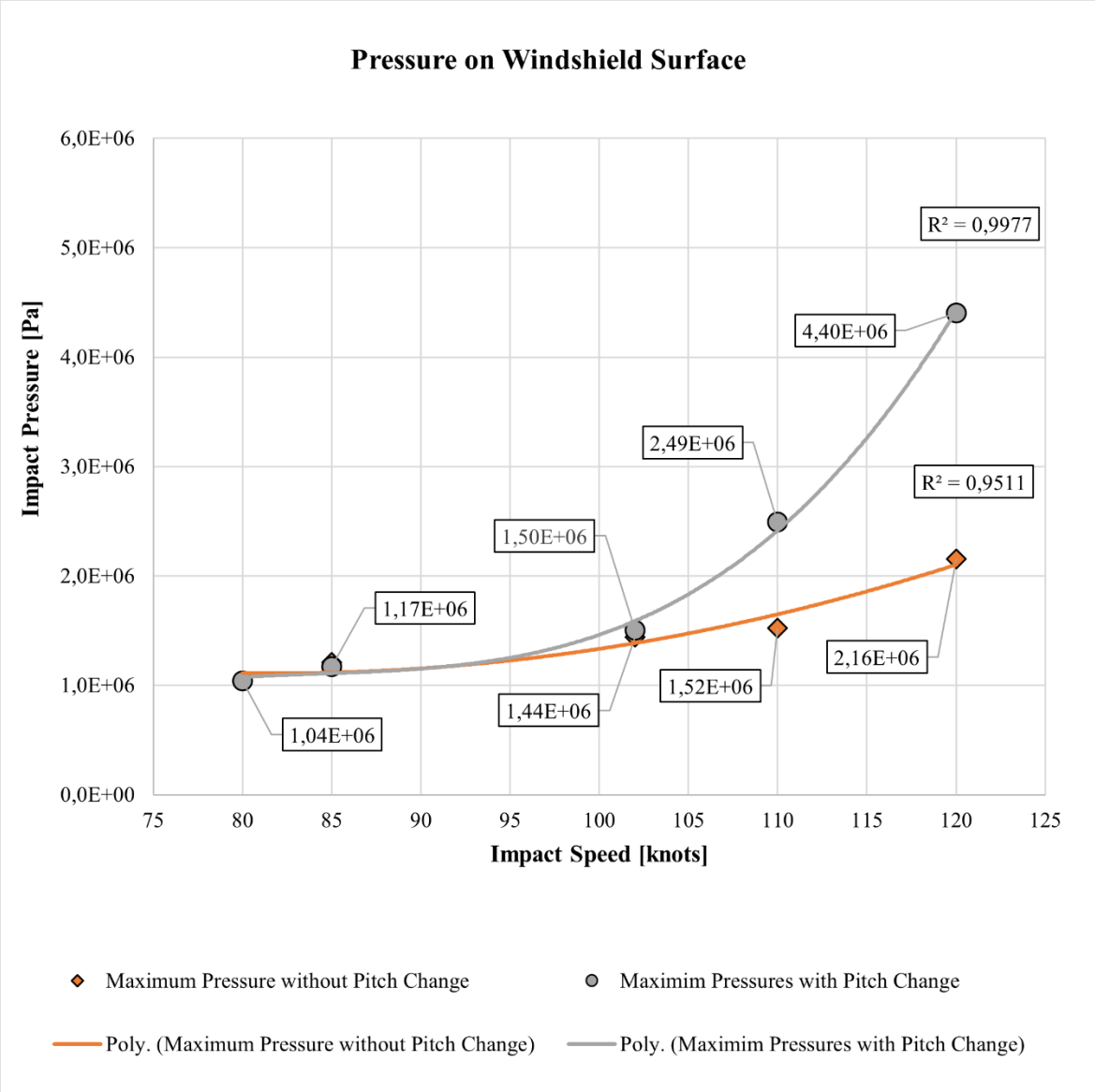

Figure 9-1 Impact Pressure Comparison

Maximum resultant forces which occurred on windscreen at impact speeds of 80, 85, 102, 110 and 120 knots were shown in Figure 9-2. Third order polynomial trend lines were created with coefficient of determination values of 0,9998 and 1 by using maximum resultant

impact force data of Strike Model 21 and Strike Model 22, respectively. Figure 9-2 shows that maximum resultant impact force increases by higher impact speeds. However, increase of maximum resultant impact force of Strike Model 22 was higher than increase of maximum resultant impact force of Strike Model 21. At the 120 knots impact speed, maximum impact forces on windshield were determined as 8,795 kilonewtons by excluding the change of helicopter pitch angle although it was 10,065 kilonewtons by including the change of helicopter pitch angle. According to analyses for 120 knots impact speed, maximum resultant impact force increases by 14,44% with including change of helicopter pitch angle change.

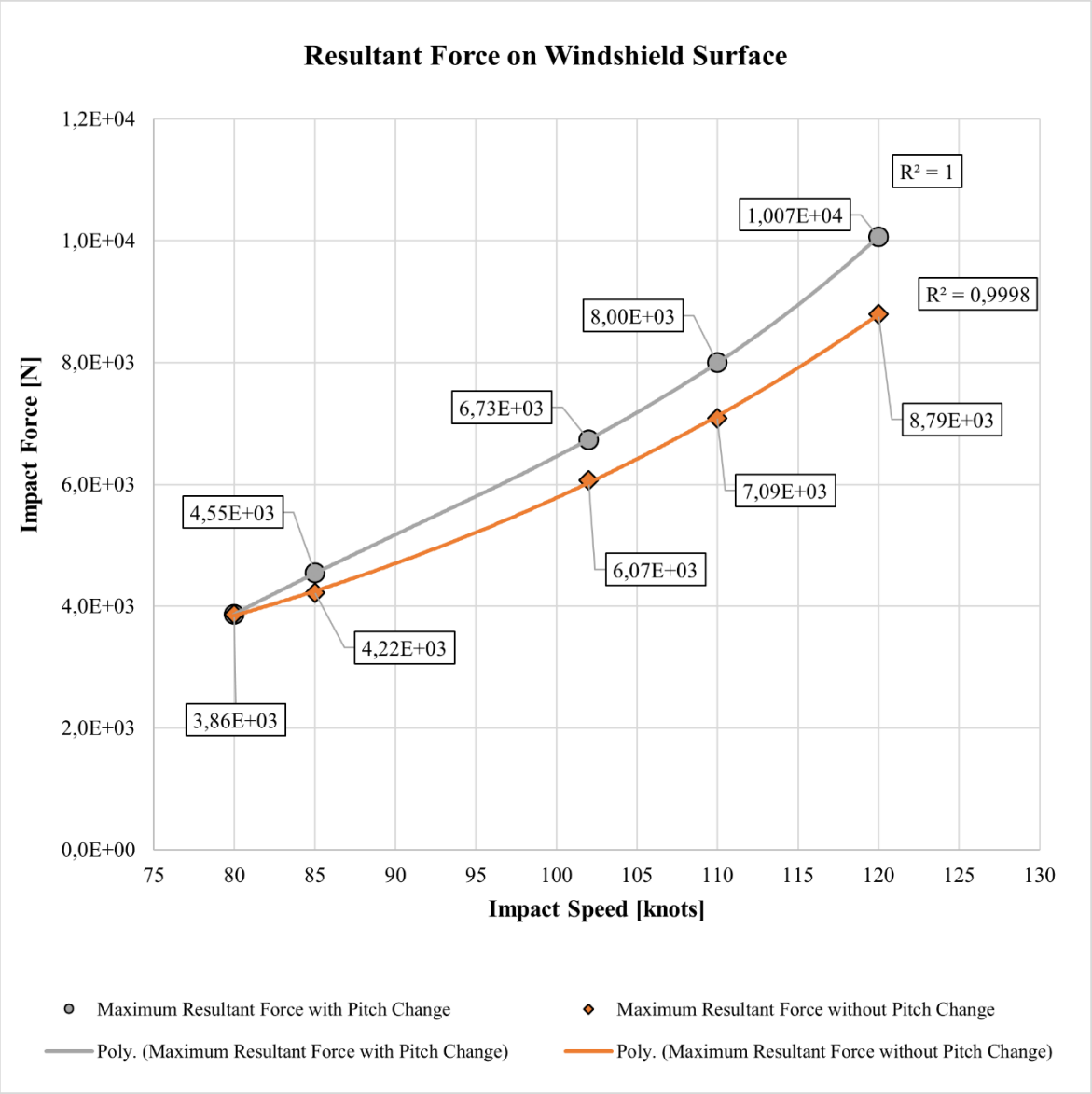

Figure 9-2 Resultant Impact Forces Comparison

Maximum normal forces which were applied perpendicular to windscreen at impact speeds of 80, 85, 102, 110 and 120 knots were shown in Figure 9-3. Third order polynomials trend lines were created with coefficient of determination values of 0,9998 and 1 by using normal component of maximum impact force data of Strike Model 21 and Strike Model 22, respectively.

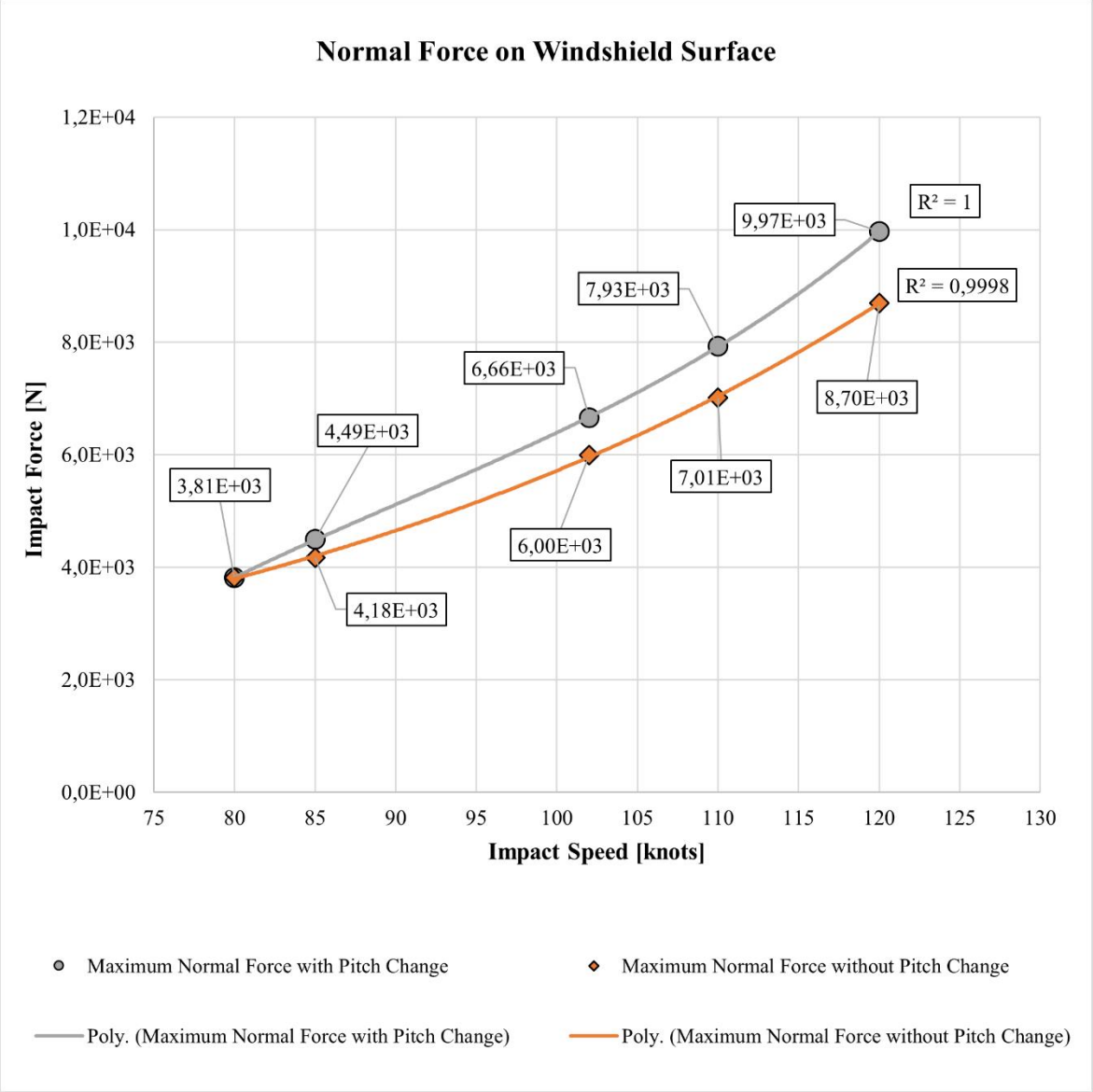

Figure 9-3 Normal Impact Forces Comparison

Similar to resultant impact force, Figure 9-3 shows that maximum impact force normal to windshield increases by higher impact speeds. However, maximum normal impact force of

Strike Model 22 was higher than maximum normal impact force of Strike Model 21. At the 120 knots impact speed, maximum normal impact forces on windshield were determined as 8,698 kilonewtons by excluding the change of helicopter pitch angle although it was 9,966 kilonewtons by including the change of helicopter pitch angle. According to analyses for 120 knots impact speed, maximum impact force normal to impact surface increases by 14,58% with including change of helicopter pitch angle.

In conclusion, the thesis study has shown that because of the flight characteristics of rotary-wing aircrafts, the bird strike incidents create more dangerous results compared to fixed-wing aircrafts because of change of pitch angle of rotary-wing aircraft.

Design of the aircrafts must comply with requirements of certification specifications and acceptable means of compliance. Therefore, rotary-wing aircrafts are designed in consideration of bird strike, like fixed-wing aircrafts. Compliance with requirements of bird strike must be shown by tests or by analysis based on tests carried out on sufficiently representative structures of similar design [1]. The study would be used as reference for bird strike analyses of rotary-wing aircrafts and the further studies would be done based on this thesis study.

10 REFERENCES

1. *Certification Specifications and Acceptable Means of Compliance for Large Rotorcraft*. 2020, European Union Aviation Safety Agency.
2. in *Part 29 Airworthiness Standards: Transport Category Rotorcraft*. Federal Aviation Administration, Department of Transportation.
3. Heimbs, S., *Computational Methods For Bird Strike Simulations: A Review*. Computers & Structures, 2011. **89**(23): p. 2093-2112.
4. *Quick Press Kit*. 2019 26 April 2019 [cited 2019 03 May 2019]; Available from: http://www.birdstrike.org/press-kit/.
5. Dolbeer, R.A. and M.J. Begier, *Wildlife Strikes to Civil Aircraft in the United States 1990-2017*. 2019.
6. Cleary, E.C., R.A. Dolbeer, and S.E. Wright, *Wildlife Strikes to Civil Aircraft in the United States 1990-2005.* Other Bird Strike and Aviation Materials, 2006. **7**.
7. *Factual Report Aviation NTSB ID: CEN09MA117*. 2010: National Transportation Safety Board. p. 17.
8. Gamble, W.H., *National Transportation Safety Board Aviation Accident Data Summary*. 2010: National Transportation Safety Board Aviation. p. 4.
9. *Sikorsky S-76C++ at Morgan City, LA - Accident Overview*. U.S. Department of Transportation Federal Aviation Administration: https://lessonslearned.faa.gov/ll_main_rotor.cfm?TabID=3&LLID_ROTO=1&LLTypeID=2.
10. *PHI Inc. Sikorsky S-76C++, N748P*. U.S. Department of Transportation Federal Aviation Administration: https://lessonslearned.faa.gov/ll_main_rotor.cfm?TabID=1&LLID_ROTO=1.
11. *Aviation Safery Network Wikibase Occurrence # 56849*. 2009: https://aviation-safety.net/wikibase/wiki.php?id=56849.
12. *NTSB Identification: CEN09MA117*. [cited 2019 April 27]; Available from: https://www.ntsb.gov/_layouts/ntsb.aviation/brief2.aspx?ev_id=20090104X12037&ntsbno=CEN09MA117&akey=1.
13. *Safety Lessons from a Fatal Helicopter Bird Strike: Sikorsky S-76C++ N748P, 4 January 2009*. [cited 2020 December 16]; Available from: http://aerossurance.com/helicopters/fatal-s76c-birdstrike-2009/.
14. Anderson, J.D., *Aircraft Performance and Design*. 1999, Boston: McGraw-Hill.
15. Lavoie, M.-A., et al., *Review of Existing Numerical Methods and Validation Procedure Available for Bird Strike Modelling.* The International Conference on Computational & Experimental Engineering and Sciences, 2007. **2**(4): p. 111--118.
16. Marinko, U., *Application of The Hydrodynamic Theory and the Finite Element Method in The Analysis of Bird Strike in a Flat Barrier.* Sci Tech Rev, 2012. **62**: p. 28-37.
17. Chizari, M., L.M. Barrett, and S.T.S. Al-Hassani, *An Explicit Numerical Modelling of the Water Jet Tube Forming.* Computational Materials Science, 2009. **45**(2): p. 378-384.

18. Hedayati, R. and M. Sadighi, *Bird strike: An Experimental, Theoretical and Numerical Investigation*. 2016: Elsevier.

19. Donea, J., et al., *Arbitrary Lagrangian – Eulerian Methods*, in *Encyclopedia of Computational Mechanics*. 2004, Wiley.

20. Khoei, A.R., et al., *Arbitrary Lagrangian-Eulerian Method in Plasticity of Pressure-Sensitive Material: Application to Powder Forming Processes.* Computational Mechanics, 2008. **42**: p. 13-38.

21. Langrand, B., et al., *Assessment of Multi-Physics FE Methods for Bird Strike Modelling-Application to a Metallic Riveted Airframe.* International Journal of Crashworthiness, 2002. **7**: p. 415-428.

22. Grimaldi, A., et al., *Parametric Study of a SPH High Velocity Impact Analysis – A Birdstrike Windshield Application.* Composite Structures, 2013. **96**: p. 616-630.

23. Barriere, L., M. Bouquet, and J.-F. Ferrero, *Bird Strike Shielding Materials: Development of A High Velocity Impact Test Platform*, in *SAMPE Europe*. 2015: Amiens, France.

24. *The Hazard Posed to Aircraft by Birds*. 2003, Australian Transport Safety Bureau.

25. Budgey, R., *The Development of a Substitute Artificial Bird by the International Birdstrike Research Group for Use in Aircraft Component Testing*. 2000: International Bird Strike Committee.

26. Wilbeck, J.S. and J.L. Rand, *The Development of a Substitute Bird Model.* The Shock and Vibration Bulletin, 1978. **Part 2**: p. 115.

27. Wilbeck, J.S., *Impact Behavior of Low Strength Projectiles*. 1978, Air Force Materials Lab Wright-Patterson AFB OH.